Application of Semi-Grand Canonical Monte Carlo (SGMC) Methods to Describe Non-Equilibrium Polymer Systems

by

Frederick E. Bernardin III

B.S., Pennsylvania State University (1990)
M.S., Carnegie Mellon University (1993)

Submitted to the Department of Chemical Engineering
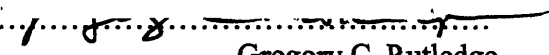in partial fulfillment of the requirements for the degree of

Doctor of Philosophy

at the

MASSACHUSETTS INSTITUTE OF TECHNOLOGY

September 2007

© 2007 Massachusetts Institute of Technology

Signature of Author...
Department of Chemical Engineering
August 27, 2007

Certified by..
Gregory C. Rutledge
Lammot DuPont Professor of Chemical Engineering
Thesis Supervisor

Certified by..
William M. Deen
Chairperson, Department Committee on Graduate Students
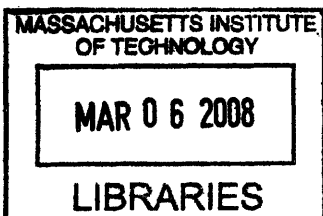
1

Application of Semi-Grand Canonical Monte Carlo (SGMC) Methods to Describe Non-Equilibrium Polymer Systems

by

Frederick E. Bernardin III

B.S., Pennsylvania State University (1990)
M.S., Carnegie Mellon University (1993)

Submitted to the Department of Chemical Engineering
in partial fulfillment of the requirements for the degree of
Doctor of Philosophy

Abstract

Understanding the structure of materials, and how this structure affects their properties, is an important step towards the understanding that is necessary in order to apply computational methods to the end of designing materials to fit very specific needs. Such needs include specific optical and mechanical properties. In polymers, the ability to easily create orientation through a variety of processes allows the production of materials that, while chemically similar, exhibit a wide variety of optical and mechanical properties. The ability to illuminate the connections between structure and optical or mechanical properties depends on the ability to reliably interpret a wide variety of experimental measurements. I assert that thermodynamic consistency and energy minimization is an integral part of this endeavor; reliable analyses of structure and properties are built upon the foundation of a minimum-free-energy ensemble of configurations that reproduces the experimental results. This project encompasses three goals, which make up this thesis: 1) to show how sets of experimental measurements are integrated into simulations to produce thermodynamically consistent, minimum-free-energy ensembles; 2) to show how these ensembles can characterize the conformations of macromolecules, which are not available from direct simulation; 3) to show how dynamic processes, which create inhomogeneous systems can be incorporated, along with experimental structural measurements, into thermodynamically consistent, minimum-free-energy ensembles.

To achieve the first of these goals, we describe the application of the Semi-Grand Canonical Monte Carlo (SGMC) method to analyze and interpret experimental data for non-equilibrium polymer melts and glasses. Experiments that provide information about atomic-level ordering, e.g. birefringence, are amenable to this approach. Closure of the inverse problem of determining the structural detail from limited data is achieved by selecting the lowest-free-energy ensemble of configurations that reproduces the experimental data. The free energy is calculated using the thermodynamic potential of the appropriate semi-grand canonical (SGC) ensemble $[NPT\Delta\mu(I)]$, as defined by the experimental data. To illustrate the method we examine uniaxially oriented polyethylene melts of average chain length up to C_{400}. The simulation results are analyzed for features not explicitly measured by birefringence, such as the density, torsion angle distribution,

molecular scale orientation and free energy, to understand more fully the underlying features of these non-equilibrium states. The stress-optical rule for polyethylene is evaluated in this way.

The second goal is achieved through multi-scale modeling, which requires the selection and preservation of information crucial to understanding the behavior of a system at appropriate length and time scales. For a description of processed polymers, such a model must successfully link rheological properties with atomic-level structure. We propose a method for the calculation of an important rheological state descriptor, the configuration tensor <QQ>, from atomistic simulations of oligomers. The method requires no adjustable parameters and can describe anisotropic polymer conformations at conditions of significant deformation. We establish the validity of the atomistic-to-macromolecular scaling by comparing the consistency of macromolecular predictions of <QQ> among different polyethylene (PE) oligomer systems. We use this method with the previously reported Semi-Grand Canonical Monte Carlo (SGMC) method to deduce macromolecular and atomic-level structural information interchangeably for systems with flow-induced orientation.

Introducing the ability to model arbitrary points in a dynamic process fulfills the third goal elaborated above. Because the characteristic relaxation times of processed polymer chains often span several orders of magnitude, it is commonly the case that partial relaxation of the chains is frozen into the final product. We report results of molecular simulations by the Semi-grand Canonical Monte Carlo (SGMC) method to study the orientation-dependent elasticity of glassy polystyrene as a function of both the system-average degree of orientation and the degree of relaxation of chain ends at a constant average degree of orientation, in accord with the tube model of Doi and Edwards. Our simulations reproduce quantitatively the experimentally observed changes in the tensile modulus E_{33} as a function of both average orientation and inhomogeneity of the orientation due to partial relaxation. The results show that the partial relaxation of the polymer chains is sufficient to explain the observed variation of mechanical properties for samples that differ in processing history, yet have the same observed birefringence.

Thesis Supervisor: Gregory C. Rutledge
Title: Lammot DuPont Professor of Chemical Engineering

Acknowledgements

I would like to thank my advisor Greg Rutledge. He has enforced a level of discipline and rigorousness that were, at times, lacking in my more free-wheeling style of inquiry; I believe that is a key element of producing the level of coherence and comprehensiveness present in my thesis. I would also like to thank the members of my thesis committee, Robert Armstrong, Bernhardt Trout, and Ken Beers, for their input on how to present this research in a way that is relevant to researchers in related, yet distinct fields.

Members of the Rutledge group, past and present (of which I have seen a complete changeover during my extended stay) deserve thanks. All of them have been helpful in a variety of ways; I mention only a few here in the interest of brevity: Pieter in 't Veld and Vikram Kuppa were valuable for their discussions of Monte Carlo methods and of how to implement them into computational routines; Jian Yu was helpful in less esoteric ways, such as helping entertain my children and at times even acting as a babysitter.

My family deserves special thanks for providing emotional and financial support (notwithstanding the relentless inquires as to the date of my eventual graduation). My children, Brooke and Ian, have been particularly helpful by making sure that I didn't get lost too deeply in my research; they have constantly reminded me about other important aspects of life.

Contents

3. Semi-Grand Canonical Monte Carlo (SGMC) Simulations to Interpret Experimental Data on Processed Polymer Melts and Glasses..54

6

4. A Method for the Estimation of Macromolecular Configurational Properties from Atomistic Simulations of Oligomers Under Nonequilibrium Conditions..............................98

5. Simulation of Mechanical Properties of Oriented Glassy Polystyrene................................118

List of Figures

9

10

List of Tables

Chapter 1

Introduction

1.1. Motivation

Since the beginnings of civilization, naturally occurring polymers, such as wool, cotton, silk, and wood have played an important role in providing the necessities of existence. Other natural polymers, such as latex rubber, subsequently provided applications that spurred the development of synthetic polymers for continually advancing industrial uses. Polymers are a class of materials which have grown to have a multitude of uses over the past century since the recognition of macromolecules in the early 1900's, replacing naturally occurring materials for a huge number of everyday uses due to relatively low weight, high strength, and elasticity. Because of their versatility, the use of these synthetic polymers has grown over the past half century from a novelty to a banality, and their application to an ever-broadening array of uses. In fact, this experience and understanding of polymers is now being applied to a new set of natural polymers in the field of biological engineering.

The connectivity of a polymer chain is a unique aspect of these compounds, which lies at the heart of their usefulness, as well as the complexity of their behavior. This connectivity accounts for the multiplicity of materials that can be created from a single monomer; by changing the connectivity among linear, branched, comb, star, rings, etc, and by varying the molecular weight of these polymers, one can tailor the resulting optical and mechanical properties. Additionally, structure and properties are affected by the stereoregularity and tacticity of the polymer chain, the ability to crystallize being one

of the most important considerations. Similar concerns are increasingly important for the understanding and control of biopolymers and the behavior of proteins; computational efforts are directed at understanding how the sequences of 'monomers' affect the ability to fold. In all fields of polymer study, the understanding of the effects of different conformations is crucial in order to enhance the efficacy of product design, and to target desired properties for future applications. Because computer experiments can isolate the effects of changes to particular features and precisely measure aspects of the materials hidden from analytical techniques, they are especially useful for such studies.

The ability to engineer materials at the nanoscale heightens the value of being able to use these precise measures to describe the properties of materials in general and polymers in particular through the use of atomistic simulations, which can focus particularly well at this length scale. Their ability to isolate different characteristics allows us to go beyond the ability to qualitatively understand the changes in the materials, and to give quantitative estimates that provide the basis for the design of new materials and for the manipulation of existing materials to extend their range of application.

Orientation in many of the age-old polymeric materials was an intrinsic characteristic that allowed their use as, e.g. fibers, and provided enhanced tensile properties. The recognition of the importance of orientation spurred the production of synthetic polymer fibers through artificial orientation processes for their use as direct replacements of their natural analogues in the production of textiles. Polymers are exceptionally well suited for this type of application because their properties are enhanced in significant ways by orientation, and because that this orientation is readily introduced into polymers, intentionally or not, through a variety of processes.

The subtler aspects of orientation remain an area of industrial and academic research interest in order to develop new materials and enhance properties of existing materials; the ways in which the manipulation of this orientation translates into the change of optical, and particularly mechanical, properties is not fully understood. At first glance, the wealth of analytical techniques available to the scientist might lead one to believe that it is simply a matter of diligence in the measuring of the polymer in order to

build up a structural model that comprehensively incorporates the distribution of conformations. However, the number of degrees of freedom is so huge that one has no possibility of building up an atomistically detailed model. In addition, even if we had such a model, the amount of structural data would still need to be distilled into a manageable number of descriptors to be of use. The apparent contradiction of "incomplete" measurements and "too much" information provided by a more complete measurement is resolved through he use of computer simulations. These simulations can provide a huge statistical sampling of possibilities which are distilled "on the fly" to provide the needed information.

This structural information is obtained by making use of some kind of model to interpret the experimental information. The model allows the organization of the huge amount of data in such a way that the underlying physical structure is explained and our understanding of the structure behind new sets of data enhanced. However, the conformations sampled by a polymer simulation are greatly affected by the way in which we integrate the analytical measurement of a non-equilibrium property such as orientation into the atomic-level description. The motivation of this thesis is to go to the heart of how we properly interpret these measurements to provide the most secure foundation for the structure-property relationships that build upon them.

1.2. Thesis Goals

The overarching theme of my thesis is the use of atomistic computer simulations to understand the structure and properties of non-equilibrium systems, particularly oriented amorphous polymer melts and glasses. My work targets three major research goals, which form the basis for publications and for individual chapters of my doctoral thesis, as well as a fourth that is a fundamental goal of any simulation work:

1. Representation of experimental non-equilibrium information.
2. Bridging atomic-molecular length scales.

3. Representation of inhomogeneous non-equilibrium systems.

4. Demonstration of ability to reproduce macroscopic observations

Below, I provide details to explain the connection among these goals and how they fit together to provide a significant contribution towards the project of understanding the nature of oriented macromolecular systems.

1.2.1. Representation of experimental non-equilibrium information.

The most fundamental goal of this research is to provide a framework for the interpretation of structural measurements of anisotropy. Ideally, we would like to provide the modeler with the least restrictive interpretation of the experiments. This allows the data to "speak for itself" and to give the modeler a fresh perspective on the problem of explaining the connection between structure and properties. The model-free interpretation has the benefit of helping the modeler avoid the pitfall of the incorporation of unnecessary variables, or worse, of incorporating a preconceived notion that is incompatible with the underlying structure.

In order to accomplish this goal, the method must: 1) provide an unambiguous methodology for the incorporation of an arbitrary experimental measurement; 2) provide insight into the microstructural details responsible for the experimental measurement. The success of both of these points is necessary to provide a useful link between the experimental measurements of structure and those of the properties of interest.

1.2.2. Bridging Atomistic-Molecular Length Scales.

The ability to interpret experimental techniques through the accomplishment of the first goal gives us a window into the local structure. The primary motive for

18

obtaining this insight into local structure is to further the understanding of how it affects the properties of industrially relevant macromolecules. To do this, one is faced with the task of making simulations of oligomers of hundreds of repeat units relevant to the configuration properties of polymers with tens, or hundreds, of thousands of repeat units. This can only be done through the determination of a proper coarse grain descriptor that "averages out" the details at the atomic level and describes the molecular level structure in a small number of parameters. Therefore, the second goal of this thesis is to provide a methodology that will facilitate the connection between the atomistic characteristics, which are accessible by simulation, and the molecular characteristics, which are only accessible through coarse graining of the atomistic) structural features.

1.2.3. Representation of inhomogeneous non-equilibrium systems.

The same feature of polymers that necessitates coarse graining, i.e., the huge span of time and length scales, has other consequences. One of these is that polymers relax to equilibrium more slowly as their length increases, because of the need for the relaxation to propagate from the ends of the chain to the center. In many cases, the time scale of the process will be of the same order as the relaxation. In these cases, it is often important to incorporate this tendency of the ends to loose their orientation more quickly than the center of the chain into molecular simulations so as to understand the development of mechanical and optical properties in oriented polymer systems. Therefore, the third goal is to provide the flexibility, when justified, to tailor the incorporation of experimental measurements to fit known underlying structural characteristics.

1.2.4. Demonstration of ability to reproduce macroscopic observations

Implicit in the goals of any computational model is that it reproduces experimental observations of the modeled system. The simulation of polymeric systems

inevitably requires making more substantial assumptions or simplifications than other atomic level simulations, because of the molecular size. Even with a "perfect" force field, one is not able to simulate the systems that we are interested in because of the limits of computational power. One must always decide "how large is large enough?" for polymer chains, so that the effects one sees are indicative of a system of much larger chains, and if they are not, "to what degree can they inform us about these larger systems?" There is always a tradeoff between ability to obtain results and the accuracy of those results. Therefore, a goal that encompasses the previous goals is to show that they reproduce aspects of experimental systems given the simulated polymer sizes. Because of the treatment of different polymers (polyethylene, polystyrene), different states (melt, glass), and quality of orientation (homogeneous, inhomogeneous), it is worthwhile to assess the strengths and limitations of the methodologies developed here side-by-side.

1.3. Thesis Organization

This section provides a brief outline of the following chapters of my thesis. The second chapter of this thesis provides a review of the literature concerning topics relevant to the understanding of the ideas developed in later chapters. This includes the discussion of analytical measurements, the inverse problem of obtaining the structure from these measurements, modeling orientation, and bridging length scales. Chapter 3 is dedicated to explaining in detail the theory and development of the Semi-Grand canonical ensemble Monte Carlo (SGMC) method as well as its practical application to describe oriented polyethylene melts on the basis of birefringence measurements. This chapter also contains more detail about the Maximum Entropy methods developed in the introduction and important characteristics that carry over to the SGMC simulations. Chapter 4 uses the information available from the techniques of the previous chapter to develop the mapping of the anisotropic structure of oligomeric simulations to the macromolecular scale anisotropic conformation properties. This chapter also

demonstrates the ability to use molecular scale conformation properties to derive the most likely local degree of anisotropy. Chapter 5 details the way in which the oriented polymers produced using the SGMC methodology can be extended to systems with inhomogeneous orientation. The specific case of calculating the tensile modulus of homogeneously and inhomogeneously oriented glassy polystyrene is provided. Chapter 6 augments the conclusions of previous chapters by linking together body of work and by evaluating the degree to which the thesis goals are satisfied. In this chapter I also highlight the most important contributions and how I believe these can be best exploited in future research.

Chapter 2

State of the Art

2.1. Orientation in dense polymer systems

2.1.1. Introduction

The ubiquitous use of polymeric materials is a consequence of their versatility; their high viscosity as melts and solutions allows them to be easily processed into materials that have a wide variety of optical and mechanical properties. This processabilty is the result of the definitive polymeric characteristic - the connectivity of macromolecular chains. By orienting the chains of atoms of the polymer molecules, we can produce materials with properties much different than those of the isotropic material, despite an identical chemical composition. Because of the molecular connectivity, the optical, and especially mechanical, properties along the chain are different from those transverse to the chain. Consequently, any residual orientation from processing, intentional or not, has predictable qualitative effects.

The orientation of the polymer molecules is the primary source of mechanical strength in fibers, of which more than 30 million tons are produced annually worldwide through processes of melt spinning, wet spinning, and dry spinning[1]. Mechanical and optical properties are modified through other processes, such as extrusion, rolling, and roll-drawing to create axial or biaxial orientation, and a significant increase in the modulus and strength in the direction of orientation[2]. Ward[3] provides an excellent

survey of the fundamental concepts involved in understanding the structure-property relationships of oriented polymers.

By adjusting processing conditions, such as temperature, molecular weight, spin line stress, or flow rate, the quality of the orientation and resulting macromolecular properties can be controlled. The tensile strength and other mechanical properties increase with orientation, but it must not be overlooked that the term 'orientation' encompasses a spectrum of qualitatively different structural possibilities. Polymer studies have consistently shown different qualities of orientation can have a measurably different impact on the mechanical properties[3].

While orientation of any quality will tend to produce the intuitively expected increase in tensile properties, it is only through careful definition of orientation, and interpretation of experimental measures of specific types of orientation, that we can analyze and explain macroscopic mechanical properties. Important considerations include the length scale over which the orientation occurs, as well as the distribution of the orientation. This is particularly relevant to the interpretation of the experimental results from analytical techniques for measuring orientation; the measurements listed below may probe different length scales, provide different information about the distribution of orientation, or both. Additionally, it is important to recognize that these measurements do not allow the definitive measurement of the full distribution of the orientation. We are always left with a multiplicity of possible distributions that are consistent with any measures of orientation, making the task of assessing the quantitative relationship between orientation and properties even more difficult; it is possible for different distributions of orientation to produce the same measured value of orientation in any given experimental determination, but to have observable differences in their mechanical properties[4].

Orientation in polymer systems in a preferred direction, at any length scale, is indicative of a *non-equilibrium* state. Although the resulting states of the polymer can be extremely long-lived, especially at or below the glass transition temperature T_g where the largest time constants become effectively infinite, they are nonetheless non-equilibrium states. Polymer processing near T_g inevitably leads to the occurrence of non-equilibrium

23

states, because the longest time scales involved in the relaxation of orientation are on the order of seconds or larger. In many polymer processes, such as fiber drawing or fiber spinning, this is advantageous because it allows the creation of highly oriented (i.e., highly non-equilibrium) polymer materials; in other cases, such as injection molding, one may prefer to avoid running near T_g to promote the relaxation of orientation at the time of cooling to provide uniform properties. Therefore, an understanding of how orientation develops, and how it dissipates, is important to all categories of processes because of the impact of orientation on the resulting properties.

2.1.2. Structure-Property-Process

While there has been relative success in the ability to describe the evolution of macroscopic flow properties, i.e., velocity and pressure, in the modeling of polymer processes, the ability to similarly model the evolution of the orientation is much more elusive, due to the visco-elastic nature of polymeric systems[5]. The triangle of relationships shown in figure 1 represents a standard conceptual framework for the understanding of materials. Importantly, without the understanding of the polymeric microstructure the link between process and property is simply one of empirical relationships and gives only a general conception of how to improve properties. Clearly orientation is an important feature of the structure, and is crucial to the understanding of the link between process and property.
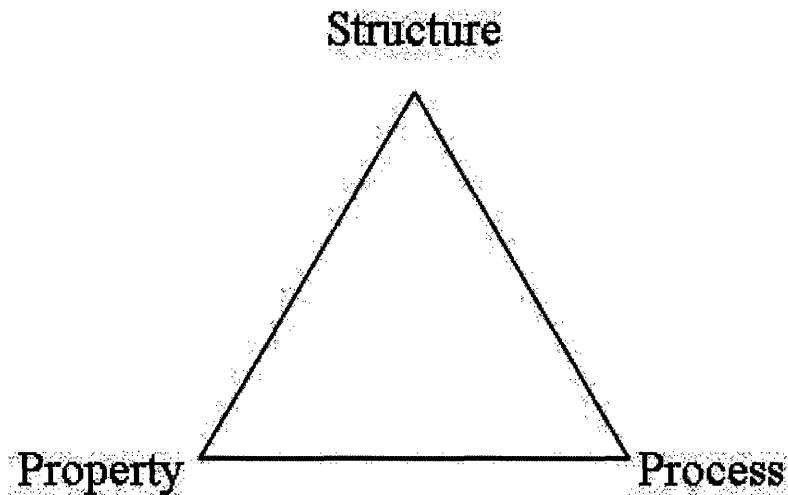
Figure 2.1. Process-property-structure triangle

A hidden, but crucial, piece of this process-property-structure triangle is the basis upon which we can claim to know the structure. A process can be controlled, and a property measured, each to a high degree of accuracy, because these are well defined by a small number of macroscopic features (temperature, flow rate, tensile strength, etc.). However, the complexity of a non-crystalline oriented structure cannot be similarly described by a consistent set of macroscopic parameters, since all non-equilibrium structures will be out of equilibrium in their own manner. The ability to gain an understanding of the relationship among structure, process and properties requires that we measure and interpret the structure of polymers for each of these non-equilibrium situations using a variety of analytical techniques. Since each analytical technique probes the microscopic structure of a material in a very specific way, distilling the complex arrangement of atoms into a modest number of macroscopic values that are particular to that technique, no analytical technique can individually define the structure. Even together, these techniques cannot unambiguously define the structure, but rather simply limit the range of possibility.

Because of this, the structure must be inferred to some degree. Here, the term 'structure' encompasses the correlations of the positions, orientations, etc., of atomic sites of a given system, with the other sites. For a completely amorphous atomic system, the

25

structure consists only of the nearest-neighbor distances, and the knowledge of the positions of neighboring sites is very limited. In contrast, the maximum amount of structure is realized by a crystal, for which the knowledge of one or a few sites that make up the "asymmetric unit" provides the knowledge of the position of all of the other sites in the system through specified symmetry operators.

It is not always appreciated that the investigator who wishes to explain the observed mechanical and/or optical behavior of complex material, such as polymers, must fill in the blanks left by experimental measurements of the structure. It is precisely during the process of filling in these blanks that the scientist must be careful not to incorporate a model or structural interpretation that is not clearly indicated by the experimental measurements of the system at hand, or by verifiable prior knowledge.

In this spirit, a more accurate conception of the structure-process-property triangle would be the process-derived property-structural measurement triangle shown in figure 2.2. This conceptual framework has the benefit of emphasizing that the structure is a complex quality that must be deciphered, rather than a readily available value that can be parameterized and correlated with the derived properties. It makes explicit the need to quantify specific structural changes in terms of the most adequate observable measurements in order to understand the underlying relationships. Without the ability to infer microscopic configuration features, especially those that may not be explicit in the measurements, we cannot gain the insight needed to extend these measurements to a general understanding of the relationship between structure and properties. This understanding is a necessary condition for computational modeling to reach its full potential as a tool to develop novel materials, and to extend the use of existing polymers, to meet the demand for increasingly specialized high-performance materials.

Structure
Measurement
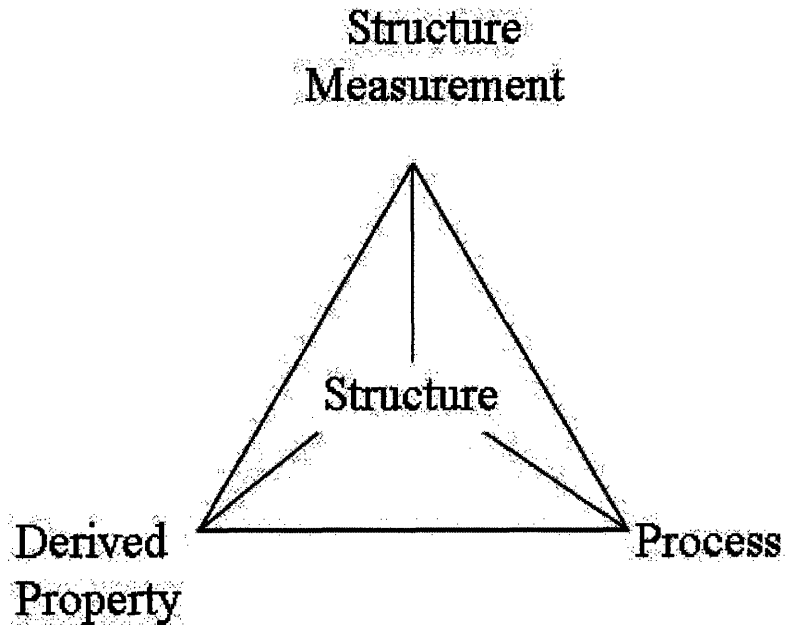
Figure 2.2. Modified process-property-structure triangle

2.1.2.1 Orientation-Induced Crystallization

In addition to the direct influence of orientation on the mechanical properties, orientation in the melt phase also influences these properties through the acceleration of the development of crystalline domains in stereo-regular polymers, including PE. In these polymers, orientation-induced crystallization occurs in the production of fibers, and consequently increases the tensile mechanical properties through an increase in the crystallinity[6]. A review of recent advances in the coupling of crystallization with the processing conditions of polymer melts is provided by[7]. Recent studies have also highlighted the importance of domains of high orientation in amorphous melts to the process of crystallization, proposing a spinodal decomposition of the melt into dense nematic domains, and less dense amorphous domains[8,9]. A similar explanation is used to account for the mesomorphic nanostructure observed to precede the formation of the crystalline domains in oriented polyethylene[10].

27

In semi-crystalline polymers, the mechanical and optical properties will be a mixture of those of the crystalline and the amorphous domains. Therefore it is also often important to independently evaluate the properties of the amorphous oriented polymer, which are distinct from the crystalline properties, because they can contribute significantly to the mechanical properties of the system[11]. Janzen[12] has carried out a parameterization of such properties using data available from several other studies of the properties of semi-crystaline PE. More recent studies have used atomistic modeling to investigate the non-crystalline and inter-phase regions in order to understand the connection between microstructure of semi-crystalline polymers and their observed properties[13].

2.2. Methods of Measurement

The methods of measuring orientation cover a wide range of length scales; some experimental techniques measure the orientation of atomic bonds while other techniques measure the macromolecular orientation, or even the orientation of morphological features. These techniques can also be characterized by their suitability for non-destructive in-line process measurements; of the techniques listed below, the techniques most readily applicable to these measurements are birefringence, IR, and Raman measurements[14]. The ability of these techniques to collect data on the same time scale as the processes of interest (~seconds) allows the direct measurement of the dynamic processes as a series of state points, whose relative structural characteristics can be used to elucidate the underlying processes. A more comprehensive assessment of the characterization of orientation through analytical techniques is provided by Cole and Ajji[15].

2.2.1. Birefringence

The refractive index of a material is proportional to its polarizability, taking on distinct values along and perpendicular to, the backbone of a polymer chain. Since the direction of the chains is random in an isotropic material, the overall refractive index is independent of the direction. However, if the polymer chain is oriented, the refractive index along the orientation direction will reflect the unequal contributions of the polarizable units. Since the contribution of monomer units to the birefringence is assumed to be additive, we can easily obtain the 2nd Legendre coefficient of segment orientation. Empirically, the ratio of normal stress difference to birefringence is constant at low values of stress (stress-optical rule), so the birefringence can be used to estimate the stress. Birefringence studies are practical on-line measurements for typical industrial applications[16, 17] in order to assess the orientation. The birefringence is often correlated with the development of mechanical properties[18, 19], although, as noted earlier this represents a simplification of the relationship between structure and properties.

2.2.2. Infrared Spectroscopy

Through the use of IR Dichroism, one can theoretically obtain more information about the orientation of the local polarizable unit than is possible through birefringence through a measurement of the angular dependence of absorbance. This is because the IR absorbance due to individual bonds, or groups of bonds, will occur at specific frequencies, which can be analyzed separately. As a consequence, this technique also requires an accurate knowledge of the transition moments in order to accurately interpret the orientation of a chain segment in terms of the orientation of these groups. Such studies have evaluated the orientation of PET, PE, and polyimides[20-22], as well as the orientation of semi-crystalline PE[23] and the orientation of amorphous chains during necking of polypropylene[24]. In off-line measurements of solid materials, IR can be used to investigate the orientation of specific layers of a solid polymer through successive

exposure and polishing through the use of surface reflectance[25]. Diffuse reflectance techniques also interact only with the surface and can be employed to avoid the limitations of transmission IR techniques applied to thick (>1cm) samples[26]. One of the weaknesses of this method is the tendency for overlap in the spectra, making it more difficult to resolve the individual intensities.

2.2.3. Raman Spectroscopy

Raman spectroscopy activates a different set of vibrational motions than does IR and is therefore complementary. Also, since Raman is a scattering technique, it is not sensitive to the thickness of the sample, as is IR. Polarized Raman spectroscopy can be used to evaluate the local orientation of the polarizable units of the polymer chain in terms of the 2nd and 4th moments of the orientation distribution function[27, 28]. This technique has been used in the analysis of many polymers including PE, PP, and nylon[29]. Changes in the vibration frequency have also been used to understand the nature of stress on the orientation of the polymer, where it is shown that the backbone vibrations are predominantly affected by the stress[30].

2.2.4. NMR

Nuclear magnetic resonance (NMR) spectroscopy is useful for the evaluation of the conformational properties of polymers because of its sensitivity of the magnetic interactions of the atomic nuclei to changes in these structural features[31]. Multi-dimensional NMR techniques allow the determination of further details of the conformations to be determined, as described by Schmidt-Rohr[32]. Analysis of oriented melt systems is accomplished by rapid quenching of the sample at a specified process condition. This technique has been applied to polystyrene samples oriented using different shear rates and different quench times to track their relaxation dynamics[33]. By

using NMR techniques such as DECODER-NMR, a very comprehensive assessment of the orientation distribution of the moieties of the polymer chain (up to the 14th moment) can be obtained[34]. Such accuracy removes much of the uncertainty of the nature of the local orientation inherent in the previously described techniques. A recent study by Wendlandt, et al.[35] gives a very comprehensive description of the procedure for determining orientation from NMR measurements. The main drawback of NMR is the required sample preparation and length of analyses, which precludes its use as a real-time diagnostic for polymer processing and limits its accuracy in the analysis of dynamic processes.

2.2.5. Neutron Scattering

Neutron scattering is extremely useful because it is the only means for evaluating the radius of gyration of molecules in dense melt systems[36]. One of the limitations of this technique is that real-time experiments are difficult for melt systems. As with NMR, melt systems are typically analyzed in the solid state, with the analysis taking into account the relaxation time preceding the quenching of the system. Small angle neutron scattering (SANS) has been used to measure the orientation of sheared polystyrene melts by Muller and coworkers[37, 38]. These studies took advantage of the ability of the range of scattering vectors to probe the orientation at different length scales to show the dependence of orientation on length scale in the shear plane. Another study aimed at an understanding of the dynamics of relaxation and orientation using SANS[39] showed that the orientation at the different length scales was not modified uniformly with changes in the processing conditions. This highlights the complexity of the orientation and the need for both the local and molecular orientation to characterize polymer systems.

2.2.6. WAXS/SAXS

X-ray studies are typically performed to assess the size and orientation of crystalline domains of polymer systems[40]. Like SANS, these X-ray techniques can assess structural features over a range of length scales. While the measurement of crystalline features of the polymer systems is not directly applicable to the scope of this thesis, characterization of the amorphous region of semi-crystalline polymers is often carried out through assessment of the component of the X-ray scattering that is not accounted for by the crystalline domains[41, 42]. These techniques are also useful for the time-resolved evolution of orientation-induced crystallinity and have been used to investigate the meso- and macroscale structure in isotactic polystyrene[43] and in isotactic polypropylene[44, 45].

2.2.7. Combination of Techniques

The recognition of the need for more comprehensive measurement of polymer systems is reflected in a number of recent studies. Combinations of these techniques have been increasingly used to obtain more comprehensive (off-line) assessments of the polymer structure. Such studies have included the Raman/X-ray studies of polypropylene[46], birefringence/X-ray studies of polyethylene and polypropylene[47], and SAXS/IR studies of polyurethane[48]. Birefringence has also been used in conjunction with optical microscopy to link morphology with the local orientation[49]. A recent development that is of particular interest has been the development by Bent and coworkers[50] of a flow cell for carrying out simultaneous measurements of SANS and birefringence on polystyrene. Similarly, a shear cell has been developed by Kumaraswamy, et al.[51] to allow visible and IR polarimetry in conjunction with light and x-ray scattering studies. The common thread of these studies is the recognition that orientation is most meaningful when we can provide a description that is grounded in mesoscopic, or molecular, orientation as well as the bond-level orientation.

2.3. Orientation as an Inverse Problem

2.3.1. Formulation of the Inverse Problem

The measurements enumerated above represent the starting point for a statistical mechanical description of a polymer system. Although these measurements can reveal important facets of the system, they do not represent an exhaustive catalogue of the interatomic correlations. Because the microscopic features cannot be comprehensively measured, we must infer them from the experimental measurements. The determination of the appropriate set of chain conformations that accounts for a given measurement belongs to a general class of problems called "Inverse Problems"[52]. Out of the countless ways in which configurations can combine to produce a particular result, we require a methodology that guides us to the best choice. For all but the simplest of problems, this is an iterative procedure that uses the limited knowledge of the energetic landscape to guide us to a representative set of conformations that describes the experiment.

Most of the analytical techniques described above provide us with a small number of moments of the orientation distribution function (odf) of the polymer chain at some length scale. The most commonly used orientation order parameter is the 2nd Legendre coefficient, $P_2(\cos\theta)= \frac{1}{2}(3\cos^2\theta-1)$, of the angle θ of the structural unit with respect to the primary axis of orientation. This is also referred to as the Herman's parameter and is common to all of the techniques. Higher order Legendre coefficients successively refine the underlying orientation distribution. For a centrosymmetric system, the odd moments of the orientation distribution vanish. Therefore, we are typically faced with the problem of obtaining a complete odf from the knowledge of the first n even Legendre terms $P_2(\cos\theta)$, $P_4(\cos\theta)$, ... , $P_{2n}(\cos\theta)$.

The importance of determining these higher moments of the odf arises from the recognition that a one-to-one correspondence between the experimental measurements and the properties of interest is only possible if the higher moments can be ignored. The

33

importance of the higher moments is not known *prima facie* and can only be assessed in a retrospective assessment of their effect on the properties of interest. As is typical for an inverse problem, our knowledge of the system is not sufficient to obtain a unique orientation distribution. Therefore, we must introduce some criteria for the solution, or chose other means of closure, to determine the most appropriate odf.

2.3.2. Solution of the Inverse Problem using Maximum Entropy

Closure to this structural inverse problem can be achieved by associating the "best" choice with the one that incorporates the minimum possible amount of additional information. The solution is thus given by the variational minimization of a cost function (maximization of entropy or equivalently minimization of information) through the method of Lagrange multipliers. Entropy is the most adequate cost function when our knowledge consists of a signal (experimental result) and no knowledge of the underlying detail (molecular structure). This procedure is known as the maximum entropy (ME) method and is attributed to Jaynes[53], although he himself credited JW Gibbs with using this same principle[54].

Maximum entropy (ME) methods allow the use of experimental information about a system, e.g. one of the moments of its distribution, to infer the most likely underlying distribution. This allows the objective interpretation of data, and ensures that no bias in the distribution is unintentionally included. Martyushev and Seleznev provide a comprehensive review of the application of ME methods as applied to the solution of non-equilibrium systems, and describe how the evolution of these systems is guided by the principles of maximum entropy generation[55]. An important feature of this method is that the entropy cost function is concave irrespective of the properties of the underlying distribution[56]. Therefore the maximization of entropy always provides us with a unique answer, which is justified as the most likely ensemble of orientations that accounts for the empirical observations.

Examples of the reconstruction of a distribution from limited number of moments, without explicitly considering the underlying molecular constraints, is given by Rodriguez, et al.[57] in which the Legendre polynomials through $P_4(\cos\theta)$ obtained from NMR are used to calculate the orientation distribution for a non-centrosymmetric rod-like azobenzene polymer. The application of ME has also been used to determine the orientation of proteins, from a more comprehensive measurement of the orientations of protein subunits[58]. The flexibility of the application of ME methods is displayed in a series of articles by Poland[59, 60] in which ME methods were used to reproduce distributions of energy, enthalpy, and end-to-end distance for polymer systems.

These studies highlight the benefits, as well as the potential difficulties, of using ME methods to analyze experimental data. ME methods provide a unique determination of the orientation (or energy, enthalpy, end-to-end distance) distribution of the relevant elements of the system, even though it contains no model with which to (possibly improperly) interpret the meaning of the measurements. The method can also be used for the subsequent development of a model since it will highlight exactly those aspects of the system that need to be more highly constrained.

ME methods however can be sensitive to the measurements (constraints) used to calculate the distributions. Measurements that provide redundant data (non-orthogonality) impede the ability of this method to work effectively. Although enforcing the orthogonality of the measurements is the best approach to resolving redundancies[61], van der Heide was able to obtain results using a "figure of merit" to bias the solution in favor of the most reliable measurements. However, this strategy has the pitfall of introducing a non-thermodynamic component to the description and jeopardizing the objectivity of the analysis, as described below for RMC. Another requirement of an effective ME analysis is that the measurements correspond with the primary axes of orientation to effectively capture the orientation moments. This is not typically a problem with orientation, since the orientation axis of a process is usually apparent.

35

2.3.2.1. Quantitative Comparison of ME Solutions

Finally, the ME methods allows a quantitative measure of the entropy of one particular distribution relative to another. The entropy is proportional to the thermodynamic potential, and thus the difference between two different conditions can be quantified in terms of the minimum amount of work required to move the system from one state to the other. However, by leaving out the microstructural details, the solution obtained using ME may not accurately reflect either the odf or the change in energy to reach the odf. By definition, the underlying odf cannot be broader than the ME solution. Therefore, one can potentially obtain a ME odf that under-represents highly oriented states ($P_2(\cos\theta) \approx 1$), resulting in overly broad distributions that understate the mechanical properties of polymers. This is a result of the non-linearity of the mechanical tensile properties, which are often marked by extremely high values at complete orientation. Other inverse methods discussed below retain the microstructural forces as part of the acceptance criteria for appropriate polymer configurations, and are less susceptible to this problem.

2.3.3. Solution of the Inverse Problem using Reverse Monte Carlo

Reverse Monte Carlo (RMC) was introduced in 1988 by McGreevy and Pusztai[62]. Since that time, the method has produced many useful contributions to the interpretation of structural measurements, especially in the interpretation of diffraction experiments[63]. Similar to the ME methods, one attempts to reproduce experimental data by appropriately constraining the system. Often RMC will include information about the microscopic interactions through the inclusion of a classical force field. However, in other respects the link to thermodynamics is broken because the experimental uncertainty of the data is equated with the variance of the underlying system, usurping the thermodynamic role of temperature. This is apparent from the form of the modified Hamiltonian, in which the goodness of fit (chi squared) contributes to the thermodynamic

potential, proportional to a modeler-selected constant. The modeler is therefore responsible for subjectively adjusting the fluctuations, and hence the thermodynamics, of the system.

In its defense, RMC was formulated in large part to provide fitting to the positions of atoms in a crystallographic lattice and has often provided satisfactory solutions without the iteration necessary for the ME method. Since one is accustomed to thinking of the movement of atoms from their sites in terms of springs, a quadratic potential, where the user-selected constant acts as a spring constant, can be a reasonable approach. However, in cases such as orientation, the system descriptor tends to be broadly distributed, making more doubtful that a Gaussian-like distribution around the average value is appropriate.

2.3.4. Solution of the Inverse Problem using Potential of Mean Force

Other techniques can be broadly categorized as potential of mean force (pmf) methods. The grouping of these methods under a single category follows that used in a recent article by Tóth and Baranyai[64], which analyzed the relative merits of these methods and RMC methods. The prototypical pmf problem is that of determining the Lennard-Jones potential of interacting spheres so as to reproduce some set of experimental data, typically a pair correlation function g(r). An early method for the determination of pair potentials from g(r) is the method of Schommers[65]. The pair potentials obtained using the Schommers method were later shown to be as good as, or better than, the potentials obtained from other methods[66]. Characteristics of Schommer's "self-consistent method" are evident in the more recently developed pmf methods.

Many of these methods make use of the ideas presented by Lyubartsev and Laaksonen[67]. They set forth a method for evaluating the adequacy of a potential through the numerical estimation of the second derivatives of the potential with respect to the interparticle positions. This evaluation serves, through a matrix inversion, as the iterative change in the potential in order to match the experimental data. The efforts in our

research group, which have aimed to model experimental data in a way that maintains thermodynamic consistency, fall into this category of methods.

Rutledge[68] systematized this approach as the semi-grand canonical Monte Carlo (SGMC) method. The contribution of this paper was to clarify the manner in which experimental data could be added to a canonical Monte Carlo NVT simulation. Using this methodology, a two-body potential was reproduced for a Lennard-Jones fluid given g(r). This approach was extended through the application to partial pair correlation functions by Bathe and Rutledge[69], where this method reproduced not only the structural characteristics but also the thermodynamic characteristics of an idealized protein system. Colhoun applied this method to describe the configurational states of PS during relaxation of orientation[70]. However, in this case an RIS model of polystyrene was used to reproduce the orientations obtained from quenching after shearing and various relaxation times. Because of this, the model did not fully account for the interactions of a dense melt or glassy system, and the orientation of the polystyrene was not connected to the thermodynamics of the system.

The EPSR method of Soper[71] refines the structure through the addition of a higher order interaction term to provide a fit to the data. The inclusion of a higher order term differentiates it from the other pmf methods included in this section. While the inclusion of the higher order terms has been successful at reproducing the structure, it has been noted by Soper that the values of these terms is very sensitive to the other assumptions about the force field.

One of the advantages of these pmf calculations is that the potential determined from these calculations can then be applied to the system to understand hidden or unmeasured aspects of the system with a justification of thermodynamic consistency. Using the evaluation of the pmf for these two-body forces, one can always arrive at a unique answer[72]. Thus, other than the three-body modifications that can be applied using EPSR, the calculated potentials objectively represent the "best" solutions to the presented inverse problem. These solutions can then be justifiably applied to a variety of other analyses including further simulations that can investigate the corresponding dynamic properties.

2.4. Effects of Polymer Dynamics

Implicit up to this point in the discussion of the computational modeling of oriented polymer systems is the assumption that orientation is homogeneous. This however, is often not the case. The very fact that we describe these simulations as 'non-equilibrium' means that if the process does not allow sufficient time to reach steady-state, polymer dynamics will play a role in the distribution of orientation along the polymer chain. This is particularly true for the process of disorientation upon cessation of the orienting force. Therefore, some background is necessary to appreciate the potential difficulty added by polymer dynamics to an already imposing problem.

Since the introduction by de Gennes of the reptation model[73], and further development of this concept by Doi and Edwards (Doi-Edwards model)[74], the idea of a polymer molecule in a dense system as being constrained in a tube defined by its neighboring chains is well accepted. Due to the nature of the tube constraints, the basic DE model consists of three characteristic times related to the motion of the polymer chain. The characteristic times $\tau_e < \tau_r < \tau_d$ represent respectively: the time for the polymer to relax between entanglements within the tube; the time for the relaxation of the contour length of the polymer chain within the tube; the time for disengagement of the chain from the tube. The DE model has been further developed to resolve discrepancies with experimental results, such as the scaling of the viscosity with molecular weight. Additional relaxation processes such as contour length fluctuations and tube reorganization, have allowed the DE model to better accord with experimental data while retaining its basic features.

The complexity of the flow behavior of polymers is a direct result of the dynamics of polymer chains characterized by τ_e, τ_r, and τ_d. These time scales, and their corresponding length scales can span several orders of magnitude. Thus, it is not surprising that the measurement of non-equilibrium states of polymers must often incorporate this dynamical behavior. Recent studies have shown how these dynamics

prevent the birefringence from being an adequate predictor of mechanical properties without considering the processing history. For example, Embry et al. showed how highly drawn samples, which had relaxed to low levels of orientation as measured by birefringence, still showed anisotropic fracture characteristics. The explanation of this phenomenon rests on a nonlinear DE tube model[75]. Previously, one of the researchers involved in the above-cited study found that a similar explanation accounted for the variability of the Young's modulus in drawn PS[4]. In each case, the highly drawn samples, after relaxation, retain some "memory" of the orientation. This is manifested in macroscopic physical properties that exhibit more anisotropy in their mechanical properties than is observed in systems that have the same orientation, but were not highly drawn.

Studies continue to explore the nature of the discrepancies of the DE model with experiments and to understand the nature of the relaxation dynamics of polymer systems. Among these, Walczak and Wool[76] have analyzed the behavior of PS with labeled chain ends to analyze the relaxation of orientation and to verify the importance of chain fluctuation to the relaxation dynamics. It is also important to note that the understanding of the initial dynamics of the oriented chains is not completely understood and is still the subject of investigation[77]. This study of the initial dynamics is made more difficult by the fact that one can only approximate the conditions of step-strain, which provide affine deformation at all length scales necessary to provide a uniformly oriented system[74].

2.5 Modeling of Polymer Process-Property-Structure

2.5.1 Parameterization of Properties

There has been a considerable effort to parameterize the relationship between optical and mechanical properties of polymers and the processing conditions. Bicerano makes a useful distinction between "fundamental properties" and "derived properties"[78]. Whereas the fundamental properties arise from the basic atomic nature of the polymer,

40

i.e. the force field interactions, the derived properties are "complex manifestations" of these fundamental properties. Applied to oriented polymers, these are reflected in properties that do not change with orientation (fundamental properties), versus those that do change (derived properties).

Parameterizing the mechanical or optical properties can give us a feel for the sensitivity of the polymer structure to processing effects on orientation[79], and is tremendously useful for the processing of commodity materials. However, it is only through the understanding of the micromechanical origins of the observed changes in the derived properties that we can hope to reliably predict the properties of existing, or more importantly, possible new polymeric materials.

2.5.2 Aggregate Model

An early step towards understanding the nature of orientation through modeling was the Single-Phase Aggregate Model of Ward[80]. This description of polymer orientation was formulated using the assumption that the mechanical properties are dependent only on the orientation of non-interacting units, whose contributions are additive. In the terms defined above, these units are assumed to contribute in an additive fashion to the same derived properties based solely on their orientation. Thus, the derived properties of a fully aligned polymer system coincide with those of a fully aligned unit of the macroscopic aggregate. A consequence of the orientational symmetry for uniaxial systems is that only the first two moments of the distribution of the non-interacting units are needed to fully specify the mechanical properties.

Therefore one would be able to form a one-to-one correspondence of the mechanical properties and orientation as measured by local probes, such as polarized Raman spectroscopy. This model is fairly successful at describing polymers such as LDPE, Nylon and PET[81]. However, polymers including HDPE and polypropylene do not follow this model, presumably because of the degree of interactions, which render the non-interactive nature of the Aggregate model less realistic[82]. These results indicate that

41

there is a significant degree of cooperative behavior, which requires a model incorporating the anisotropic interactions of the fundamental properties of the polymer.

2.5.3. Atomistic Modeling of Properties

With current computational power, the most fundamental level at which dense amorphous polymer systems can be investigated is at the atomic level. Atomic-level simulations use the fundamental properties defined by an empirical force field to predict of the derived properties that result from an imposed microstructure. This strategy has successfully reproduced correlations in the orientations of neighboring chains, and the appearance of ordered domains as revealed by experimental WAXS/SAXS measurements[83]. MC simulations of Yong[84] further underscore the importance of understanding the atomic level interactions by showing that excluded volume effects and chain packing are heterogeneous and are important considerations in the modeling of orientation.

The atomistic modeling of oriented polymers can proceed using Monte Carlo (MC) methods or through the use of molecular dynamics (MD). Although knowledge of MC methods is sufficient to understand the subsequent chapters, a brief review of MD is also given to help understand its limitations for modeling polymer orientation. For both types of simulations, the ability to reproduce the stress-optical behavior, as determined from the change in birefringence for a given deviatoric stress, provides a validation of results. The verification of this relationship rests on the ability to sample atomistic conformations in order to calculate the stress through the virial relationship, and the birefringence through the polarizability tensor. MC studies that evaluate the stress-optical relationship have been performed by Mavrantzas and Theodorou for polyethylene[85, 86] and by Cail, et al, for PET[87].

Modeling at the atomic level allows the detailed assessment of the oriented microstructure relating to a set of conditions, which may be unobtainable in the laboratory. This ability is particularly useful for the analysis of semi-crystalline polymers

such as polyethylene, as described above, where isolation of the contribution of each of the phases is not feasible in the laboratory.

2.5.4. Monte Carlo Modeling

Since the development of the Metropolis algorithm[88] the growth in the application of MC methods has relied more on the development of innovative algorithms than by increase of computing power[89]. One important development for polymer simulation was the introduction of variable connectivity moves[90], which allow the rapid equilibration of internal segments of polyethylene chains, and has provided the means for equilibration of atomistic PE chains of up to C_{6000}[91]. The advantage of MC modeling is that we are able to make short cuts, through unphysical moves, to the non-equilibrium state point of a system. This is useful for the exploration of steady-state non-equilibrium state points, whose orientation is well described by a small number of orientation descriptors. This is especially true for state points that lie far from equilibrium and are not easily reached using MD simulations.

Mavrantzas and coworkers have provided the most relevant set of MC studies for oriented polymer melts[85, 86, 92, 93]. Their approach is similar to the potential of mean force calculations discussed above in that the choice of variables provides a thermodynamically consistent description of the system. Although the particulars of the methodology differed over this set of papers, their choice of descriptor for the orientation was based on the average conformation tensor <QQ>, consistent with macroscopic rheological equations of state.

These studies by Mavrantzas and coworkers were carried out for polyethylene chains of lengths from C_{24} to C_{1000}. The connection to macroscopically observed quantities was made through the birefringence of these oriented chains. This set of studies also provided results on the relationship between molecular ordering and properties including local orientation, stress-optical behavior, and the nature of the free energy changes. The last paper in this series[93] incorporated the GENERIC formalism as

43

developed by Ottinger[94]. The GENERIC formalism is specifically designed to describe a thermodynamically admissible evolution of any system in terms of the effects on energy and entropy, defined respectively by reversible and dissipative matrices. The results of the polymer simulations were interpreted in terms of homogeneous time-independent systems, even though the GENERIC framework provides the basis for obtaining the time evolution to reach a non-equilibrium state defined by a particular potential. Thus, the GENERIC model contains the potential for more extensive application to polymer systems. However, despite the rigor of the approach, or perhaps because of it, there is a serious limitation in the ability with which one can simulate polymer systems of realistic size; continuing with the conformation tensor as the "coarse grain descriptor", one would be faced with impossibly large simulations in order to evaluate industrially relevant polymer systems.

In its application to polymer melts by Mavrantzas and coworkers, the GENERIC model has similarities to the SGMC methodology. The current state of atomistic modeling using the SGMC methodology as well as a comparison with the GENERIC model is presented in Chapter 3.

2.5.5. Molecular Dynamics Modeling

Molecular Dynamics modeling is more intuitive than Monte Carlo; a molecular dynamics simulation proceeds according to Newton's laws of motion. As a consequence of the explicit representation of time, MD simulations can be used for the calculation of dynamical properties. However, in order to produce orientation in a polymer system, the strain rates involved in MD simulations are orders of magnitude beyond what is experimentally possible, due to the small time steps that can be accommodated by the simulation. This can result in conformations that are not representative of those found in experimental results. This was noted in MD studies of poly(vinyl phenol)[95] in which the side chains felt an unrealistic amount of stress, creating high energy states in which the side groups were oriented in the flow direction. Additionally, the time scale of the

44

simulations does not allow the incorporation of the relaxation of the polymer chain ends predicted by the DE model. Nevertheless, these studies can often reproduce the derived mechanical properties of polymers, as is the case with polystyrene by Lyulin[96] and of PE by Yashiro[97]. Other MD studies have modeled dynamic behavior not accessible by MC simulations, such as the polymer crystallization of PE[98-101].

2.6. Scale-Bridging

Because of the huge number of degrees of freedom, atomistic simulations of polymers are limited to a direct description of small systems and/or short time scales. In order to allow the results of these atomistic simulations to inform studies of macroscopically observable phenomena, they must be connected to simplified models, which are capable of accessing larger size and time scales. Considerable progress has been made in the ability to link different scales through 'hierarchical' modeling[102, 103]. An overview of recently developed computational methods for linking atomistic simulations to the predictions of thermal, mechanical, and rheological properties is given by Theodorou[104]. The successful coarse graining of a polymer model allows degrees of freedom that are not directly relevant to the properties under investigation, to be averaged and removed from the simulation. Obviously, coarse grain models that are adequate for the description of one polymer characteristic may not be adequate to describe another. With this in mind, the coarse graining described below represents methodologies that are relevant to the simulation of oriented polymer systems.

2.6.1. Coarse-graining RIS

Much of polymer theory has been developed using the recognition that, at some macroscopic level, polymers have general characteristics that do not depend on their specific chemical nature. This commonality underlies the derivation of scaling laws by

de Gennes[72] through the application of statistical segments that act as links in a freely jointed chain. In this way, the unique chemical interactions of a polymer system are contained in the nature of these links.

One strategy for connecting the local chain properties with macroscopic conformation properties is by applying the Rotational Isomeric States (RIS) model[105]. The RIS model ignores the explicit interactions among chains and reduces the possible conformations to a large, but finite, number of possibilities. Cail and coworkers used RIS models of PE and PET to investigate their orientation behavior[106]. They studied the stress-strain and the birefringence-strain data and found that these simulations were not successful at representing the mechanical and optical responses simultaneously. This same group has also made use of the scale invariance arguments to coarse grain using local measurements of orientation (NMR and birefringence) for polyethylene networks[107], while noting that the properties determined in this fashion are order-of-magnitude because they ignore higher moments of orientation. These difficulties are symptomatic of the problem of developing a broadly applicable coarse grain model.

2.6.2. Coarse graining, Bead-spring

Another typical approach to coarse graining is the use of bead-spring models, for which the specific spring constants, equilibrium distances, and intermolecular forces represent the specific chemical characteristics[108]. While this approach requires a significant investment to determine the coarse grained positions and potentials, the procedure has been systematized in order to facilitate these coarse grained analyses[109]. The resulting coarse grain models allow the simulation of realistic-size polymer chains.

There has been a significant development of the use of these bead-spring models to provide closure to macroscopic fluid dynamics equations[110]. These "micro-macro" approaches utilize a multi-scale approach in which mesoscopic simulations and a coarse-grained microscopic bead-spring simulation pass information back-and-forth. The coarse grained microscopic model assumes the role of the constitutive model needed in order to

46

provide closure to the macroscopic governing equations. Similar to the GENERIC framework, the conformation tensor can be connected with the deviatoric stress to provide a link with the processing conditions. In this case however the model is not atomistic, and so sacrifices a level of detail to provide the connection at the macroscopic level. While this microscopic coarse grain model provides the closure that is necessary to solve the set of momentum and mass conservation equations, and allows the evaluation of the macroscopic stress tensor through a stochastic analysis of the corresponding microscopic system, these methods do not truly consider the chemical specificity of the system at a fundamental (atomic) level. Typically there is no explicit interaction among the molecules; these are included in a mean-field fashion. Such simplifications are a necessary sacrifice in order to allow the number of time-steps required to obtain useful information at the macroscopic level. While the descriptions of these bead-spring models is expected to be good for regions in which the orientation does not contain a significant enthalpic component, for conditions of high deviatoric stress (highly oriented chains), the models used in these approaches will systematically underestimate the stress that corresponds to an orientation state[111]. Chui has employed a conceptually similar poly-bead model to obtain rheological and structural information of coarse-grained PE[112]. The Chui model builds in capability for non-Gaussian distribution of the mean-square distance of sites at the length scale of several coarse grained bonds. However, at the scale of a single coarse-grained bond, the model strictly assumes a Gaussian distribution of the mean-square length and will be subject to a lesser degree of underestimation than a purely bead-spring model.

2.7. Summary

Several topics have been covered in this chapter that are relevant to the following chapters of this thesis. It is worthwhile to briefly summarize the most important ideas:

- Experimental techniques provide only the measure of a specific aspect of the structure; structure is a many-dimensional concept that cannot be entirely captured by any set of experiments.

- In order to make a comprehensive determination of the microstructure, we must solve an Inverse Problem; there are a number of techniques available for the closure of these Inverse Problems.

- Polymer dynamics are often important to consider along with the experimental measurements in the determination of structure.

- Atomistic modeling of polymers provides important insight into the connection between structure and properties.

- Scale-bridging is an active area of research because of the inability of simulations to provide information at all length and time scales, and because of the difficulties involved in coarse-graining.

2.8. References

[1] K.E. Perepelkin, *Fibre Chem* **2001**, *33*, 249.

[2] A. Ajji, N. Legros, M.M. Demoulin, *Adv Perform Mater* **1998**, *5*, 117.

[3] *Structure and Properties of Oriented Polymers*; Ward, I. M., Ed.; Chapman and Hall: London, 1997.

[4] A. De Francesco and R.A. Duckett., *Polymer* **2004**, *45*, 8005.

[5] R. Pantani, A. Sorrentino, V. Speranza, G. Titomanlio, *Rheol Acta*, **2004**, *43*, 109.

[6] R.Y. Qian, *J Macromol Sci B* **2001**, *B40*, 1131.

[7] G. Kumaraswamy, *J Macromol Sci-Pol R* **2005**, *C45*, 375.

[8]   Olmstead, P. D.; Poon, W. C. K.; McLeish, T. C. B.; Terrill, N. J.; Ryan, A. J. *Phys. Rev. Lett.* **1998**, *81*, 373.

[9]   K. Kaji, K. Nishida, T. Kanaya, G. Matsuba, T. Konishi, M. Imai., *Adv Polym Sci* **2005**, *191*, 187.

[10]   N. Stribeck, R. Bayer, P. Bosecke, A. Camarillo, *Polymer* **2005**, *46*, 2579.

[11]   J.C. Rodriguez-Cabello, J. Martin-Monge, J.M. Lagaron, J.M. Pastor, *Macromol Chem Physic* **1998**, *199*, 2767.

[12]   J. Janzen, *Polym Eng. Sci.* **1992**, *32*, 1242.

[13]   P.J. in 't Veld, M. Hutter, G.C. Rutledge, *Macromolecules* **2006**, *39*, 439.

[14]   P.D. Coates, S.E. Barnes, M.G. Sibley, E.C. Brown, H.G.M. Edwards, I.J. Scowen, *Polymer* **2003**, *44*, 5937.

[15]   K.C. Cole and A. Ajii., Chapter 3 in *Solid phase processing of polymers*, I.M. Edward, P.D. Coates and M. Dumoulin, Eds., Carl Hanser, Munich, 2000.

[16]   D.C. Angstadt, J.P. Coulter, *Polym Eng Sci* **2006**, *46*, 1691.

[17]   H.F. Shan, J.L. White, *J Appl Polym Sci* **2004**, *93*, 9.

[18]   M.H. Hong, J.L. White, *Int Polym Proc* **2002**, *17*, 53.

[19]   A. GhanehFard, P.J. Carreau, P.G. Lafleur, *Int Polym Proc* **1997**, *12*, 136.

[20]   L.S. Saunders, I.M. Ward, J.I. Cail, R.F.T. Stepto, *Polymer* **2007**, *48*, 1360.

[21]   C. Pellerin, M. Pezolet, P.R. Griffiths, *Macromolecules* **2006**, *39*, 6546.

[22]   C. Bungay, T.E. Tiwald, *Thin Solid Films* **2004**, *455-56*, 272.

[23]   C. Yan, J.M. Zhang, D.Y. Shen, S.K. Yan, *Chinese Sci Bull* **2006**, *51*, 2844.

[24]   Y.H. Song, K.H. Nitta, N. Nemoto, *Macromolecules* **2003**, *36*, 1955.

[25]   H.B. Daly, K.C. Cole, B. Sanschagrin, K.T. Nguyen, *Polym Eng Sci* **1999**, *39*, 1982.

[26]   J.A.J Jansen, J.H. Vandermaas, A.P. Deboer, *Macromolecules* **1991**, *24*, 4278.

[27]   J. Purvis, D.I. Bower and I.M. Ward. *Polymer* **1973**, *14*, 398.

[28]   G.Y.U. Nikolaeva, L.E. Semenova, K.A. Prokhorov, S.A. Gordeyev, *Laser Phys* **1997**, *7*, 403.

[29]   Y.J. Wu, Y.Z. Xu, Y. Zhao, D.J. Wang, S.F. Weng, J.G. Wu, D.F. Xu, *Spectrosc Spect Anal* **2005**, *25*, 1408.

[30]   P.R. Griffiths, D.B. Chase, R.M. Ikeda, J.W. Catron, *Appl Spectrosc* **2002**, *56*, 809.

[31]   A.J. Brandolini, Ch.9 in *NMR Spectroscopy Techniques*, M.D. Bruch (ed.), Marcel Dekker, New York, 1996.

[32]   K. Schmidt-Rohr and H.W. Spiess, *Multidimensional Solid-state NMR and Polymers*, Academic Press, London, 1994.

[33]   F.L. Colhoun, R.C. Armstrong, G.C. Rutledge, *Macromolecules* **2001**, *34*, 6670.

[34]   M.Y. Liao and G.C. Rutledge, *Macromolecules* **1997**, *30*, 7546.

[35] M. Wendlandt, T.A. Tervoort, J.D. van Beek, U.W. Suter, *J. Mech. Phys. Solids* **2006**, *54*, 589.

[36]   *Polymers and Neutron Scattering*, J.S. Higgins and H.C. Benoit, Oxford Univ. Press, New York, 2002.

[37]   R. Muller, J.J. Pesce, C. Picot, *Macromolecules* **1993**, *26*, 4356.

[38]   R. Muller, C. Picot Y.H. Zang, D. Froelich, *Macromolecules* **1990**, *23*, 2577.

[39]   J. Healy, G.H. Edward, R.B. Knott, *Physica B* **2006**, *385(Part 1 Sp. Iss. SI)*, 620.

[40]   P.E. Lopes, M.S Ellison, W.T. Pennington, *Plast Rubber Compos* **2006**, *35*, 294.

[41]   A. Blim, E. Oldak, A. Wasiak, L. Jarecki, *Polimery* **2005**, *50*, 48.

[42]   P.C. van der Heijden, L. Rubatat, O. Diat, *Macromolecules* **2004**, *37*, 5327.

[43]   M.C.G. Gutierrez, G.C. Alfonso, C. Riekel, F. Azzurri, *Macromolecules* **2004**, *37*, 478.

[44]   P.K. Agarwal, R.H. Somani, W.Q. Weng, A. Mehta, L. Yang, S.F. Ran, L.Z. Liu, B.S. Hsiao, *Macromolecules* **2003**, *36*, 5226.

[45]   A. Nogales, B.S. Hsiao, R.H. Somani, S. Srinivas, A.H. Tsou, F.J. Balta-Calleja, T.A. Ezquerra, *Polymer* **2001**, *42*, 5247.

[46]   S.F. Ran, D.F. Fang, I. Sics, S. Toki, B.S. Hsiao, B.R. Chu, *Rev Sci Instrum* **2003**, *74*, 3087.

[47]   J.L. White, D.M. Choi, C.H. Choi, *Arab J Sci Eng* **2002**, *27*, 69.

[48]   H.S. Lee, S.R. Yoo, S.W. Seo, *J Polym Sci Pol Phys* **1999**, *37*, 3233.

[49]   V.N. Kalashnikov, M.G. Tsiklauri, *Colloid Polym Sci* **1996**, *274*, 1119.

[50]   J.F. Bent, R.W. Richards, T.D. Gough, *Rev Sci Instrum* **2003**, *74*, 4052.

[51]   G. Kumaraswamy, R.K. Verma, J.A. Kornfield, *Rev. Sci. Instrum.* **1999**, *70*, 2097.

[52]   P.C. Sabatier, *J Math Phys* **2000**, *41*, 4082.

[53]   E.T. Jaynes, *Phys Rev* **1957**, *106*, 620.

[54]   E.T. Jaynes, in: *The Maximum Entropy Formalism*, R. Levine, M. Tribus (Eds.), MIT Press, Cambridge, MA, 1979.

[55]   L.M. Martyushev, V.D. Seleznev, *Phys Rep* **2006**, *426*, 1.

[56]   S. Abe, *J. Phys A - Math. Gen* **2003**, *36*, 8733.

[57]   V. Rodriguez, F. Lagugne-Labarthet, C. Sourisseau, *Appl Spectrosc* **2005**, *59*, 322.

[58]   U.A. van der Heide, S.C. Hopkins, Y.E. Goldman, *Biophys J* **2000**, *78*, 2138.

[59]   D. Poland, *J Chem Phys* **1995**, *102*, 2604.

[60]   D. Poland, *J Chem Phys* **2000**, *112*, 6554.

[61]   N. Agmon, Y. Alhassid, R.D. Levine, *J. Comp. Phys.* **1979**, *30*, 250.

[62]   R.L. McGreevy, L. Pusztai, *Mol Simul* **1988**, *1*, 359.

[63]   R.L. McGreevy, J Phys - Condens Mat **2001**, *13*, R877.

[64]   G. Tóth, A. Baranyai, *J Phys. - Condens. Mat* **2005**, *17*, S159.

[65]   W. Schommers, *Phys Lett A* **1973**, *43*, 157.

[66]   W. Schommers, *Phys Rev A* **1983**, *28*, 3599.

[67]   A.P. Lyubartsev, A. Laaksonen, *Phys Rev E* **1995**, *52*, 3730.

[68]   G.C. Rutledge, *Phys Rev E* **2001**, *63*, 021111.

[69]   M. Bathe, G.C.Rutledge, *J Comput Chem* **2003**, *24*, 876.

[70]   F.L. Colhoun, R.C. Armstrong, G.C. Rutledge, *Macromolecules* **2002**, *35*, 6032.

[71]   A.K. Soper, *Mol. Phys.* **2001**, *99*, 1503.

[72]   R.L. Henderson, *Phys Lett* **1974**, *49A*, 197.

[73]   *Scaling Concepts in Polymer Physics*, P.-G. de Gennes, Cornell Univ. Press, Ithica, NY, 1979.

[74]   *The Theory of Polymer Dynamics*, M. Doi and S.F. Edwards, Oxford Univ. Press, New York, 1994.

[75]   J. Embery, R.S. Graham, R.A. Duckett, D. Groves, M. Collis, M.R. Mackley, T.C.B. McLeish, *J Polym Sci Pol Phys* **2007**, *45*, 377.

[76]   W.J. Walczak, R.P. Wool, *Macromolecules* **1991**, *24*, 4657.

[77]   L. Messe, R.E. Prud'homme, *J Polym Sci Pol Phys* **2000**, *38*, 1405.

[78]   *Prediction of Polymer Properties*, J. Bicerano, Marcel Dekker, New York, 2002.

[79]   A. Ghaneh-Fard, *J Plast Film Sheet* **1999**, *15*, 194.

[80]   I.M. Ward, *Proc Phys Soc* **1962**, *80*, 1176.

[81]   P.K. Biswas, *Coll. Polym. Sci.* **1984**, *262*, 623.

[82]   *Mechanical Properties of Solid Polymers*, I.M. Ward and D.W. Hadley, John Wiley & Sons, W. Sussex, England, 1993.

[83]   G. Allegra, S.V. Meille, *Adv Polym Sci* **2005**, *191*, 87.

[84]   C.W. Yong, P.G. Higgs, *Macromolecules* **1999**, *32*, 5062.

[85]   V.G. Mavrantzas, D.N. Theodorou, *Macromol Theor Simul* **2000**, *9*, 500.

[86]   V.G. Mavrantzas, D.N. Theodorou, *Comput Theor Polym Sci* **2000**, *10*, 1.

[87]   J.I. Cail, L.S. Saunders, R.F.T. Stepto, I.M. Ward, *Polymer* **2007**, *48*, 1379.

[88]   N. Metropolis, A.W. Rosenbluth, M.N. Rosenbluth. A.H. Teller, E. Teller, *J. Chem. Phys.* **1953**, *21*, 1087.

[89]   *Simulation Methods for Polymers*, M. Kotelyanskii and D.N. Theodorou (eds.), Marcel Dekker, New York, 2004.

[90]   P.V.K. Pant, D.N. Theodorou, Macromolecules 28:7224 (1995)

[91]   A. Uhlherr, S.J. Leak, N.E. Adam, P.E. Nyberg, M. Doxastakis, V.G. Mavrantzas, D.N. Theodorou, Comput. Phys. Commun. 144:1 (2002)

[92]   V.G. Mavrantzas, D.N. Theodorou, *Macromolecules 31*:6310 (1998)

[93]   V.G. Mavrantzas, H.C. Ottinger, *Macromolecules 35*:960 (2002)

[94]   H.C. Öttinger, *Phys Rev E* **1998**, *57*, 1416.

[95]   P. Gestoso, J. Brisson, J Polym Sci Pol Phys, 40:1601 (2002)

[96]   A.V. Lyulin, N.K. Balabaev, M.A. Mazo, M.A.J. Michels, *Macromolecules* **2004**, *37*, 8785.

[97]   K. Yshiro, T. Ito, Y. Tomita, *Int J Mech Sci* **2003**, *45*, 1863.

[98]   M.J. Ko, N. Waheed, M.S. Lavine, G.C. Rutledge, *J Chem Phys* **2004**, *121*, 2823.

[99]   A. Koyama, T. Yamamoto, K. Fukao, Y. Miyamoto, *J Macromol Sci Phys* **2003**, *B42*, 821.

[100] A. Koyama, T. Yamamoto, K. Fukao, Y. Miyamoto, *Phys Rev E* **2002**, *65*, 050801.

[101] M.S. Lavine, N. Waheed, G.C. Rutledge, *Polymer* **2003**, *44*, 1771.

[102] F. Muller-Plathe, *Chemphyschem* **2002**, *3*, 754.

[103] *Bridging Time Scales: Molecular Simulations for the Next Decade*, P. Nielaba, M. Maraschal, G. Ciccotti (eds.), Springer, Berlin, 2002.

[104] D.N. Theodorou, Mol Phys. **2004**, *102*, 147.

[105] *Statistical Mechanics of Chain Molecules*, P. Flory, Oxford Univ. Press, New York, 1989.

[106] J.I. Cail, R.T.F. Stepto, I.M. Ward, *J Macromol Sci Phys* **2005**, *B44*, 843.

[107] M.E. Ries, M.G. Brereton, I.M. Ward, J.I. Cail, R.F.T. Stepto, *Macromolecules* **2002**, *35*, 5665.

[108] K. Kremer, in *Multiscale Modeling and Simulation*, S. Attinger and P. Koumoutsakos (eds.), Springer, Berlin, 2004.

[109] H. Meyer, O. Biermann, R. Faller, D. Reith, F. Muller-Plathe, *J Chem Phys* **2000**, *113*, 6264.

[110] Laso M and Ramirez J. in *Multiscale Modeling of Polymer Properties*, M. Laso and E.A. Perpete (eds.), Elsevier, Amsterdam, 2006.

[111] I. Ghosh, G.H. McKinley, R.A. Brown, R.C. Armstrong, *J. Rheol.* **2001**, *45*, 721.

[112] C. Chui, M.C. Boyce, Macromolecules **1999**, *32*, 3795.

Chapter 3

Semi-Grand Canonical Monte Carlo (SGMC) Simulations to Interpret Experimental Data on Processes Polymer Melts and Glasses

3.1. Introduction

One of the hallmarks of polymers is the ease with which they can be processed into anisotropic materials. The persistence of these anisotropic states, despite their inherently non-equilibrium nature, is the key to the versatile optical and mechanical properties of polymers. Deducing the microstructure of these anisotropic states from their observed properties is, by its very nature, an inverse problem; the enormous number of structural degrees of freedom at the atomic scale ensures that even the most sophisticated battery of measurements will leave the structure severely underdetermined. Statistical mechanics provides various tools whereby a representative sample of these degrees of freedom can be averaged to calculate a corresponding measurable macroscopic property. Semi-Grand Canonical Monte Carlo (SGMC) is one such tool that allows the simulation of anisotropy in an otherwise homogeneous system by identifying each structural unit by one or more of its measurable anisotropic features. We can thus speak of a set of "physical isomers" or "physical species" which differ from each other only in their orientation. The systems are distinguished by the orientation distribution function (ODF) of these species.

Experimental data are incorporated into the SGMC simulation through the normalization of an experimental observable to match the concentration of a corresponding physical species[1]. For the uniaxially oriented systems studied here, the physical species are structural units that are distinguished according to the angle θ they form with the axis of orientation. For example, birefringence depends on the second Legendre coefficient $P_2(\cos\theta)$ of the polarizable structural units. Similarly, infrared dichroism depends on $P_2(\cos\theta)$ of the dipole of an IR-active structural unit of the molecule. Raman depolarization ratios depend on the values of both $P_2(\cos\theta)$ and the fourth Legendre coefficient $P_4(\cos\theta)$ of the relevant scattering unit. Multidimensional NMR can, in principle, provide data for the entire ODF. For highly oriented samples, DECODER-NMR and several related NMR techniques[2-4] have been shown to be particularly powerful; values for Legendre coefficients up to $P_{14}(\cos\theta)$ have been reported by these methods[5]. The reader is directed to Ward[6] for more detail on the techniques and interpretation of measurements of oriented polymer systems.

From the information provided by these experimental techniques, one can attempt to reconstruct the full ODFs, for example through the use of Maximum Entropy (ME) methods[7] or Reverse Monte Carlo (RMC)[8]. Maximum entropy methods produce a unique and unbiased distribution function for a set of experimental constraints. However, these methods ignore important energetic interactions within the system, possibly resulting in an unphysical solution. RMC, on the other hand, can account for the chemical interactions among sites in the system, but equates measurement uncertainty with thermal fluctuations in the system, in a manner inconsistent with thermodynamics. Obviously, as experimental measurement techniques improve, the thermodynamics of the system should be unaffected.

SGMC is distinguished from other inverse methods by its consideration of the specific chemical and thermodynamic features of a system that may be out of equilibrium. The result is a simulation incorporating all available information about the system in a thermodynamically consistent manner. Thus, we obtain not only a more reliable estimate of the incomplete features of the orientation distribution, but also a basis for estimating the other non-equilibrium characteristics of the system. We can obtain

estimates of torsion angle distributions, changes in free energy, orientation on different length scales, density, and other measures which are not accessible using either experimental measurements, or ME and RMC methods. It is this wealth of microscopic-level information that justifies the more intense computational expense of an SGMC simulation. We demonstrate this method for a variety of systems that span the range of orientation observed in experimental polyethylene melt studies[9-11] as well as higher orientations that have been simulated for polyethylene melts by molecular dynamics[12,13].

3.2. Theory

3.2.1. Semi-Grand Canonical (SGC) Ensemble

The SGC ensemble is obtained by the identification of each of the N sites in a system with one of several species types, indicated by a component or speciation matrix, $\mathbf{I}$; $\mathbf{I}_i$ is a vector component of $\mathbf{I}$ that designates the specific species type of site i^{14}. Rewriting equations 41 and 48 of Briano and Glandt[14] to express the SGC partition function Υ and the probability density $p(\mathbf{I})$ of the species in terms of the conjugate potential function $\mu(\mathbf{I}_i)$ we obtain the equations that provide the basis for the SGMC method:

$$\Upsilon = \frac{\exp(-\beta N \mu_r)}{N!} \int_{\mathbf{I}_1} \cdots \int_{\mathbf{I}_N} q^N Z_N \exp(\beta \sum_{i=1}^{N} \mu(\mathbf{I}_i)) \prod_{i=1}^{N} d\mathbf{I}_i \qquad (3.1)$$

$$p(\mathbf{I}) = \frac{1}{\Upsilon} \frac{q^N}{N!} \int_{\mathbf{I}_2} \cdots \int_{\mathbf{I}_N} Z_N \exp(\beta \sum_{i=1}^{N} (\mu(\mathbf{I}_i) - \mu_r)) \prod_{i=2}^{N} d\mathbf{I}_i \qquad (3.2)$$

where $Z_N = \int \exp\left(-\beta U\left(\mathbf{r}^N\right)\right) dr^N$ is the canonical configuration integral; q is a scaled internal partition function (assumed to be constant, for the purposes of this work); μ_r is a reference potential whose value is constrained by fixing the system size to be N.

This speciation yields the non-equilibrium SGC [$NVT\Delta\mu(\mathbf{I})$] ensemble (where $\Delta\mu(\mathbf{I}) = \mu(\mathbf{I}) - \mu_r$) by transformation of the canonical [NVT] ensemble (or analogously

56

[*NPTΔμ*(I)] from [*NPT*]). In the [NVTΔμ(I)] ensemble, the probability density and importance criterion necessary to satisfy the detailed balance condition follow directly from eq. 3.2:

$$\ln p(\mathbf{r}^N, \mathbf{I}) \propto -\beta \left[U(\mathbf{r}^N) - \sum_{i=1}^{N} \Delta\mu(\mathbf{I}_i) \right]$$ (3.3)

$$p_{acc} = \min\left\{ 1, \exp\left(-\beta \left[U(\mathbf{r}^N)_{new} - U(\mathbf{r}^N)_{old} - \right. \right. \right.$$

$$\left. \left. \left. \sum_{i=1}^{N} \left(\mu(\mathbf{I}_i)_{new} - \mu(\mathbf{I}_i)_{old} \right) \right] \right) \right\}$$ (3.4)

Methods for the iterative determination of $\mu(\mathbf{I})$ to reproduce the desired $p(\mathbf{r}^N, \mathbf{I})$ have been reported elsewhere[1,15,16]. The value of μ_r may be determined *a posteriori* by methods such as thermodynamic integration or the self-consistent histogram method[17]. In general, it is unnecessary to evaluate μ_r since it is a constant and does not affect the distributions.

A system that is physically inhomogeneous, yet chemically homogeneous, can be simulated in the SGC ensemble by choosing a physical, rather than chemical, variable to identify each site. This was originally demonstrated for a Lennard-Jones (LJ) fluid by identifying each site by the (*N*-1) pair-wise intermolecular distances the site forms with the other sites in the system, i.e. its contribution to the radial distribution function (RDF); the conjugate potential determined by iteration in this case is just the conventional two-body interaction potential[1]. The same identification was subsequently evaluated for intra- as well as intermolecular interaction potentials using the Gō model[18] for proteins as a test case[14]. Procedurally similar methods to determine interaction potentials have been proposed and justified on different grounds by Soper[19], Lyubartsev, et al.[20], Müller-Plathe[21] and most recently Jain et al[22]. However, the process of speciation to construct a simulation in the SGC ensemble is more general. It can solve not only for the potentials intrinsic to materials, but also for potentials or fields that perturb the system out of equilibrium. Colhoun, et al, originally employed this capability to follow the relaxation of polystyrene molecular conformations after shearing[23]. In that work, the use of the SMAS-DECODER NMR method allowed the determination of the full ODF prior to its use in a SGMC simulation. In this work we consider the use of SGMC to study

systems given only incomplete information about the ODF, as is more commonly the case from birefringence and the other measurement methods mentioned earlier.

The motivation for using a Monte Carlo method to study non-equilibrium states is that the method samples the optimal ensemble of configurations that reproduces the available observations (i.e. the experimental measurements). Relative to molecular dynamics, the Monte Carlo method permits the introduction of non-physical moves that sample phase space more efficiently. The structures produced by a non-equilibrium molecular dynamics simulation (NEMD) may be sensitive to the rate of deformation employed in the simulation, which typically exceeds by several orders of magnitude those available experimentally. In contrast, the SGMC method constructs a molecular model that reproduces the available experimental data assuming only the applicability of the force field. The result is a quasi-equilibrium state that can be identified closely with a perturbation on the time scale of the delay between experimental measurements. Ultimately, the goal of modeling building is to anticipate behavior that is not obvious from the experimental measurement. A real strength of molecular modeling is the ability to query the simulated ensemble and quantify characteristics of the most probable ensemble of molecular configurations. These characteristics, which may not be accessible by conventional analytical techniques, provide a window into the structural changes taking place in the polymer melt. This is not to say that the extracted characteristics of the system are the true ones, but rather that they are the most probable ones given the limited information available. The method also allows the evaluation of complementary sets of experimental data, either individually or jointly, to determine whether they are consistent and non-degenerate in the information they provide about the state of the system.

3.2.2. Maximum Entropy: The Moments Problem

Nearly a half-century ago, Jaynes showed the equivalence of the Maximum Entropy (ME) estimates of information theory and the ensembles obtained from statistical

mechanics[24]. The ME estimate involves an iterative calculation of a potential conjugate to each of the independent constraints using the method of Lagrange multipliers[25]. These constraints are the measured (or known) values of the system, which are then "simulated" in an ensemble that holds their conjugate potentials constant. Therefore, the adaptation of this approach is not simply a mathematical convenience. Our statistical approach to modeling ensembles makes this evaluation of a potential *identical* to the statistical mechanical description of the most likely non-equilibrium ensemble that is consistent with our knowledge of the system.

The application of this method to determine a full distribution of any characteristic from a finite number of its moments is known as the 'Moments Problem'[26]. This is relevant to the measurement of the second moment of an orientation distribution, e.g. through birefringence, to obtain an estimate of the properties of the system. The SGMC method provides a means for adapting ME methods to complex interacting systems. In its simplest form, an ensemble with $U(\mathbf{r}^N)\equiv 0$, the SGMC method becomes identical to the ME method. The Lagrange multipliers are analogous to $\Delta\mu(\mathbf{I})$ in eq. 3.3 (e.g. μ_k, $k=0$ to K, see eq. 3.5 below) and maximize the entropy S subject to the constraint that the known values of the K moments match their ensemble averages $\langle h_k(\mathbf{I})\rangle$.

In general, the SGMC potential function $\mu(\mathbf{I})$ can be written as the summation of a set of basis functions:

$$\mu(\mathbf{I}) = \sum_{k=0}^{K}\mu_k h_k(\mathbf{I}) = \mu_0 + \sum_{k=1}^{K}\mu_k h_k(\mathbf{I}) \tag{3.5}$$

The moments $<h_k>$ and the change in entropy ΔS with respect to the condition $\mu(\mathbf{I})=0$ for a non-interacting system are then found to be[24]:

$$\langle h_k(\mathbf{I})\rangle = \int h_k(\mathbf{I})p(\mathbf{I})d\mathbf{I} = \int h_k(\mathbf{I})\exp\left\{\beta\sum_{k=0}^{K}\mu_k h_k(\mathbf{I})\right\}d\mathbf{I} \tag{3.6}$$

$$\frac{\Delta S}{k_B} = -\int p(\mathbf{I})\ln p(\mathbf{I})d\mathbf{I} = -\beta\sum_{k=0}^{K}\mu_k\langle h_k(\mathbf{I})\rangle \tag{3.7}$$

where μ_0 is chosen such that $p(\mathbf{I})$ is normalized. The convexity of the functional form of eq. 3.7 ensures a unique solution for $\mu(\mathbf{I})$, if one exists[27]. This uniqueness can be extended to interacting systems by recognizing that weighting states (e.g., by their interaction energies) does not affect the existence of a unique solution[28]. This property guarantees the closure of the inverse problem being solved here by SGMC.

One potential difficulty with reconstructing a detailed atomistic system from a limited set of measured moments is that the Lagrange multipliers may oscillate and not converge as the size of the basis set K increases for a non-orthogonal basis set[29]. This problem is resolved through orthonormalization of the basis sets as discussed below. With both SGMC and ME methods, the nature of the experimental data will guide the choice of the basis functions as well as the number of terms used in the basis set K to provide a best solution to the inverse problem of estimating the complete distribution.

3.2.3. Molecular Representation

The selection of physical isomers is motivated by the experimental measurement of the physical organization of the molecules. Significantly, for most of the experimental methods mentioned in the Introduction, these physical isomers will be local in nature, involving only one or a few bonds.

For a polymeric system comprised of N atoms or sites, distributed among N_{ch} chains, the Cartesian coordinate of the ith site of the jth chain can be written $\mathbf{r}_{i,j}$. The intramolecular coordinates are equivalently represented in terms of connector vectors $\mathbf{q}_{i,j}^{(m)}$ of the n_j sites in each chain. The superscript m indicates the number of bonds spanned by the connector. Connector vectors that coincide with the backbone bonds are represented as:

$$\mathbf{q}_{i,j}^{(1)} = \mathbf{r}_{i+1,j} - \mathbf{r}_{i,j}; \quad i = 1, 2, \ldots, n_j - 1 \tag{3.8}$$

Other connector vectors can be similarly defined; for example, next-nearest neighbor sites in polyethylene, which provide an estimate of the local chain direction, are represented:

$$\mathbf{q}_{i,j}^{(2)} = \mathbf{r}_{i+2,j} - \mathbf{r}_{i,j}; \quad i = 1, 2, \ldots, n_j - 2 \tag{3.9}$$

and the end-to-end vector $\mathbf{Q}_j$ of chain j is defined as:

$$\mathbf{Q}_j = \mathbf{q}_j^{(n_j - 1)} = \mathbf{r}_{n_j, j} - \mathbf{r}_{1, j} \tag{3.10}$$

For molecules with rigid intramolecular bonds and bond angles, $\mathbf{q}^{(1)}_{i,j}$ and $\mathbf{q}^{(2)}_{i,j}$ are fixed in magnitude, and they can be described unambiguously by their corresponding unit vectors $\mathbf{e}^{(1)}_{i,j}$ and $\mathbf{e}^{(2)}_{i,j}$:

$$\mathbf{e}_{i,j}^{(1)} = \frac{\mathbf{q}_{i,j}^{(1)}}{\left|\mathbf{q}_{i,j}^{(1)}\right|}$$

$$\mathbf{e}_{i,j}^{(2)} = \frac{\mathbf{q}_{i,j}^{(2)}}{\left|\mathbf{q}_{i,j}^{(2)}\right|} \tag{3.11a, 3.11b}$$

However, the magnitude of $\mathbf{Q}_j$ will not, in general, be fixed, necessitating both an orientation (unit vector) and scalar magnitude to characterize its distribution.

Application of the SGMC method requires the conservation of the total number of speciated elements. For a monodisperse polymer system, n_j is constant and the number of connector vectors is strictly conserved and equal for each molecule. In general, we use variable-connectivity moves to simulate polymer systems, in which N and N_{ch} are fixed but $\{n_j\}$ are not. For such systems, the number of connector vectors is not conserved for $\mathbf{q}_{i,j}^{(m)}$ if $m > n_{min}$, the shortest chain in the simulation, violating this fundamental requirement of the SGMC method. However, for all cases considered here, the size of the structural units is smaller than n_{min} and so is always conserved. For fixed N_{ch}, the number of end-to-end connectors is conserved by construction, making the set $\{\mathbf{Q}_j\}$ a viable physical isomer in the SGC ensemble, despite m being larger than n_{min}.

3.2.4. Selection of Basis Set

In general, equation 3.3 can be written as:

$$\ln p(\mathbf{r}^N, \mathbf{I}) \propto -\beta \left[U(\mathbf{r}^N) - \sum_{i=1}^{N} \sum_{k=0}^{K} \mu_k h_k(\mathbf{I}_i) \right] \tag{3.12}$$

where now $h(\mathbf{I})$ represents a generalized basis function. Colhoun et al.[23] provided a demonstration of the SGMC method for molecular orientation, effectively using a boxcar function for the multidimensional speciation of a polymer system based on the polar angles of $\mathbf{e}^{(2)}{}_{i,j}$, $I \equiv \{\cos\theta^{(2)}, \phi^{(2)}\}$, where $\cos\theta^{(2)} = \mathbf{e}^{(2)}_{i,j} \cdot \mathbf{e}_x$ and

$\tan\phi^{(2)} = \left(\mathbf{e}^{(2)}_{i,j} \cdot \mathbf{e}_y\right)\Big/\left(\mathbf{e}^{(2)}_{i,j} \cdot \mathbf{e}_z\right)$. The corresponding uniaxial form $I \equiv \{\cos\theta^{(2)}\}$ of this basis set is:

$$
\begin{aligned}
p(\cos\theta^{(2)}) &= \sum_{k=1}^{K} h_k(\mathbf{I}_i) \\
&= \sum_{k=1}^{K} c_k \left[H(\cos\theta^{(2)} - \cos\theta^{(2)}_{k-}) - H(\cos\theta^{(2)} - \cos\theta^{(2)}_{k+}) \right]
\end{aligned}
\tag{3.13}
$$

where $H(x)$ is the Heaviside function and $\cos\theta^{(2)}_{k+}$ and $\cos\theta^{(2)}_{k-}$ are the upper and lower limits of the kth bin. The resolution of the histogram is limited only by the numerical precision, or the ability to populate each bin statistically during a single simulation.

As the number of bins becomes large, it is often more practical to represent $p(\cos\theta^{(m)})$ as a series of continuous basis functions. For $\mathbf{e}^{(1)}_{i,j}$ or $\mathbf{e}^{(2)}_{i,j}$, a particularly relevant form is the polynomial expansion for the ODF using basis functions of the form $h_k\left(\mathbf{e}^{(2)}\right) \equiv \left(\mathbf{e}^{(2)t} \cdot\right)^k \Big/ k!$, where the superscript t denotes the transpose. For cases involving connector vectors described in this work, the ODF generally exhibits mirror symmetry, and odd-order terms in $e_i^{(m)}$ average to zero. The ODF then becomes:

$$
\begin{aligned}
\ln p\left(\mathbf{e}^{(2)}\right) &= A_0^{(2)} + \frac{1}{2}\mathbf{e}^{(2)t} \cdot \mathbf{A}_2^{(2)} \cdot \mathbf{e}^{(2)} + \ldots \\
&= \sum_{k=0}^{K/2} \frac{\left(\mathbf{e}^{(2)t} \cdot\right)^{2k}}{(2k)!} \mathbf{A}_{2k}^{(2)}
\end{aligned}
\tag{3.14}
$$

We can obtain a polynomial expansion over the interval $[-1,1]$ in x, y and z by expanding eq. 3.14:

$$
\ln p\left(\mathbf{e}^{(2)}\right) = A_0^{(2)} + \sum_{j=x,y,z} A_{2,j}^{(2)} \cos^2\theta_j^{(2)} + \ldots
\tag{3.15}
$$

which produces a distribution by specifying $\{\langle \cos^{2k}\theta_j^{(2)} \rangle\}$ and determining the conjugates $\{A_{2k,j}^{(2)}\}$, for $j=x, y, z$, as in the Moments Problem discussed above. Upon

62

application of the Gram-Schmidt orthonormalization, one obtains the Legendre polynomial expansion:

$$\ln p\left(\mathbf{e}^{(2)}\right) = A\,'^{(2)}_{0} + \sum_{j=x,y,z} A\,'^{(2)}_{2,j} P_2\left(\cos\theta_j^{(2)}\right) + \dots \tag{3.16}$$

This form suggests a new set of species types or physical isomers that are defined by the polynomials, $P_{2k}(\cos\theta^{(2)})$. These are linearly related to the original isomers defined by $\cos^{2k}\theta^{(2)}$, and provide an equivalent expression for $\ln p(\mathbf{e}^{(2)})$. The leading term $A\,'^{(2)}_{0}$ is constant and may be dropped. Equation 3.12 then takes the specific form:

$$\ln p(r^N, \{P_{2k}^N\}) \propto -\beta\left[U(\mathbf{r}^N) - \sum_{i=1}^{N}\sum_{k=1}^{K/2}\sum_{j=x,y,z} \mu^{(2)}_{2k,j} P_{2k}(\cos\theta_{i,j}^{(2)})\right] \tag{3.17}$$

where $\mu_{2k,j}^{(2)}$ can be directly identified as $A\,'^{(2)}_{k,j}/\beta$ in eq. 3.16. Because $P_2(\cos\theta_x^{(2)})$ is typically proportional to the birefringence, eq. 3.17 can be truncated after $k=1$ and $\mu_{2k,y}^{(2)}$ $=\mu_{2k,z}^{(2)} =0$ to obtain an appropriate form for use with these measurements. Similarly, other measures of uniaxial orientation will be truncated after $k=1$ (infrared), $k=2$ (Raman), or some $k>2$ (NMR).

3.2.5. Relation to Melt Elasticity

While we have been motivated by the nature of experimental measurements to simulate orientation in polymers using a local orientation potential, Mavrantzas and coworkers were motivated by studies of melt elasticity in elongational flows and proposed a new free energy function for a flow-oriented polymer melt in terms of new, molecular structural variables. This resulted in a similar description of non-equilibrium polymer systems in terms of the conformation tensor[30-32] or, alternatively, in terms of the normal modes[33]. They defined the conformation tensor for chain j, $\mathbf{c}_j$, as:

$$\mathbf{c}_j = \frac{3\mathbf{Q}_j\mathbf{Q}_j}{\langle Q_j^2\rangle_0} \tag{3.18}$$

where $\langle Q_j^2 \rangle_0$ is the mean squared end-to-end distance of the jth chain in the unperturbed state. The selection of c_j as the structural parameter to describe the non-equilibrium state space was inspired by its prevalence in rheological models of polymer systems and by the intuition that it accurately represents the "slowest" degrees of freedom, those most likely to deviate from their equilibrium values under conditions of flow. The probability distribution can then be written, to within an additive constant, as:

$$\ln p(\mathbf{Q}_j) = \boldsymbol{\alpha} : \mathbf{c}_j \qquad (3.19)$$

where $\boldsymbol{\alpha}$ is a new thermodynamic potential conjugate to c_j.

Despite their differences in origin and motivation, we believe that there exists an intimate connection between the approach of Mavrantzas and coworkers and the SGMC ensemble approach elaborated here. Comparing the two approaches can offer some insight into both methods. To show this, we start with eq. 3.14, substitute $\mathbf{Q}_j/Q_j$ for $\mathbf{e}^{(2)}$, invoke mirror symmetry as before and truncate the expansion at the second moment term. Doing so, we obtain:

$$\ln p(\mathbf{Q}_j) = \frac{1}{2}\frac{(\mathbf{Q}_j)^t \cdot \mathbf{A}_2 \cdot \mathbf{Q}_j}{Q_j^2} = \frac{1}{2}\frac{\mathbf{A}_2 : \mathbf{Q}_j\mathbf{Q}_j}{Q_j^2} \qquad (3.20)$$

We next define two new variables, Λ^2_j and $\mathbf{S}_j$, to represent the size and orientation, respectively, of the conformation tensor of chain j with respect to its undeformed state:

$$\Lambda^2_j = \frac{tr(\mathbf{Q}_j\mathbf{Q}_j)}{\langle Q_j^2 \rangle_0} \qquad (3.21a)$$

$$\mathbf{S}_j = \left(3\mathbf{e}_j^{(Q)}\mathbf{e}_j^{(Q)} - \mathbf{I}\right)/2 \qquad (3.21b)$$

The diagonal elements of $\mathbf{S}_j$ are the second Legendre polynomials of the vector $\mathbf{Q}_j$ with respect to the three Cartesian axes, and $\mathbf{S}_j$ is traceless. Using these definitions, the conformation tensor for chain j defined by eq. 3.18 can be written as follows:

$$\mathbf{c}_j = \frac{3\mathbf{Q}_j\mathbf{Q}_j}{\langle Q_j^2 \rangle_0} = \Lambda^2_j(2\mathbf{S}_j + \mathbf{I}) \qquad (3.22)$$

while eq. 3.20 becomes:

$$\ln p(\mathbf{Q}_j) = \frac{\mathbf{A}_2 : \mathbf{c}_j}{6\Lambda_j^2} = \frac{1}{6}\mathbf{A}_2 : (2\mathbf{S}_j + \mathbf{I}) \tag{3.23}$$

Comparison of eq. 3.19 and eq. 3.23 suggests that $\mathbf{A}_2 = 6\Lambda_j^2 \boldsymbol{\alpha}$ and one can write:

$$\ln p(\mathbf{Q}_j) = 2\Lambda_j^2 \boldsymbol{\alpha} : \mathbf{S}_j + \Lambda_j^2 tr(\boldsymbol{\alpha}) \tag{3.24}$$

In the SGC ensemble, $\mathbf{A}_2 = 3\beta\boldsymbol{\mu}_2^{(Q)}$, where $\boldsymbol{\mu}_2^{(Q)}$ has been defined as the end-to-end vector orientation potential. The tensors $\boldsymbol{\mu}_2^{(Q)}$ and $\boldsymbol{\alpha}$ can *always* be specified to obtain the equality $2\boldsymbol{\alpha} = \beta\boldsymbol{\mu}_2^{(Q)}$. In general, the form of $\boldsymbol{\alpha}$ (and therefore $\beta\boldsymbol{\mu}_2^{(Q)}$ in this comparison) is specified by the velocity gradient tensor for a given flow[33]. For the special case of traceless $\boldsymbol{\alpha}$ such that for a general uniaxial elongational flow[33], the melt elasticity approach can be reproduced by SGMC using:

$$\ln p(\mathbf{r}^N, \mathbf{Q}^{N_{ch}}) = -\beta\left[U(\mathbf{r}^N) - \sum_{j=1}^{N_{ch}} \Lambda_j^2 \left(\boldsymbol{\mu}_2^{(Q)} : \mathbf{S}_j\right)\right] \tag{3.25}$$

Since $\mathbf{S}$ is also traceless, it turns out that any arbitrary value can be added to the diagonal components of $\boldsymbol{\mu}$ in eq. 3.25 with no effect on the resulting distribution of $\mathbf{Q}$ produced by simulation. Therefore, as a matter of practicality in this work, the melt elasticity approach with a uniaxial traceless $\boldsymbol{\alpha}$ was reproduced using a form of $\beta\boldsymbol{\mu}$ with a single non-zero component $\beta\mu_{xx}{=}3\alpha_{xx}$ ($={-}6\alpha_{yy} ={-}6\alpha_{zz}$) in eq. 3.25; subtracting $\alpha_{xx}\mathbf{I}$ from this form recovers the original $\beta\boldsymbol{\mu}_2^{(Q)}$ with no change on the distribution of $\mathbf{Q}$ obtained by simulation.

Instead of coupling the physical potential to the conformation tensor, it may be desirable in some circumstances to introduce a second speciation parameter for the chain size, Λ^2_j. This is consistent with rheological models such as the "pompon" model described by Öttinger[34] and employed by Mavrantzas and Öttinger[33], in which independent variables for orientation $\mathbf{S}_j$ and stretch Λ_j^2 are defined. We introduce a second potential $\mu_2^{(\Lambda)}$ for the chain size and rewrite the orientation potential as $\mu_2^{(S)}$ to clarify its coupling to $\mathbf{S}_j$. The probability density becomes:

$$\ln p(\mathbf{r}^N, \mathbf{Q}^{N_{ch}}) = -\beta\left[U(\mathbf{r}^N) - \sum_{j=1}^{N_{ch}}\left(\boldsymbol{\mu}_2^{(S)} : \mathbf{S}_j\right) - \mu_2^{(\Lambda)}\sum_{j=1}^{N_{ch}}\Lambda_j^2\right] \tag{3.26}$$

Eq. 3.26 has the form of physical isomerism defined by a two-dimensional speciation variable, $\{S, \Lambda^2\}$, in which the variables are separable and independent. A similar approximation was also recognized by Mavrantzas and Theodorou[32].

The separation of physical isomerism into two components, based on orientation (the S_j term) and size (the Λ^2_j term), as shown in Eq. 3.26 reveals an interesting difference from the use of the conformation tensor; application of $\boldsymbol{\mu}^{(S)}_2$ with $\mu^{(\Lambda)}_2=0$ produces only rotational forces that do not contribute to the system pressure. In contrast, application of $\boldsymbol{\alpha}$ (or similarly, $\boldsymbol{\mu}_2^{(\varnothing)}$) or $\mu^{(\Lambda)}_2$ results in stretching forces. These stretching forces are responsible for the pressure changes documented previously[30] and create a contribution to the pressure that is not coupled to the volume, but rather to the applied physical potential. In those simulations, the system pressure P is the trace of the sum of the volume-coupled term $b\mathbf{I}$ and the stress due to the applied physical potential $\boldsymbol{\tau}^{(\mu)}$ as shown in eq. 8 of reference 30. The pressure contribution of the potential is traceless only if the potential acts exclusively on the orthonormalized components of the direction of a non-rigid unit, as is the case for $\boldsymbol{\mu}^{(S)}$, with no direct effect on the size. Derivation of the stresses due to orientation and their numerical validation against the simulated virial stresses are given in the Appendix (section 3.6).

3.3. Simulation Method

We use the united atom polyethylene model originally proposed by Paul et al.[35] with modifications described by Veld et al[36]. The force field is:

$$E = E_{b,i} + E_{\theta,i} + E_{\tau,i} + E_{LJ,ij}$$

$$= \frac{1}{2}k_b(b_i - b_0)^2 + \frac{1}{2}\frac{k_\theta}{\sin^2\theta_0}(\cos\theta_i - \cos\theta_0)^2 + \sum_{i=1}^{3}k_{\tau,i}(1 - \cos i\varphi) \quad (3.27)$$

$$+ 4\varepsilon\left[\left(\frac{\sigma}{r_{ij}}\right)^{12} - \left(\frac{\sigma}{r_{ij}}\right)^{6}\right]$$

66

with the following parameters: k_b=37.61 kJ/mol/nm^2, b_0=1.53 nm, k_θ=502.1 kJ/mol, θ_0=68.0 degrees, $k_{\tau,1}$=6.69 kJ/mol, $k_{\tau,2}$=-3.63 kJ/mol, $k_{\tau,3}$=13.56 kJ/mol, ε=390.95 J/mol and σ=0.4009 nm. The Lennard-Jones (LJ) cutoff is 2.5σ with a corresponding long-range energy correction.

During a simulation, the following Monte Carlo moves were employed: (1) site translation; (2) reptation; (3) re-bridging[37]; (4) end rotation; (5) end-bridging[38]; and (6) volume change. In the site translation move, the Cartesian coordinates of a single site were changed by a random displacement within a range whose maximum was adjusted to maintain a targeted acceptance of 50%. In the reptation move, a site was removed from one end of a chain and appended to the other end of the same chain or to the end of a different chain, while keeping the bond length and angle constant; the new torsion angle was perturbed from the old one by a random value adjusted to maintain 50% acceptance. In the rebridging move, three consecutive sites were selected at random from the middle of the chain and a nonlinear equation was solved to determine alternative configurations of these three sites that reconnect the chain sections, while keeping bond lengths and angles constant; the move was selected randomly from among these alternative configurations. In the end rotation move, the torsion at a randomly selected chain end was perturbed by a random amount within a range whose maximum was adjusted to maintain the targeted acceptance of 50%. In the end-bridging move, three consecutive sites in the vicinity of a chain end were selected. A nonlinear equation was solved, as in re-bridging, except that the sites were placed so as to connect part of the original chain to the end of its neighbor. In the volume change move, the edge length of the simulation cell was changed by a small random amount, within a range whose maximum was adjusted to maintain the targeted acceptance of 50%, and the chain centers-of-mass were displaced affinely. The attempt frequency and typical fraction of accepted moves (for the isotropic melt) were, respectively: site translation, 0.55 and 0.50; reptation, 0.11 and 0.13; re-bridging, 0.11 and 0.20; end rotation, 0.11 and 0.50; end bridging, 0.11 and 0.10. Volume changes were attempted, on average, once every N moves with an acceptance of 0.50.

The use of variable connectivity moves (reptation and end-bridging) means that the molecular weight of the chains is not fixed during a simulation. The resulting

67

molecular weight (or chemical) polydispersity is controlled through the introduction of conventional residual chemical potentials μ_{MW} for chains of different molecular weight. The subscript MW is used to distinguish this chemical potential from the orientation potential introduced earlier. The following choice of μ_{MW} ensures a flat molecular weight distribution whose polydispersity index is 1.09[39]:

$$\mu_{MW} = 0, \quad for \ \frac{1}{2}\frac{N}{N_{ch}} \leq N_{sites} \leq \frac{3}{2}\frac{N}{N_{ch}}$$

$$\mu_{MW} = -\infty, \quad otherwise \tag{3.28}$$

The parameters used for the simulations were chosen to allow comparison to previously published work[30,33,39] as well as to evaluate the effects of orientation potentials applied to different choices of connector vector in the $[NN_{ch}PT\mu_{MW}\Delta\mu(I)]$ ensemble. In each case the simulations were run with the force field pressure contribution $P=1$ atm, temperature $T=450K$, and μ_{MW} as specified by eq. 3.28. Simulations were run for 2×10^5 to 1×10^6 MC cycles. Block averages of the orientation were used to verify the convergence of the error around the mean value obtained for the simulation. The "local" orientation potential applied to next-nearest neighbor vectors $q^{(2)}$ was of the form prescribed by eq. 3.17 with $K=2$ and only $\mu_{2,x}^{(2)}$ nonzero (the subscript x on $\theta_{i,j,x}^{(2)}$ and $\mu_{2,x}^{(2)}$ is omitted henceforth for simplicity):

$$\mu = \mu_2^{(2)} \sum_{j}^{N_{ch}} \sum_{i}^{n_j} P_2(\cos\theta_{i,j}^{(2)}) \tag{3.29}$$

The orientation potentials employed for each of four system sizes are shown in Table 3.1. For each chain length, an additional simulation with three quarters as many chains was run at the highest orientation potential to ensure that system size effects were negligible.

Table 3.1. Values of orientation potential $\mu_2^{(2)}$ used with eq. 3.29 (in units of kT)

ID	N	N_{ch}	Orientation Potential $(\mu_2^{(2)}/kT)$
C_{24}	768	32	0, 0.025, 0.05, 0.075, 0.1, 0.15, 0.2, 0.25, 0.3, 0.35, 0.4, 0.45
C_{78}	3120	40	0, 0.025, 0.05, 0.075, 0.1, 0.15, 0.2, 0.25, 0.3
C_{156}	3120	20	0, 0.025, 0.05, 0.075, 0.1, 0.15, 0.2, 0.25
C_{400}	3200	8	0, 0.025, 0.05, 0.075, 0.1

Two "molecular" orientation potential forms were tested by applying a potential to the vector $\mathbf{Q}_j$. Their forms were as follows:

$$\mu = \mathbf{\mu}_2^{(S)} : \sum_j^{N_{ch}} \mathbf{S}_j \tag{3.30}$$

with all the components $\mu^{(S)}_{2,ij}=0$ except $\mu^{(S)}_{2,xx}$. In this case, eq. 3.30 simplifies to a form analogous to eq. 3.29, with $\theta_{t,j}^{(2)}$ replaced by the orientation angle $\theta_j^{(Q)}$ formed by the end-to-end vector $\mathbf{Q}_j$ of chain j with respect to the orientation direction:

$$\mu = \mu_{2,xx}^{(S)} \sum_j^{N_{ch}} P_2\left(\cos\theta_j^{(Q)}\right) \tag{3.31}$$

Similarly, the orientation potential given by eq. 3.25 takes the form:

$$\mu = \mu_{2,xx}^{(Q)} \sum_j^{N_{ch}} \Lambda_j^2 P_2(\cos\theta_j^{(Q)}) \tag{3.32}$$

Henceforth, the subscript xx on $\mu_{2,xx}^{(S)}$ and $\mu_{2,xx}^{(Q)}$ are also dropped for simplicity of notation. The orientation potentials employed with eqs. 3.31 and 3.32 are shown in Table 3.2.

Table 3.2. Values of orientation potential used with eq. 3.31 and eq. 3.32 (in units of kT)

MW	N_{sites}	N_{ch}	Physical Isomer Potential	
			$\mu_2^{(S)}/kT$	$\mu_2^{(Q)}/kT$
C_{24}	768	32	0, 0.7, 1.0, 1.4, 3.0	0, 0.9, 1.8, 2.7, 3.6
C_{78}	3120	40	0, 0.4, 0.8, 1.2, 1.6	0, 0.6, 1.2, 1.8, 2.4

3.4. RESULTS AND DISCUSSION

3.4.1. Simulations using the local orientation potential, $\mu_2^{(2)}$

3.4.1.1. Orientational Order and Density.

Fig. 3.1 shows $<P_2(cos\theta^{(2)})>$ as a function of $\mu_2^{(2)}$ for the four different chain lengths listed in Table 3.1. This plot shows that at small orientation potentials, the relationship between $<P_2(cos\theta^{(2)})>$ and $\mu_2^{(2)}$ is linear and independent of the chain length. At larger orientation potential, the orientation order parameter $<P_2(cos\theta^{(2)})>$ increases more sharply, an effect which becomes more pronounced for the longer chains. The differences in response for the different chain lengths can be traced to the lower fraction of chain ends in systems with longer chains. Chains ends tend to reduce the system density and to exhibit greater orientational freedom. Both of these effects necessitate a higher orientation potential to realize a given level of system orientation. Fig 3.2 shows the computed density for systems of different chain length and increasing orientation. The isotropic densities are consistent with the values calculated from the polyethylene equation of state developed by von Meerwall et al[40]. Just as with the orientation, the density behavior changes qualitatively around $\mu_2^{(2)} = 0.15kT$: for $\mu_2^{(2)} < 0.15kT$, the density is roughly constant, while for $\mu_2^{(2)} > 0.15kT$ it increases dramatically. This upturn occurs at a normal stress difference of 15-20 MPa. As shown in the conformation analyses to follow, the two regions suggested by Fig 3.1 and Fig 3.2 correspond to

70
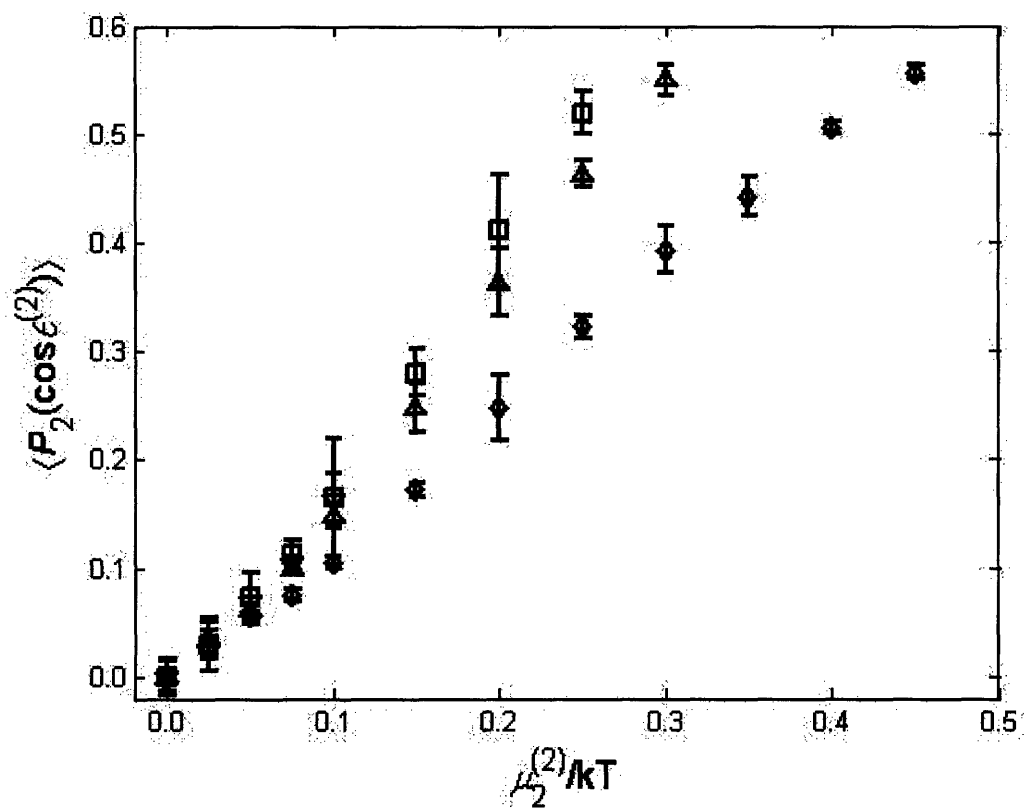
Figure 3.1. $<P_2(\cos\theta^{(2)})>$ of polymer chains as a function of orientation potential for C_{24}
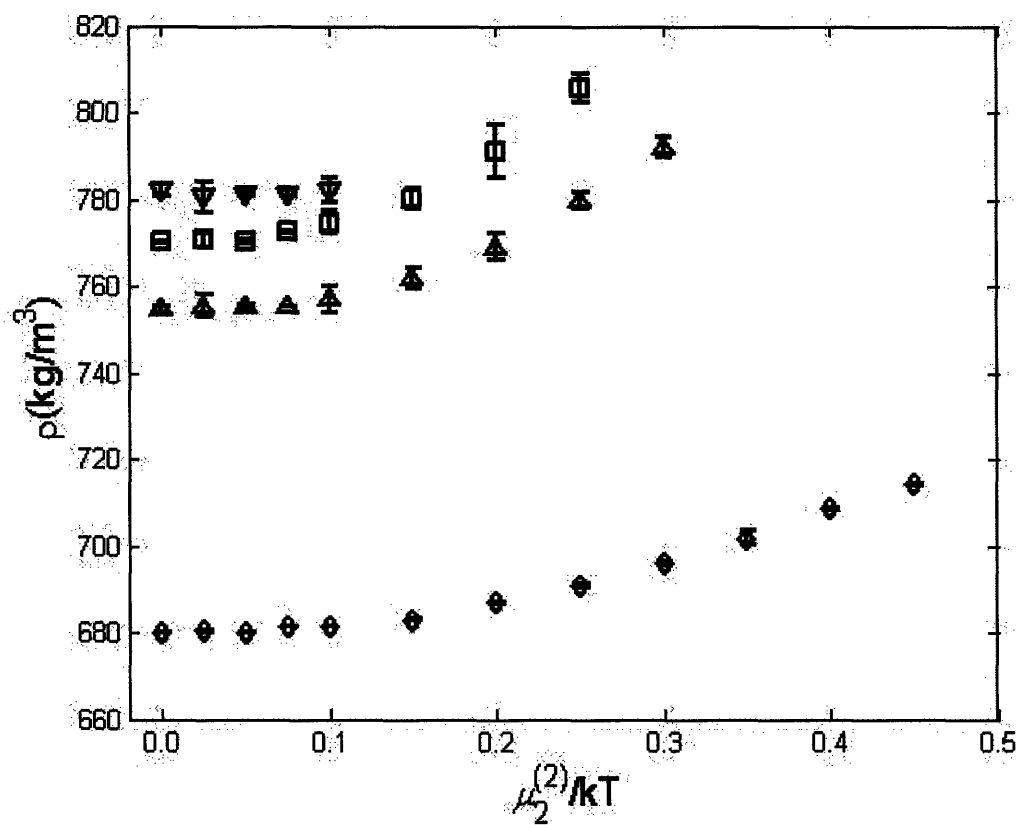
($\lozenge$), C_{78} ($\triangle$), C_{156} ($\square$), C_{400} ($\triangledown$).

Figure 3.2. System density as a function of orientation potential for C_{24} ($\lozenge$), C_{78} ($\triangle$), C_{156} ($\square$), C_{400} ($\triangledown$).

rotation of the *principal axes* of the molecule at low potential, followed by deformation of the molecule and an increase in the number of *trans* torsions at high potential. The latter allows for densification as chains become aligned.

3.4.1.2. Molecular Conformation.

For each individual chain, the radius of gyration tensor is determined from the outer product of the individual intramolecular connector vectors:

$$\mathbf{R}_{g,j}^2 = n_j^{-2} \sum_{i=1}^{n_j-1} \sum_{i'>i}^{n_j} \mathbf{q}^{(i'-i)} \mathbf{q}^{(i'-i)} \tag{3.33}$$

The eigenvalues of this tensor define an ellipsoid that characterizes the size and shape of the molecule, while the eigenvectors define the principal axes and the molecular frame of reference. Averaging the radius of gyration tensor over all chains j and then obtaining the eigenvalues results in a system average molecular shape in the laboratory frame of reference, defined by the orientation potential. Alternatively, determining the eigenvalues molecule by molecule, sorting the eigenvalues for each molecule in decreasing order (i.e. $\lambda_1 > \lambda_2 > \lambda_3$) and then averaging each λ_i over all chains j results in a system averaged molecular shape in the molecular frame of reference, defined by the principal axes of each molecule. The asphericity of the molecule is defined as:

$$a = 1 - \frac{\lambda_2^2 + \lambda_3^2}{2\lambda_1^2} \tag{3.34}$$

where the eigenvalues correspond to those averaged in either the laboratory or the molecular frame of reference. For an isotropic system, the asphericity in the laboratory frame is zero, while that in the molecular frame is significantly different from zero[41]. As shown in Fig 3.3, the asphericity in the laboratory frame increases dramatically at low orientation potential, with little change in asphericity in the molecular frame. This is indicative of rotation of the principal axes of the molecules in response to the orientation potential, with little change in the size or shape of the molecules. At high orientation potential, the molecular asphericity increases, indicative of deformation and

73
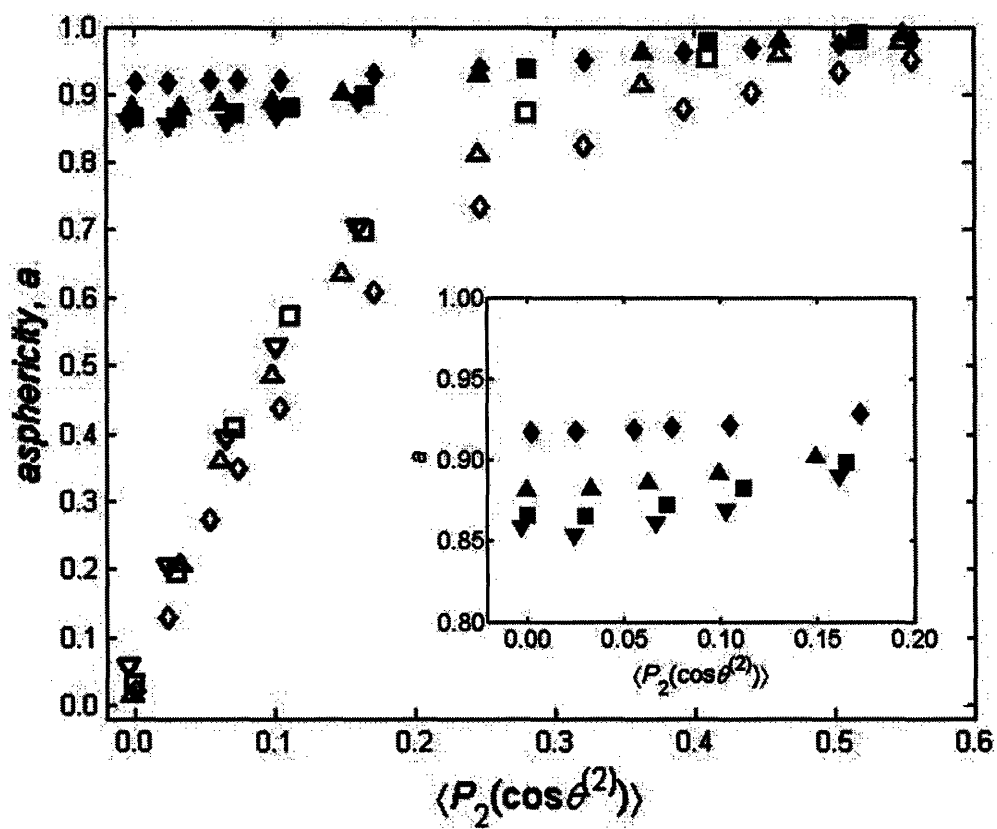
Figure 3.3. Molecular asphericity as a function of orientation order parameter $<P_2(\cos\theta^{(2)})>$; laboratory reference for C_{24} ($\lozenge$), C_{78} ($\triangle$), C_{156} ($\square$), C_{400} ($\triangledown$); molecular reference for C_{24} ($\blacklozenge$), C_{78} ($\blacktriangle$), C_{156} ($\blacksquare$), C_{400} ($\blacktriangledown$). Inset – expanded view of molecular asphericity for low orientation order parameters.

elongation of the molecules. The point at which this change in the behavior of the radius of gyration occurs is commensurate with the changes in density and local orientation order parameter $<P_2(\cos\theta^{(2)})>$ mentioned previously.

Molecular size and shape are altered primarily through unraveling of the molecule via torsional rearrangement. The torsion angle distribution of the molecule thus provides another way to assess whether the orientation is occurring through rotation or deformation of the molecule. Figure 3.4 shows the fraction of torsions in the *trans* state as a function of increasing orientation potential, where torsion angles between $-\pi/3$ and $+\pi/3$ radians were considered to be in the *trans* state. For $\mu_2^{(2)} < 0.15kT$, the *trans* fraction is little changed; for $\mu_2^{(2)} > 0.15kT$, it increases, indicative of an unraveling of the chain.

A comparison of Fig 3.2 and Fig 3.4 reveals that a correlation exists between density and fraction of torsions in the *trans* state. This correlation is shown explicitly in Fig 3.5. It has been proposed that such a relationship could be responsible for the formation of a dense liquid phase in coexistence with a less dense liquid by spinodal decomposition, due to spontaneous segregation of trans-rich regions from trans-poor regions in the melt[42]. Evidence in favor of this spinodal decomposition has been suggested based on small angle X-ray diffraction data on polymer melts[43,44]. The length scale of density fluctuations is on the order of 10-100 nm, larger than the simulations performed here. Thus, the oriented melt phases produced by the SGMC simulation are representative volume elements of the dense liquid phase, and can be used to estimate the free energy of such phases relative to that of the isotropic melt. A first principles analysis of the spinodal decomposition mechanism is thus possible by this approach, but it is beyond the scope of the current work.

3.4.1.3. End-to-End Vector.

We next consider the change in the end-to-end vector of the molecules as the orientation potential is applied for the systems described in Table 3.1. In Fig. 3.6 and Fig. 3.7, molecular orientation order parameter, $<P_2(\cos\theta^{(Q)})>$, where $\theta^{(Q)}$ is the angle
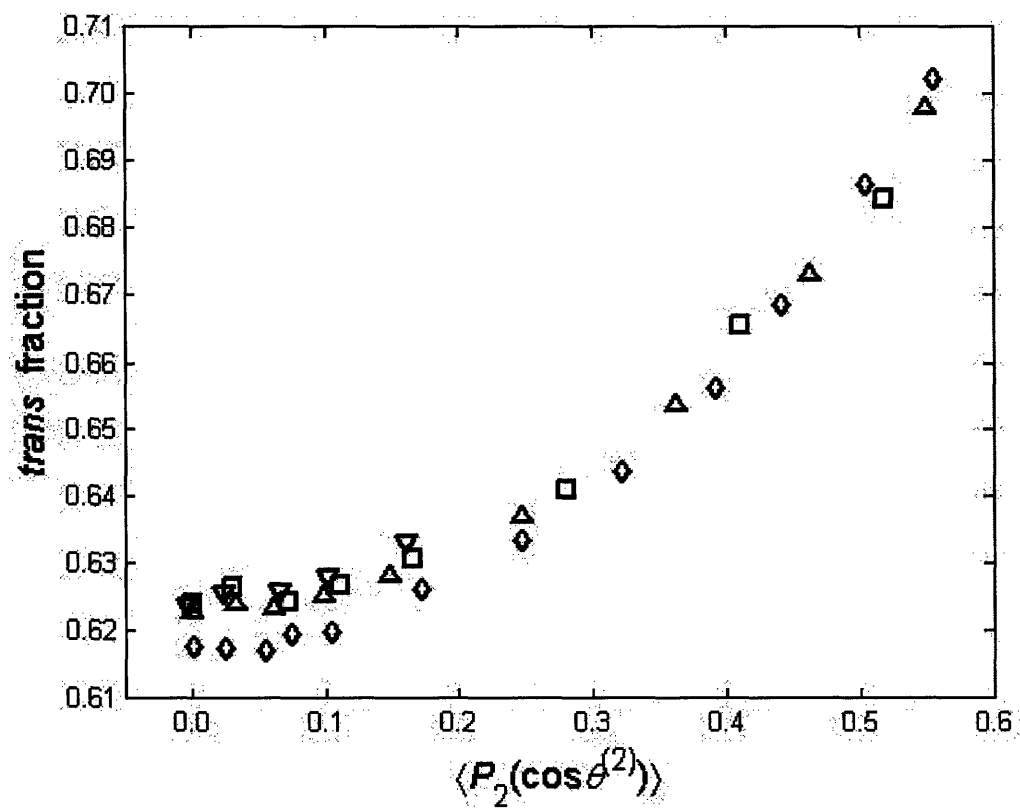
Figure 3.4. Fraction of *trans* bonds as a function of orientation order parameter $<P_2(\cos\theta^{(2)})>$ for C_{24} ($\lozenge$), C_{78} ($\triangle$),C_{156} ($\square$), C_{400} ($\triangledown$).
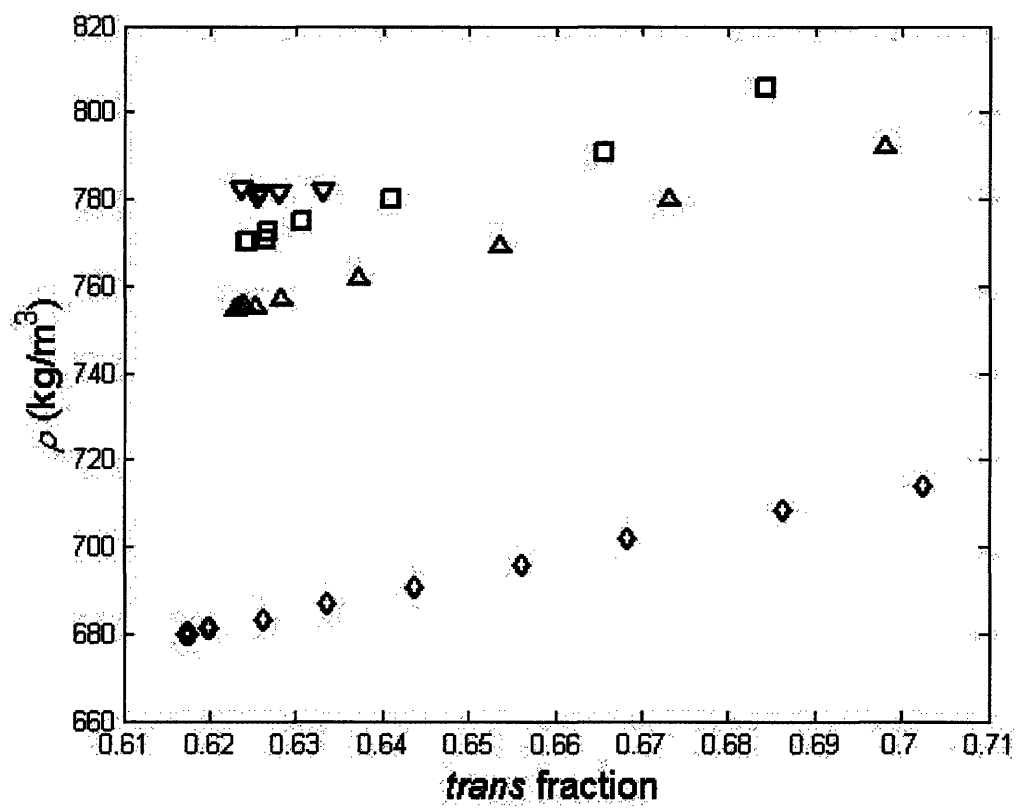
Figure 3.5. Density as a function of the fraction of *trans* bonds for C_{24} ($\lozenge$), C_{78} ($\triangle$),C_{156} ($\square$), C_{400} ($\triangledown$).

formed by the end-to-end vector of the molecule with the orientation axis, and molecular size, Λ^2, respectively, are plotted against the local orientation order parameter, $<P_2(\cos\theta^{(2)})>$, to show the changes in orientation and size of the molecules. At low orientation, the molecular orientation order parameter is roughly proportional to the local orientation order parameter, while the molecular size is essentially unchanged; this regime corresponds to rotation of the principal axes of the molecules in the direction of orientation. Subsequent increases in $<P_2(\cos\theta^{(2)})>$ produce relatively smaller changes in $<P_2(\cos\theta^{(Q)})>$ but larger changes in $<\Lambda^2>$, consistent with significant deformation of the polymer molecules. This effect is stronger for the longer chains.

3.4.2. The Stress-Optical Coefficient

Orientation plays a primary role in the development of birefringence. As the molecules orient, the difference in the optical properties along the chain and perpendicular to the chain produce an increasingly birefringent material. The empirical observation that the birefringence, Δn, is proportional to the normal stress difference $\Delta\tau=\tau_{xx}-\tau_{yy}$ at low $\Delta\tau$ is known as the stress-optical rule. The stress-optical coefficient is defined as:

$$C \equiv \frac{\Delta n}{\Delta \tau} \tag{3.35}$$

This proportionality holds true in regions without significant molecular deformation. The normal stress difference $\Delta\tau$ can be measured through the determination of the forces originating with the physical isomeric potential as shown in the appendix to this chapter, and the birefringence Δn is calculated as described by Mavrantzas and Theodorou[31]:

$$\Delta n = \frac{2}{9\pi} \frac{N}{V} \frac{(n^2+2)^2}{n} (\alpha_{11}^{(opt)} - \frac{\alpha_{22}^{(opt)} + \alpha_{33}^{(opt)}}{2}) \left\langle P_2(\cos\theta^{(2)}) \right\rangle \tag{3.36}$$

The values of the diagonal elements of the optical polarizability tensor $\alpha^{(opt)}$ represent the principal components for a fully trans conformation of PE. The values, $\alpha^{(opt)}{}_{11}=2.458$, $\alpha^{(opt)}{}_{22}=1.903$ and $\alpha^{(opt)}{}_{33}=1.458$, were obtained from Mavrantzas and Theodorou[31] and assume an equilibrium bond angle complement of $68°$; N/V is the number density of

78
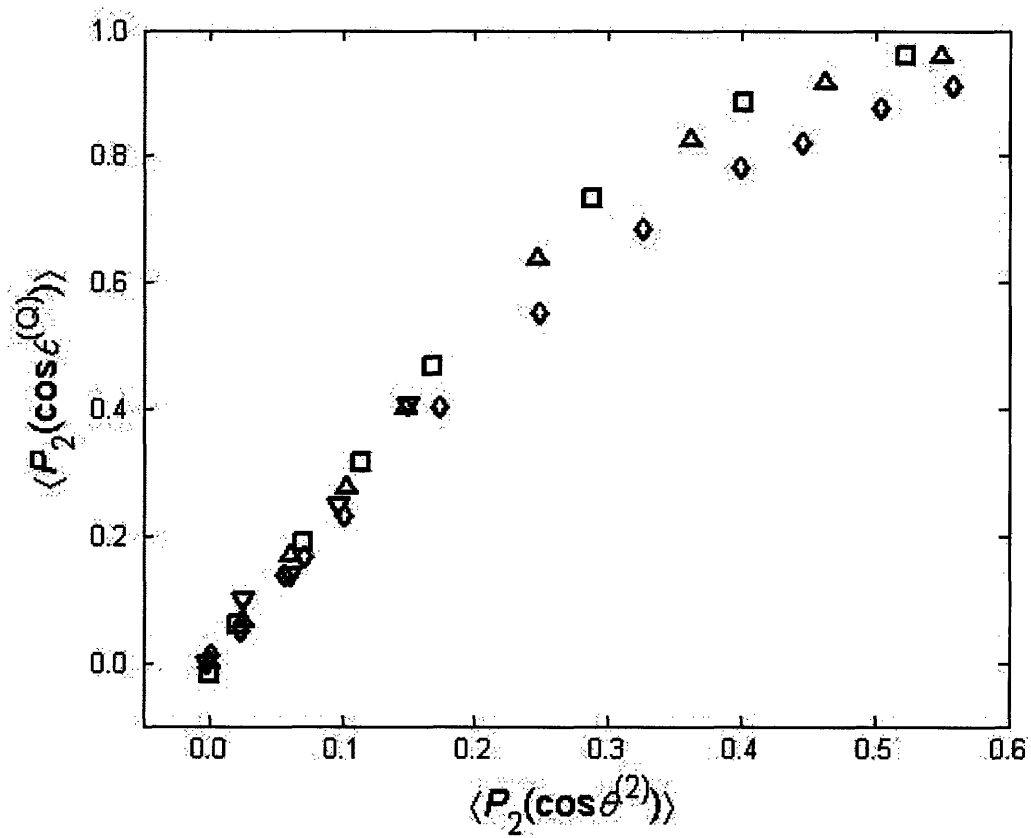
Figure 3.6. Molecular orientation order parameter versus local orientation order parameter for C_{24} ($\lozenge$), C_{78} ($\triangle$), C_{156} ($\square$), C_{400} ($\triangledown$).
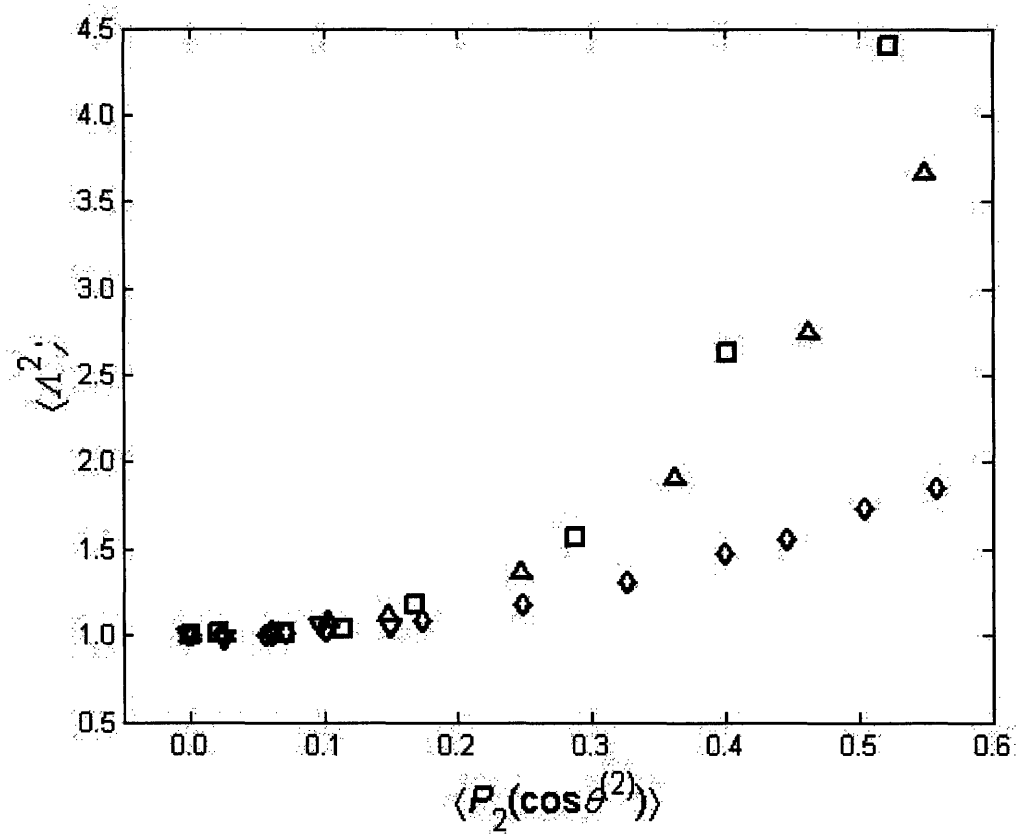
Figure 3.7. Molecular size as a function of local chain direction for C_{24} ($\lozenge$), C_{78} ($\triangle$),C_{156} ($\square$), C_{400} ($\triangledown$).

polarizable species; The refractive index n of polyethylene is described by the following relation[45]:

$$\rho(g/cc) = 0.3276\frac{n^2-1}{n^2+2} \qquad (3.37)$$

While the birefringence is most strongly affected by orientation, it is also dependent on density, as apparent from eqs 3.36 and 3.37.

From a series of simulations, Mavrantzas and Theordorou[31,32] calculated C for polyethylene to within 35% of its experimentally observed value. They attributed the error to the intrinsic stiffness of their intramolecular potential, but acknowledged that the observed length dependence of this quantity could indicate artifacts in the simulation due to the choice of state variable. The accurate calculation of C is significant in the current context, since Δn depends primarily on the local chain direction, and $\Delta\tau$ is sensitive to the manner in which the orientation potential is applied.

Reported experimental values of C for polyethylene melts are 2.0 GPa^{-1} (403K)[46] and 2.2 GPa^{-1} (413K)[47]. Fig. 3.8 shows the plot of $\Delta\tau$ vs. Δn, with an expanded view of the region at low $\Delta\tau$ shown in fig. 3.9. Fig. 3.9 shows that the relationship is approximately linear for $\Delta\tau<15$ MPa. At larger $\Delta\tau$, the relationship becomes non-linear, coincident with the crossover from molecular rotation to molecular deformation. Changes in birefringence due to density account for only about 5% of C for the highest orientations of C_{24}, C_{78}, and C_{156}.

Two linear regressions of the data are shown in Fig. 3.9: The lower regression uses all of the points below 4MPa and yields an estimate for the stress optical coefficient C of 2.1 GPa^{-1}; the upper regression uses all of the points shown except the C_{24} points > 7MPa and yields a C of 2.4 GPa^{-1}. Both are in good agreement with the experimental data. One notable feature of these results is that they do not reproduce the large MW dependence seen by Mavrantzas and Theodorou[31,32] in which C exhibited a maximum for C_{78}, with a value almost 3 times that obtained for high molecular weight polyethylene. As shown in Figure 3.10, our results indicate that C approaches an asymptotic value of about 2.5 GPa^{-1} for high molecular weight polyethylene. The shape of this curve mirrors
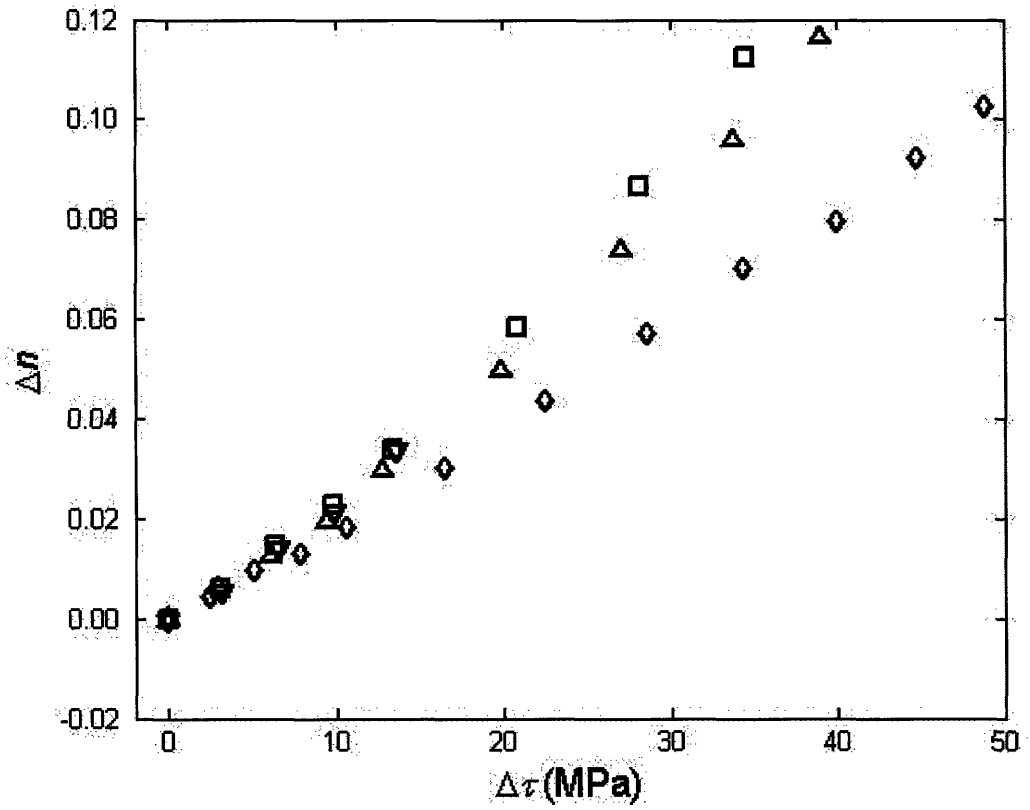
Figure 3.8. Birefringence as a function of normal stress difference for C_{24} (◊), C_{78} (△),C_{156} (□), C_{400} (▽).
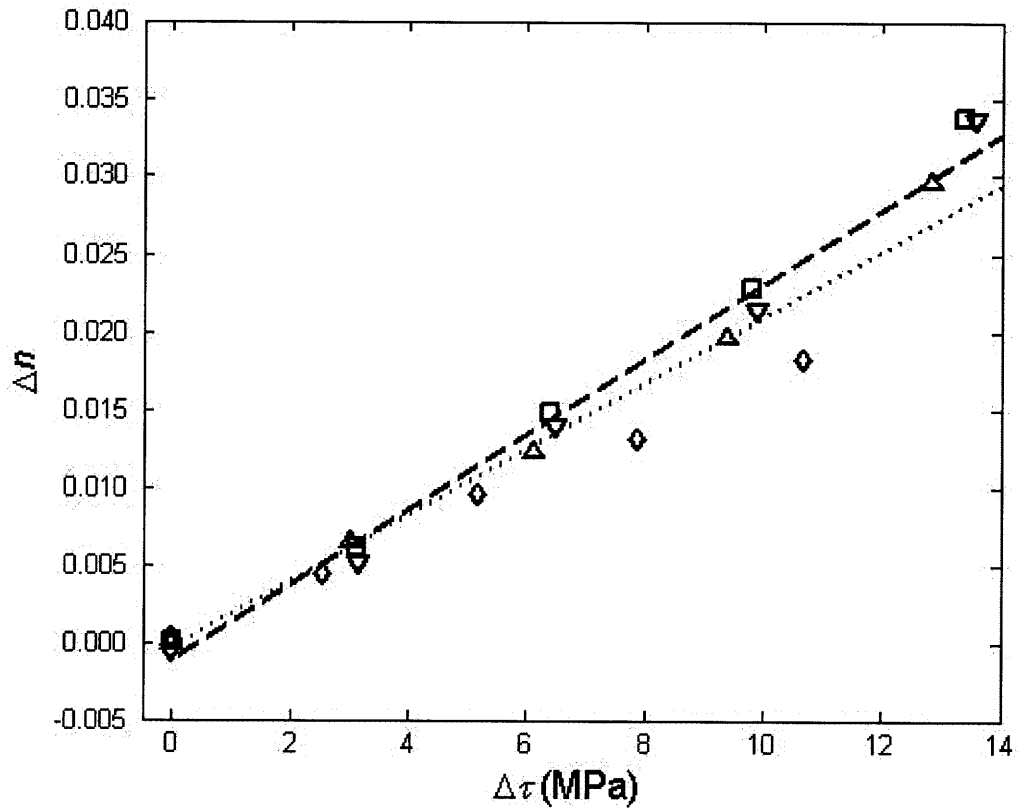
Figure 3.9. Birefringence as a function of normal stress difference for C_{24} ($\Diamond$), C_{78}

($\triangle$),C_{156} ($\square$), C_{400} (∇). The lower line represents a fit of the data below $\Delta\tau=7$ MPa; the

upper line uses all of the points shown except for the C_{24} data above $\Delta\tau=7$ MPa.
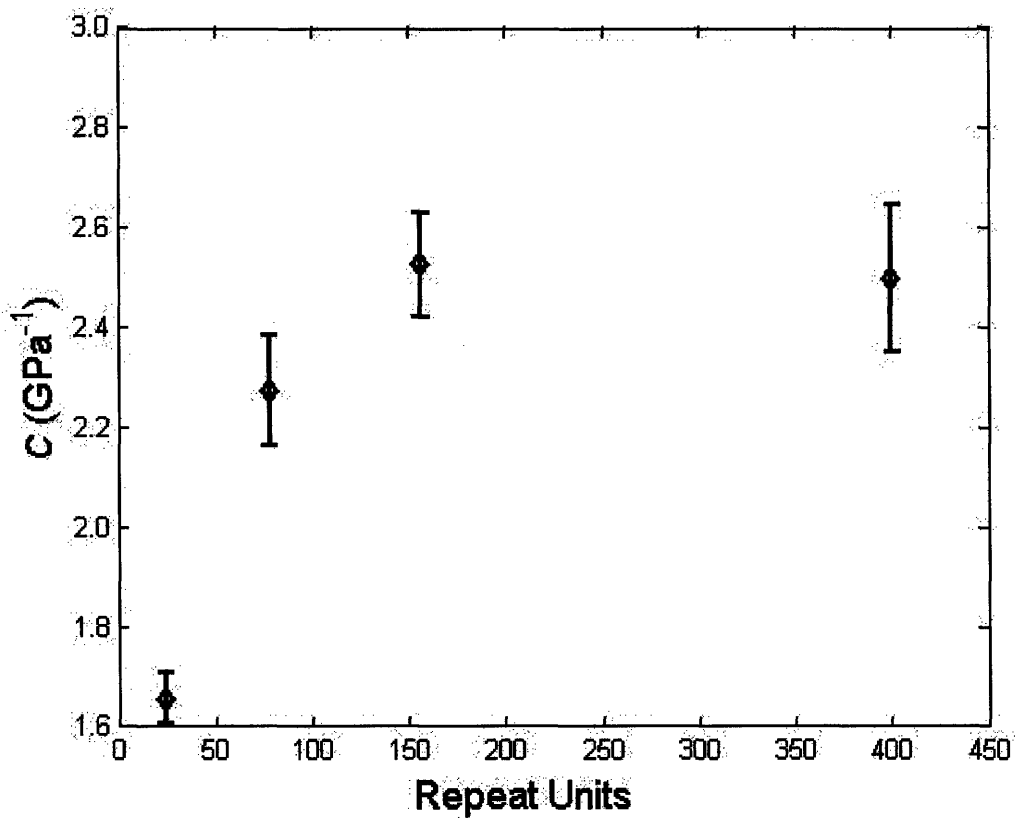
Figure 3.10. Stress Optical Coefficient (C) as a function of number of repeat units; Each point is a regression of the data shown in Figure 3.9.

that of the simulated isotropic refractive index n, which also reaches its asymptotic value at a chain length of about 150 carbons.

3.4.3. Work of orientation

The SGMC method minimizes the free energy of the system simulated. A useful consequence of this is that one can obtain the reversible work of orientation through a thermodynamic integration with respect to the orientation potential μ. The work of orientation is taken with reference to the isotropic state at the same pressure and temperature. We computed the integral using the self-consistent histogram method[17]. Fig. 3.11 shows that the work of orientation for the potential defined in eq. 3.29 is molecular weight-dependent and that it requires less work to orient the longer chains. The ability to calculate the free energy allows us to determine the relative contributions of the loss of entropy and of the change in enthalpy, as shown in Fig. 3.12. We observe that the enthalpic contribution to the work of orientation is comparable for all four molecular weights; the greater work required to orient the C_{24} chains is due to the larger entropy to be overcome for this low molecular weight system.

3.4.4. Simulations using the End-to-End Potentials, $\mu_2^{(S)}$ and $\mu_2^{(Q)}$

The results presented in the preceding section were generated exclusively through the application of a local orientation potential, according to eq. 3.29. Next, we discuss results from simulations using the potentials (eqs. 3.31 and 3.32) acting on Q_j. The potential described by eq. 3.32 in particular reproduces simulations similar to those of refs. 30-33 for the case of a traceless α tensor and a single conformation tensor model. The traceless form of α is consistent with the kinematic interpretation presented in ref. 33 for uniaxial elongational flow. Unfortunately, there are non-trivial differences in the polyethylene force field, in the applied potential, and in the measured quantities between

85
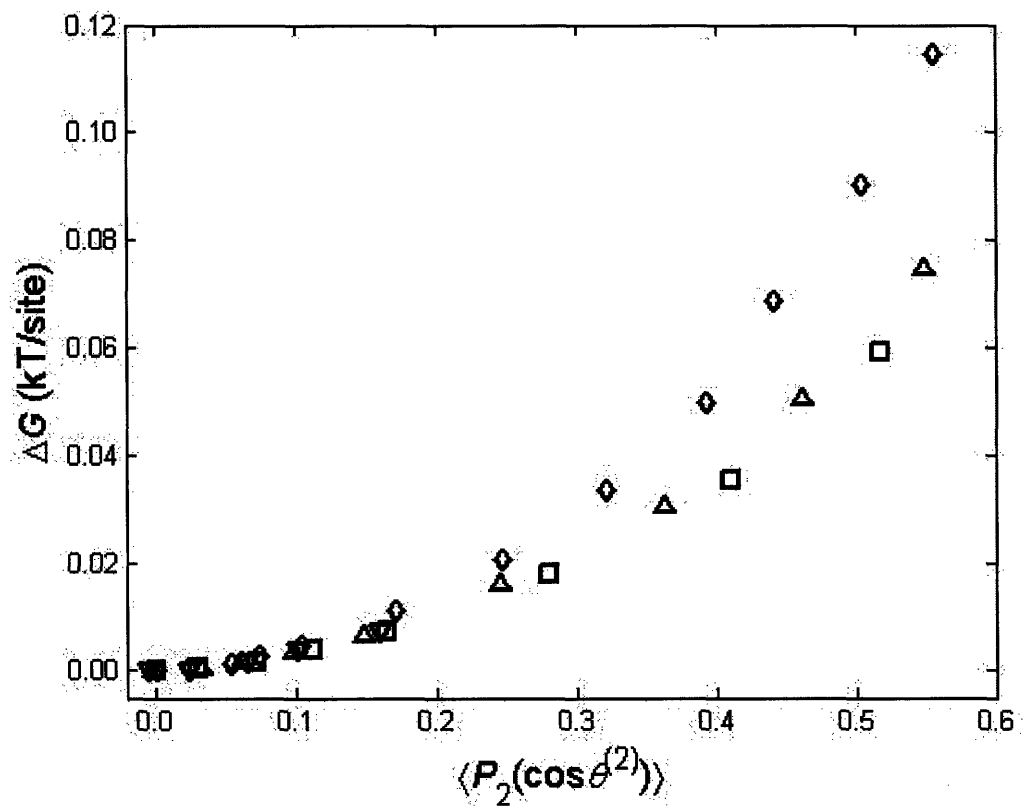
Figure 3.11. Free energy as a function of orientation order parameter for C_{24} ($\lozenge$), C_{78} ($\triangle$),C_{156} ($\square$), C_{400}($\triangledown$).
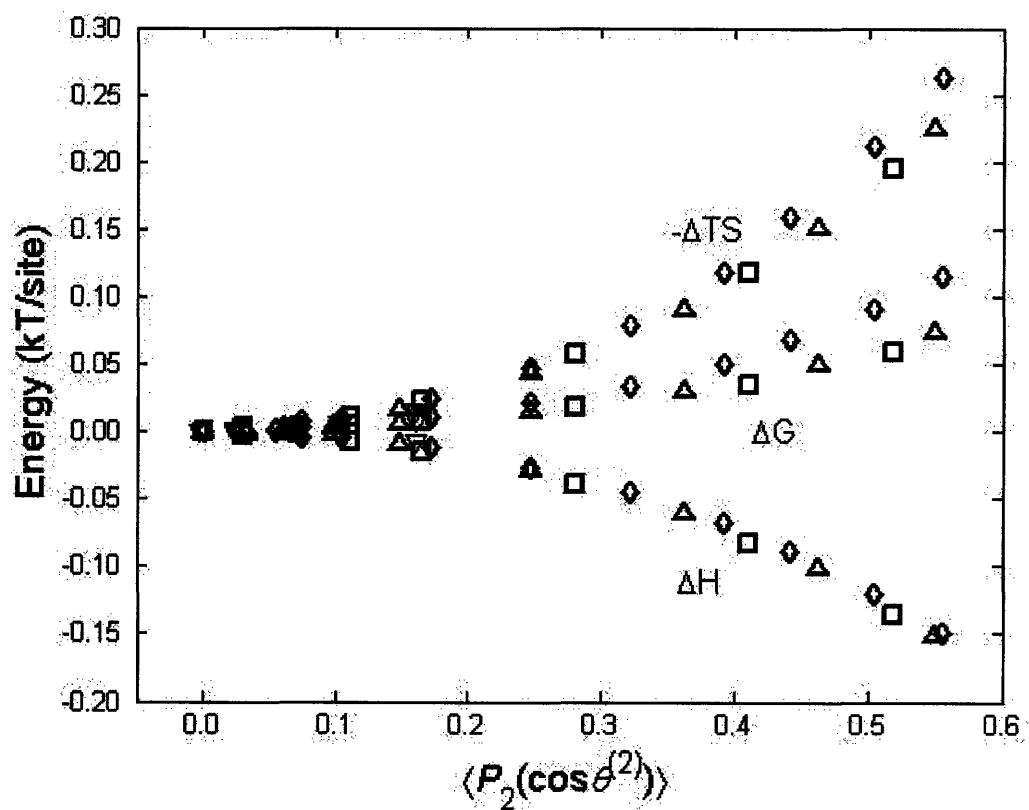
Figure 3.12. Contributions to the free energy as a function of orientation for C_{24} ($\Diamond$), C_{78} ($\triangle$), C_{156} ($\square$), C_{400} (∇).

the present work and those referenced: refs. 30-32 use an α that is not traceless; ref. 33 employs a traceless α, but applies it to a multiple conformation tensor model based on normal modes rather than as defined in refs. 30-32 and in eq. 3.18 here. Nevertheless, the response of the conformation tensor components $<c_{xx}>$ and $<c_{yy}>$ versus $\Delta\tau$ from the C_{78} simulations using eq. 3.32 are in reasonable accord with the corresponding first normal modes plotted in Fig. 1 of ref. 3.33 (data not shown) and confirm the analogous behavior of the two approaches.

Of course, in the spirit of modeling experimental data, the SGMC approach presented here presupposes some knowledge about the chain conformation, such as the conformation tensor predicted by rheological modeling. The melt elasticity approach presumes instead a kinematic interpretation of α in terms of velocity gradients[33]. Either way, the information provided to the simulation is molecular in nature rather than local, as was the case for birefringence measurements. Thus, it may produce a qualitatively different picture of the ordering of the molecule. One of the most striking demonstrations of this is the relationship between $<P_2(\cos\theta^{(2)})>$ and $<P_2(\cos\theta^{(Q)})>$ shown in Fig. 3.13. Compared to Fig 3.6, the local orientation $<P_2(\cos\theta^{(2)})>$ is much lower for the same $<P_2(\cos\theta^{(Q)})>$ when the potential is applied to the end-to-end vectors. The two end-to-end potentials produce similar results even though one acts on both the orientation and size of the conformation tensor while the other acts only on the orientation of the principal axes of conformation tensor. The proportionality between $<P_2(\cos\theta^{(Q)})>$ and $<P_2(\cos\theta^{(2)})>$ is molecular weight dependent for all values of the molecular orientation potentials $\mu^{(Q)}_2$ and $\mu^{(S)}_2$. This contrasts with the situation for $\mu^{(2)}_2$, which is molecular-weight independent for $\mu^{(2)}_2 < 0.15kT$. This can be explained by the nature of the potential in the two instances. For the end-to-end potential, if the entire chain is properly equilibrated, one expects additivity of the local orientation such that $<P_2(\cos\theta^{(Q)})> \approx (n_j-1)<P_2(\cos\theta^{(2)})>$, because of the long-range correlation. For a local orientation potential, the correlations along the chain contour and thus the persistence length are independent of chain length, provided the chains are of sufficient length. This is exactly what we observe; the best-fit slopes of the lines in Fig. 3.13 are 79 and 22, in good agreement with

88
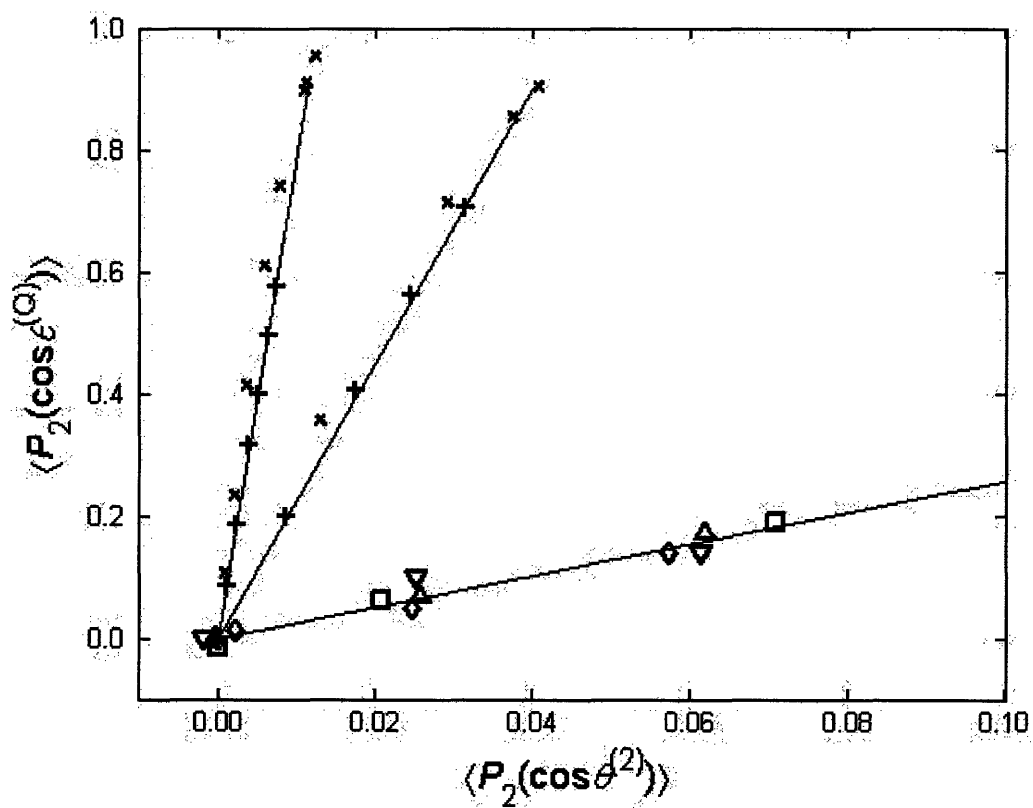
Figure 3.13. Molecular orientation order parameter as a function of local orientation order parameter. Application of the local potential $\mu_2^{(2)}$ for C_{24} ($\Diamond$), C_{78} ($\triangle$),C_{156} ($\square$), C_{400} (∇); application of the end-to-end potential $\mu_2^{(S)}$ (+) and $\mu_2^{(Q)}$ (x) for C_{24} (intermediate line) and C_{78} (leftmost line). Lines are best-fit with slopes of 79, 22, and 2.5.

$(\langle n_j \rangle - 1)$ for $\langle n_j \rangle = 78$ and 24, respectively. For the local orientation, the slope is about 2.5 and independent of chain size for low degrees of orientation.

3.5. Conclusion

We describe a general strategy for using Monte Carlo simulation in the semi-grand canonical ensemble to study non-equilibrium polymer systems. The method takes advantage of a generalized treatment of speciation of a system to encompass physical species, as well as chemical species; the thermodynamics are otherwise unaltered. The physical speciation is then allowed to be polydisperse and the distribution transformed so that a more convenient set of species types is defined for the case of orientation. Assigning potentials to one or more members of the new list of physical species allows the method to be applied to a wide variety of experimental methods; it is sufficient that the measured property can be computed as an ensemble average of individual molecular conformations. We have shown how the local orientation, characterized through measurements of birefringence for example, can be used to infer information about the molecular shape, torsion distributions, and work of orientation. These results produce the most likely ensemble of structures by taking the least restrictive interpretation of the data.

For the specific case of polyethylene, our results confirm two qualitatively different mechanisms for orientation, also observed by Mavrantzas and Theodorou[30], with a transition occurring at a normal stress difference of approximately 15-20 MPa for all molecular weights studied. Below this point, the molecular axes undergo rotation with little molecular deformation. We also observe a proportionality between the local and end-to-end orientation order parameters $\langle P_2(\cos\theta^{(2)}) \rangle$ and $\langle P_2(\cos\theta^{(Q)}) \rangle$ that is independent of the molecular weight. We estimate the stress-optical coefficient in good agreement with the literature values and find it to be relatively insensitive to molecular weight for C_{78} and higher. The most important factor that limits the range of applicability of the stress-optical rule is the degree to which orientation occurs primarily through molecular rotation; changes in the density account for a small part of the non-linearity in

the SOC. At higher normal stress difference, the molecules experience significant deformation, as characterized by the *trans* fraction of torsions, the end-to-end vectors, and the asphericity of the molecules.

We also show that different results are obtained depending on whether the orientation is applied locally, to bond segments, or at the molecular level, to the end-to-end vector. The latter is well described by the additivity of the local order parameter. Studies probing oriented polyethylene melts simultaneously at different length scales would provide guidance as to which of these physical potentials is more relevant. Bent and coworkers[48] have performed simultaneous birefringence and SANS measurements of non-equilibrium polystyrene melts. However, such experiments are currently lacking for polyethylene, to the best of our knowledge.

3.6 Appendix - Normal Stress Calculation

We demonstrate the calculation of the virial stress contributions of the terms containing $\mu_2^{(Q)}$ (eq. 3.25) and $\mu_2^{(S)}$ (eq. 3.26) for which the end-to-end vector is Q_j. The results for the end-to-end connector can be generalized to other connector vectors.

Contribution of $\mu_2^{(S)}$:

We are concerned only with the diagonal components of the virial tensor since: (1) off-diagonal components are *on average* zero; and (2) only the diagonal components contribute to the pressure and to the normal stress difference. Thus, only one subscript is used to specify the component of the tensors $\mu_2^{(S)}$ and $\mu_2^{(Q)}$, and the subscript '2' is dropped to simplify notation. The trace of the virial stress due to the applied physical potential $\mu^{(S)}$ for an individual end-to-end vector (or connector vector) is calculated as:

$$tr\left(\mathbf{W}^{(\mu)}\right) = \sum_i W_{ii}^{(\mu)} = \sum_i Q_i \frac{\partial}{\partial Q_i}\mu^{(S)} : \mathbf{S} = \sum_i Q_i \frac{\partial \sum_j \mu_j^{(S)} P_2(Q_j)}{\partial Q_i} \qquad (3.38)$$

where i and j both index Cartesian coordinates. Performing the partial differentiation for $P_2(Q_j) = \frac{1}{2}\left(3Q_j^2/|\mathbf{Q}^2| - 1\right)$, eq. 3.38 becomes:

$$tr\left(\mathbf{W}^{(\mu)}\right) = 3\sum_i\left(\mu_i^{(S)}\frac{Q_i^2}{\left|\mathbf{Q}^2\right|} - \frac{Q_i^2}{\left|\mathbf{Q}^2\right|}\sum_j\mu_j^{(S)}\frac{Q_j^2}{\left|\mathbf{Q}^2\right|}\right)$$

$$= 3\left(\sum_i\mu_i^{(S)}\frac{Q_i^2}{\left|\mathbf{Q}^2\right|} - \sum_j\mu_j^{(S)}\frac{Q_j^2}{\left|\mathbf{Q}^2\right|}\right) = 0 \qquad (3.39)$$

Eq 3.39 shows that there is no change in the pressure of the system due to the application of an arbitrary $\{\mu_i^{(S)}\}$.

Defining $M_i = \mu_i^{(S)}Q_i^2/\left|\mathbf{Q}^2\right|$ and taking the sum over the N_μ interactions in the system volume V, the normal stress difference for a uniaxial potential is seen to be:

$$\Delta\tau^{(\mu)} = \frac{N_\mu\left\langle W_{xx}^{(\mu)} - W_{yy}^{(\mu)}\right\rangle}{V} = \frac{N_\mu}{V}\left\langle M_x - M_y + \frac{Q_y^2 - Q_x^2}{\left|\mathbf{Q}^2\right|}\sum_j M_j\right\rangle \qquad (3.40)$$

Contribution of $\mathbf{\mu}_2^{(Q)}$:

Similarly, the trace of the virial stress due to a the applied physical potential $\mathbf{\mu}^{(Q)}$ for an individual end-to-end vector (or connector vector) can be calculated:

$$tr\left(\mathbf{W}^{(\mu)}\right) = \sum_i W_{ii}^{(\mu)}$$

$$= \sum_i Q_i\frac{\partial}{\partial Q_i}\Lambda^2\mathbf{\mu}^{(Q)} : \mathbf{S} \qquad (3.41)$$

$$= \frac{1}{2\left\langle\left|\mathbf{Q}^2\right|\right\rangle_0}\sum_i Q_i\frac{\partial\sum_j\mu_j^{(Q)}\left(3Q_j^2 - \left|\mathbf{Q}^2\right|\right)}{\partial Q_i}$$

Partial differentiation obtains the following expression for the pressure contribution:

$$tr\left(\mathbf{W}^{(\mu)}\right) = \frac{1}{\left\langle\left|\mathbf{Q}^2\right|\right\rangle_0}\sum_i Q_i^2\left(3\mu_i^{(Q)} - \sum_j\mu_j^{(Q)}\right) \qquad (3.42)$$

If we consider a traceless form of $\mathbf{\mu}$ ($=2\mathbf{\alpha}$) the final result is:

$$tr\left(\mathbf{W}^{(\mu)}\right) = \frac{3\sum_i\mu_i^{(Q)}Q_i^2}{\left\langle\left|\mathbf{Q}^2\right|\right\rangle_0} \neq 0 \qquad (3.43)$$

The contribution to the pressure will therefore be:

92

$$\Delta P^{(\mu)} = \frac{N_\mu tr(\mathbf{W}^{(\mu)})}{V} = \frac{3N_\mu}{V}\left\langle \frac{\sum_i \mu_i^{(Q)} Q_i^2}{\langle|\mathbf{Q}^2|\rangle_0} \right\rangle \qquad (3.44)$$

This accounts for the necessary introduction of a conjugate variable to the volume of $P=3b+\Delta P^{(\mu)}$ where b is the conjugate thermodynamic variable to volume in the constant pressure simulations.

Comparison of normal stresses using the virial equation, and the orientation fluctuations

Eq. 3.40 can be used to calculate the normal stress difference from a local physical isomer potential by replacing N_μ with the number of interactions N-$2N_{ch}$ and $\mathbf{Q}$ with $\mathbf{q}^{(2)}$. Alternatively, one could obtain this quantity from the average virial stresses. However, the use of eq. 3.40 is more accurate. Figure 3.14 shows a comparison of the two methods for calculating the normal stress differences for the series of simulations on C_{78} chains using a local isomer potential $\mu_2^{(2)}$. The error bars are only shown for the normal virial stress differences for clarity; the error bars on the normal stress differences calculated using eq. 3.41 are one half, or less, the size of the error bars on the virial. This shows the consistency of this approach with the simulation results.

93
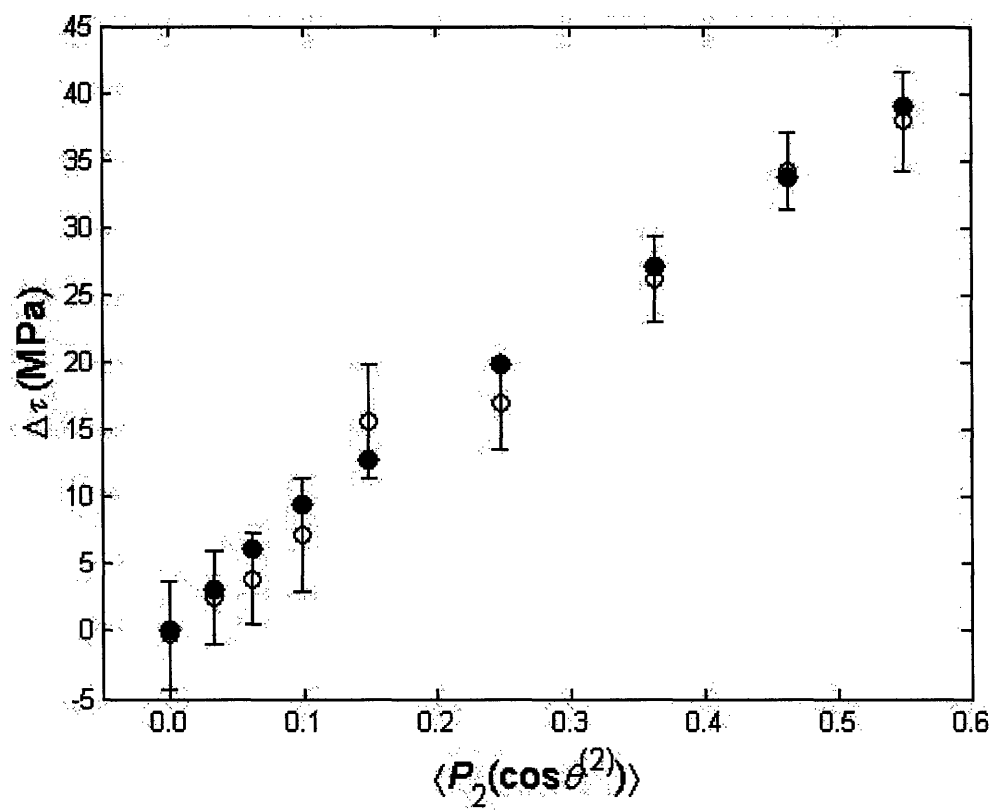
Figure 3.14. Open circles, with error bars represent the normal stress difference measured using the molecular virial stress; the filled circles represent the normal stress difference calculated from eq. 3.41.

3.7 References

[1]   G.C. Rutledge, *Phys. Rev. E* **2001**, *63*, 021111.

[2]   K. Schmidt-Rohr, M. Hehn, D. Schaeffer, H.W. Spiess, *J. Chem. Phys.* **1992**, *97*, 2247.

[3]   R.H. Lewis, H.W. Long, K. Schmidt-Rohr, H.W. Speiss, *J. Mag. Res., Ser. A* **1995**, *115*, 26.

[4]   P. Robyr, B.H. Meier, R.R. Ernst, *Chem. Phys. Lett.* **1991**, *187*, 471.

[5]   M.Y. Liao, G.C. Rutledge, *Macromolecules* **1997**, *30*, 7546.

[6]   *Structure and Properties of Oriented Polymers*; I.M. Ward, Ed.; Chapman and Hall: London, 1997.

[7]   L.M. Martyushev, V.D. Seleznev, *Phys. Rep.* **2006**, *426*, 1.

[8]   R.L. McGreevy, *J. Phys. Cond. Matt.* **2001**, *13*, R877.

[9]   I.M. Fouda, H.M. Shabana, *Polym. Int.* **1999**, *48*, 181.

[10]   M.A. Mabrouk, M.A. Shams-Eldin, *Pure Appl. Opt.* **1996**, *5*, 929.

[11]   H. Shan, J.L. White, *J. Appl. Poly. Sci.* **2004**, *93* 9.

[12]   M.J. Ko, N. Waheed, M.S. Lavine, G.C. Rutledge, *J. Chem. Phys.* **2004**, *121*, 2823.

[13]   A. Koyama, T. Yamamoto, K. Fukao, Y. Miyamoto, *J. Macromol. Sci. Phys.* **2003**, *B42*, 821.

[14]   J.G. Briano, E.D. Glandt, *J. Chem. Phys.* **1984**, *80*, 3336.

[15]   M. Bathe, G.C. Rutledge, *J. Comput. Chem.* **2003**, *24*, 876.

[16]   N.B. Wilding, *J. Chem. Phys.* **2003**, *119*, 12163.

[17]   A.M. Ferrenberg, R.H. Swendsen, *Phys. Rev. Lett.* **1989**, *63*, 1195.

[18]   N. Gō, *Annu. Rev. Biophys. Bioeng.* **1983**, *12*, 183.

[19]   A.K. Soper, *Chem. Phys.* **1996**, *202* 295.

[20]   A.P. Lyubartsev, A. Laaksonen, *Phys. Rev. E* **1995**, *52*, 3730.

[21]   H. Meyer, R. Biermann, R. Faller, D. Reith, F. Muller-Plathe, *J. Chem. Phys.* **2000**, *113*, 6264.

[22]   S. Jain, S. Garde, S.K. Kumar, *Ind. Eng. Chem. Res.* **2006**, *45*, 5614.

[23]   F.L. Colhoun, R.C. Armstrong, G.C. Rutledge, *Macromolecules* **2002**, *35*, 6032.

[24]   E.T. Jaynes, *Phys. Rev.* **1957**, *106*, 620

[25]   M. van Gurp, *J. Rheol.* **1998**, *42*, 1269.

[26]   A. Tagliani, *J. Math. Phys.* **1993**, *34*, 326.

[27]   L.R. Mead, N. Papanicolaou, *J. Math. Phys.* **1984**, *25*, 2404.

[28]   S. Guiasu, *Information Theory with Applications*, McGraw-Hill Intl.: New York, 1977; Chapter 4.

[29]   N. Agmon, Y. Alhassid, R.D. Levine, *J. Comp. Phys.* **1979**, *30*, 250.

[30]   V.G. Mavrantzas, D.N. Theodorou, *Macromolecules* **1998**, *31*, 6310.

[31]   V.G. Mavrantzas, D.N. Theodorou, *Comp. Theor. Polym. Sci.* **2000**, *10*, 1.

[32]   V.G. Mavrantzas, D.N. Theodorou, *Macromol. Theor. Sim.* **2000**, *9*, 500.

[33]   V.G. Mavrantzas, H.C. Öttinger, H. C. *Macromolecules* **2002**, *35*, 960.

[34]   H.C. Öttinger, *Rheol. Acta* **2001**, *40*, 317.

[35]   W. Paul, D.Y. Yoon, G.D. Smith, *J. Chem. Phys.* **1995**, *103*, 1702.

[36]   P.J. in't Veld, M. Hutter, G.C. Rutledge, *Macromolecules* **2006**, *39*, 439.

[37]   L.R. Dodd, T.D. Boone, D.N. Theodorou, *Mol. Phys.* **1993**, *78*, 961.

[38]   P.V.K. Pant, D.N. Theodorou, *Macromolecules* **1995**, *28*, 7224.

[39]   V.G. Mavrantzas, T.D. Boone, E. Zervopoulou, D.N. Theodorou, *Macromolecules*, **1999**, *32*, 5072.

[40]   E. von Meerwall, S. Beckman, J. Jang J, W.L. Mattice, *J Chem Phys* **1998**, *108*, 4299.

[41]   K. Solc, *J. Chem Phys.* **1971**, *55*, 335.

[42]   P.D. Olmstead, W.C.K. Poon, T.C.B. McLeish, N.J. Terrill, A.J. Ryan, *Phys. Rev. Lett.* **1998**, *81*, 373.

[43]   M. Imai, K. Kaji, *Polymer* **2006**, *47*, 5544.

[44]   A.J. Ryan, J.P.A. Fairclough, N.J. Terrill, P.D. Olmstead, W.C.K. Poon, *Faraday Discuss.* **1999**, *112*, 13.

[45]   R.K. Krishnaswamy, J. Janzen, *Polym. Test.* **2005**, *24*, 762.

[46]   D.W. Saunders, *Trans. Faraday Soc.* **1956**, *52*, 1425.

[47] H. Janeschitz-Kriegl, *Polymer Melt Rheology and Flow Birefringence*; Springer-Verlag: Berlin, 1983.

[48] J.F. Bent, R.W. Richards, T.D. Gough, *Rev. Sci. Inst.* **2003**, *74*, 4052.

Chapter 4

A Method for the Estimation of Macromolecular Configurational Properties from Atomistic Simulations of Oligomers under Non-equilibrium Conditions

4.1. Introduction

Rheologists and others who study melt phase flows are interested in both the molecular-scale and continuum scale properties of polymer melts. For example, the configuration tensor <QQ>, defined as the ensemble averaged outer product of the end-to-end vector **Q** of the melt phase molecules, is often assumed to provide information necessary and sufficient to predict the stress on a macromolecule using, e.g., the Giesekus model[1,2]. Since the time and length scales necessary to describe polymers span several orders of magnitude, a multiscale modeling strategy is required to link the atomic-level structural information with the behavior of <QQ>, from which rheological phenomena can be understood.

A typical strategy is to represent a polymer as a series of beads and springs, e.g. finite extensibility nonlinear elastic dumbbell (FENE) models[3]. However, such models have been found to underestimate the experimentally measured stress required to obtain a given value of <QQ> in strong extensional flow[4]. The discrepancies of the FENE model can be attributed to its configuration distribution, which is always Gaussian and fails to reproduce the non-Gaussian behavior that accompanies breakdown of the stress-optical relationship[5]. The method presented here provides a quantitative description of

the principal components of <**QQ**> valid even at conditions where the stress-optical rule is no longer valid.

We accomplish this by applying a local orientational bias to the polymer chain, which accurately reproduces the stress-optical relationship for polyethylene, as we have shown in Chapter 3. The fundamental difference between this approach and that of applying stresses to the chain ends is analyzed by Picu et al.;[6] we have also discussed this in detail in Chapter 3. An important outcome of such oriented, nonequilibrium simulations is the ability to determine a direction-dependent persistence length of a polymer under uniaxial deformation, which turns out to be a rapidly convergent function of the simulated oligomer size.

We demonstrate our method using polyethylene (PE), the prototypical chain molecule, as its structural simplicity allows the simulation of relatively high molecular weight systems. However, our ultimate goal is to characterize the conformations of more complex molecules for which atomistic simulation is much more challenging. For example, even the pendant methyl groups of polypropylene severely reduce the efficacy of state-of-the-art variable-connectivity Monte Carlo moves that make the cited PE simulations possible[7]. Without such moves, effectively sampling conformations of dense atomistic systems of more than a few dozen monomers is difficult and time-consuming.

The approach developed here allows us to make predictions about high molecular weight polymers in oriented flows based on simulations of relatively low molecular weight oligomers. The ability to make such predictions from simulations of oligomers of only a few persistence lengths allows the structural investigation of a much broader array of industrially relevant materials at highly oriented conditions. We also show how the reverse procedure allows us to probe the likely atomic-level structure corresponding to a measured or simulated <**QQ**>.

4.2. Method

4.2.1. Configurational Properties

We consider a polymer system consisting of N_{ch} chains for which the Cartesian coordinate of the ith site of the jth chain can be written $\mathbf{r}_{i,j}$. The coordinates $\mathbf{r}_{i,j}$ represent the full set of N_j atomic backbone sites associated with chain j. The full set of intramolecular backbone coordinates is equivalently represented by a set of $n_j = N_j - 1$ connector vectors as:

$$\mathbf{q}_{i,j} = \mathbf{r}_{i+1,j} - \mathbf{r}_{i,j}, \quad i = 1, 2, \ldots, N_j - 1 \tag{4.1}$$

As in Chapter 3, we make use of a "local chain direction" defined by the vector joining next-nearest neighbors along the chain (see figure 4.1b), such that the relevant connector vectors are defined as follows, now with $n_j = (N_j - 1)/2$:

$$\mathbf{q}_{i/2,j} = \mathbf{r}_{i+1,j} - \mathbf{r}_{i-1,j}, \quad i = 2, 4, \ldots, N_j - 1 \tag{4.2}$$

The local chain direction is preferable because: (1) experimental measurements, such as birefringence, are traditionally interpreted in terms of the orientation of the local chain direction, since it is the smallest segment for which full alignment coincides with that of the chain; (2) the chain direction is a much smoother function of position along the chain than the bond direction. Other connector vectors can similarly be defined. Figure 4.1 shows different possible representations of an atomistic polymer chain, all of which are consistent with eq. 4.5 below.

The square of the jth end-to-end vector $\mathbf{Q}_j$ can be represented in the connector vector notation as:

$$\left\langle \mathbf{Q}_j \cdot \mathbf{Q}_j \right\rangle = \sum_i^{n_j} \left\langle \mathbf{q}_{i,j} \cdot \mathbf{q}_{i,j} \right\rangle + 2 \sum_i^{n_j-1} \sum_{i'>i}^{n_j} \left\langle \mathbf{q}_{i,j} \cdot \mathbf{q}_{i',j} \right\rangle \tag{4.3}$$

where the brackets denote an ensemble average. By defining $k = |i - i'|$ as the contour distance between the vectors and summing over i, eqn. 4.3 can be rewritten as:

$$\left\langle Q_j^2 \right\rangle = n_j \left\langle q^2 \right\rangle + 2 \sum_{k=1}^{n_j-1} (n_j - k) \left\langle \mathbf{q} \cdot \mathbf{q}_{k,j} \right\rangle \tag{4.4}$$
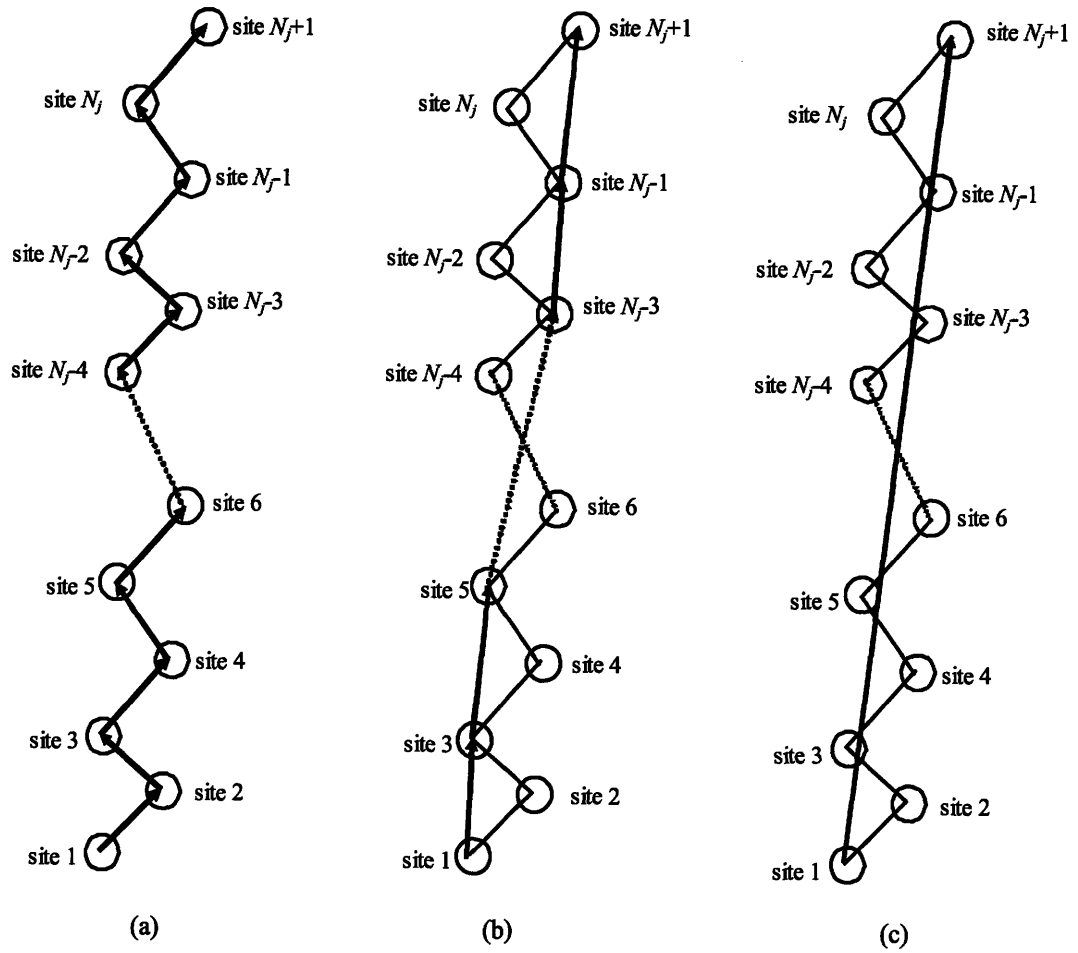
Figure 4.1. Representation of chain using: (a) $N_j - 1$ bond vectors; (b) $(N_j-1)/2$ chain direction vectors; (c) end-to-end vector. Dotted lines refer to sections of arbitrary length in the middle of the chain.

101

where $\langle \mathbf{q} \cdot \mathbf{q}_{k,j} \rangle$ represents the average of the dot product of all vector pairs displaced by k vectors along the backbone of chain j.

By choosing Cartesian axes that coincide with the principal axes α of $\langle \mathbf{Q}_j \cdot \mathbf{Q}_j \rangle$, the configuration tensor is diagonalized, with three nonzero components. Upon rearrangement we obtain:

$$\langle Q_j^2 \rangle = \sum_{\alpha=1,2,3} \langle Q_{j,\alpha}^2 \rangle$$

$$= n_j \sum_{\alpha=1,2,3} \left(2 \sum_{k=0}^{n_j-1} \left\{ (1-\frac{k}{n_j}) \langle \mathbf{q} \cdot \mathbf{q}_{k,\alpha} \rangle \right\} - \langle q_\alpha^2 \rangle \right) \qquad (4.5)$$

$$= n_j \sum_{\alpha=1,2,3} \langle q_\alpha^2 \rangle \left(2\ell_{p,\alpha} - 1 \right)$$

It should be noted that eqn. 4.5 is rigorously true for any chain comprising n_j connectors, and does not depend on the specific choice of representation used for the chain. The summation over k produces the scaled persistence vector component $\ell_{p,\alpha,}$ where the quantity $<q_\alpha^2>$, the mean squared length of the connector vectors, acts as a scaling factor. The persistence of the polymer chain is thus a direction-dependent quantity that depends on both its specific chemical properties *and* the orientation imposed by the processing conditions. Eq. 4.5 provides the corresponding magnitude of the principal components $\langle Q_{j,\alpha}^2 \rangle$ used in the rheological modeling of the system.

To obtain the parameters necessary to calculate ℓ_p, we make use of the Flory theorem[8], which states that real polymer chains in a melt behave as ideal chains for sufficiently large contour distances. This condition requires that all interactions are short-ranged[9], and implies a limiting form of $\langle \mathbf{q} \cdot \mathbf{q}_{k,\alpha} \rangle$ that is exponential in k. Thus, beyond some segmental separation $k{\geq}k^*$ the following relationship holds for the components of the average dot product of contour segments:

$$\langle \mathbf{q} \cdot \mathbf{q}_{k,\alpha} \rangle = A_\alpha \exp(-k\tau_\alpha) \qquad (4.6)$$

Eqn. 4.6 permits the determination of $\ell_{p,\alpha}$ from the k-dependence of the connector vector correlation function, which can be written for the special case of $k^*=0$ as:

$$\ell_{p,\alpha}\Big|_{k^*=0} = \frac{A_\alpha}{\langle q_\alpha^2 \rangle} \sum_{k=0}^{n_j-1} \left\{ (1 - \frac{k}{n_j}) \exp(-k\tau_\alpha) \right\}$$

$$= \frac{A_\alpha}{\langle q_\alpha^2 \rangle} \left\{ \frac{(1 - \exp[-n_j\tau_\alpha]}{1 - \exp[-\tau_\alpha]} + \right. \tag{4.7}$$

$$\left. \frac{\exp[-\tau_\alpha](1 - n_j \exp[-(n_j-1)\tau_\alpha] + (n_j-1)\exp[-n_j\tau_\alpha])}{n_j(1 - \exp[-\tau_\alpha])^2} \right\}$$

In the limit of large molecules ($n_j \to \infty$), eq. 4.7 simplifies to the relationship:

$$\ell_{p,\alpha}\Big|_{k^*=0} = \frac{A_\alpha}{\langle q_\alpha^2 \rangle} \left\{ \frac{1}{1 - \exp[-\tau_\alpha]} \right\} \tag{4.8}$$

For small τ_α, eq. 4.8 further simplifies to the mathematical equivalent of the wormlike chain model with τ_α being the inverse of the wormlike chain persistence length scaled by the bond length.

For real polymers, eq. 4.6 only applies beyond some segmental separation k^*. Thus, eq. 4.7 may require a correction term for $k<k^*$. Fortunately, the correction term is readily evaluated in a simulation of oligomers, by choosing the smallest k^* for which the values of A_α and τ_α have converged. The true value of the persistence length to be used in eqn. 4.5 is obtained by replacing the first k^* terms of eqn. 4.7 with the value obtained directly from an oligomer simulation. The true persistence $\ell_{p,\alpha}$ can then be calculated as the persistence given by eq. 4.7, $\ell_{p,\alpha}|_{k^*=0}$, modified by the short range correction for $k^* \neq 0$:

$$\ell_{p,\alpha} = \ell_{p,\alpha}\Big|_{k^*=0} + \sum_{k=0}^{k^*-1} \left(\langle \mathbf{q} \cdot \mathbf{q}_{k,\alpha} \rangle - A_\alpha \exp(-k\tau_\alpha) \right) \tag{4.9}$$

The preceding equations and their application represent the proposed method for calculating the anisotropic configurational tensor of macromolecules from the properties of simulations of oriented oligomers. It consists of:

1) Performing a simulation in the semigrand canonical ensemble, as described in Chapter 3 with chains of length $n_j \gg k^*$ and a finite orientation potential, to generate ensembles of oriented melt-like configurations. From these simulations, the averages $\langle \mathbf{q} \cdot \mathbf{q}_{k,\alpha} \rangle$ are obtained.

103

2) Fitting simulated data for $\langle \mathbf{q} \cdot \mathbf{q}_{k,\alpha} \rangle$ for $k \geq k^*$ using eqn. 4.6 to obtain A_α and τ_α for $\alpha=1,2,3$; the value of k^* is determined as the smallest value for which A_α and τ_α are independent of k^*. $\langle q_\alpha^2 \rangle$ and the short range correction terms are then obtained from the simulated data by direct evaluation of $\langle \mathbf{q} \cdot \mathbf{q}_{k,\alpha} \rangle$ for $k<k^*$.

3) Determining ℓ_p using eqns. 4.7 and 4.9.

4) For any polymer of length $n_j{}' \gg n_j$ accessible by simulation, the components of $\langle \mathbf{Q}_j \cdot \mathbf{Q}_j \rangle$ are obtained using eqn. 4.5.

Although we present results exclusively in terms of <QQ>, the radius of gyration $r_g{}^2$ and its components can be calculated by equating $\mathbf{Q}_j$ in eq. 4.5 with the vector between two points in a chain separated by n_j bonds. This allows the evaluation by summation over all pairs in an average chain. In the long-chain limit, the 1/6 proportionality between $\langle \mathbf{Q}_j \cdot \mathbf{Q}_j \rangle$ and $r_g{}^2$ can be used.

Finally, the order parameter used for orientation is the second Legendre coefficient, defined as:

$$P_2(\mathbf{q}_{i,j}) = \frac{3}{2} \frac{q^2_{i,j,\alpha=1}}{q^2_{i,j}} - \frac{1}{2} \qquad (4.10)$$

Here, $\alpha=1$ corresponds to the axial direction in a uniaxially oriented system.

4.2.2. Simulation Procedure

The Semi-Grand Canonical Monte Carlo (SGMC) is a thermodynamically consistent method for incorporating experimental measurements into an otherwise unconstrained simulation of a system at equilibrium[10]. We impose a physical potential that acts on the orientation of the local chain direction vector $\mathbf{q}_{ij}$ as explained in detail in Chapter 3. The acceptance criterion for the SGMC simulation of uniaxially oriented molecules described by birefringence measurements differs from that of the

104

corresponding isotropic *NPT* simulations by the addition of a single measure of anisotopy $P_2(\mathbf{q})$ and its thermodynamic conjugate, the scalar physical potential μ, to the Hamiltonian. In this case, μ plays the role of an orienting field; increasing μ results in an increased average orientation $<P_2(\mathbf{q})>$. The relative probability of a configuration is related to the thermodynamic variables as follows:

$$\ln(p) \propto -\beta \left[U(r^N) + PV - \mu \sum_{i,j} P_2(\mathbf{q}_{i,j}) \right] + N \ln V \qquad (4.11)$$

To obtain properties representative of the full chain, we simulate an oligomer sufficiently long to capture fully the short range correlations due to the specific chemical nature of the polymer. For polyethylene, the characteristic ratio is about $7^{[11]}$, significantly smaller than the typical number of monomer units in the chains used in these simulations.

SGMC simulations of oligomeric alkanes with average chain lengths of C_{24}, C_{78}, and C_{156}, were performed using a modification of the united atom force field originally proposed by Paul et al.$^{[12,13]}$. This force field was previously shown to yield good results for PE melt structure and dynamics$^{[12]}$ and, in Chapter 3, for the stress-optical coefficient of PE in oriented melts. Site translation, reptation, rebridging, end-rotation, end-bridging and volume change moves were all used to ensure rapid and complete sampling. The end-bridging move in particular leads to polydispersity in the chain length. For each of the three systems reported here, the polydispersity was 1.09. The ranges of chain lengths for each system were: C_{12} to C_{36} for the C_{24} system; C_{39} to C_{117} for the C_{78} system; and C_{78} to C_{234} for the C_{156} system. For complete details, the reader is referred to Chapter 3. Simulations were run at pressure $P=1$ atm and temperature $T=450$ K. Simulations ran for 2×10^5 to 1×10^6 cycles after equilibration of the orientation. The physical isomer potentials used with eqn. 4.11 are listed in Table 4.1.

Table 4.1. Physical Potentials applied in [$NPT\Delta\mu$] ensemble.

MW	N	N_{ch}	Physical Isomer Potential μ (in units of kT)
C_{24}	768	32	0, 0.025, 0.05, 0.075, 0.1, 0.15, 0.2, 0.25, 0.3, 0.35, 0.4, 0.45
C_{78}	3120	40	0, 0.025, 0.05, 0.075, 0.1, 0.15, 0.2, 0.25, 0.3
C_{156}	3120	20	0, 0.025, 0.05, 0.075, 0.1, 0.15, 0.2, 0.25

4.3. Results and Discussion

4.3.1 Correlation Parameters.

Fig. 4.2 shows a semi-log plot of the correlation of $\langle \mathbf{q} \cdot \mathbf{q}_{k,\alpha} \rangle$ for selected values of μ and chain size C_{78}. It illustrates graphically the procedure for determining the parameters τ_α, A_α, and k^*. The value of τ_α is determined from the slope of the fit to the semi-log plot for $k \geq k^*$, and A_α from the corresponding intercept using a weighted nonlinear least-squares regression. Fig. 3 shows the estimates of A_α and τ_α and their 95% confidence limits as a function of k^* for the transverse component of the C_{78} system with μ=0.15. The uncertainty in the estimated parameters is typically 3 to 5 %. From the deviations in A_α and τ_α estimated by $k^*<2$ from their asymptotic values, we conclude $k^*=2$ to be appropriate for this case. For the axial component, even $k^*=0$ does not introduce significant error. Other chemistries may be different, however; in general, we expect that k^* depends on the stiffness of the chain and the choice of $\mathbf{q}$ vector used to represent the chain.

Figs. 4.4 and 4.5 shows the parameters A_α and τ_α obtained using different molecular weights and different local orientation potentials. The values for these parameters are consistent over the chain lengths studied and highlight their intrinsic nature.
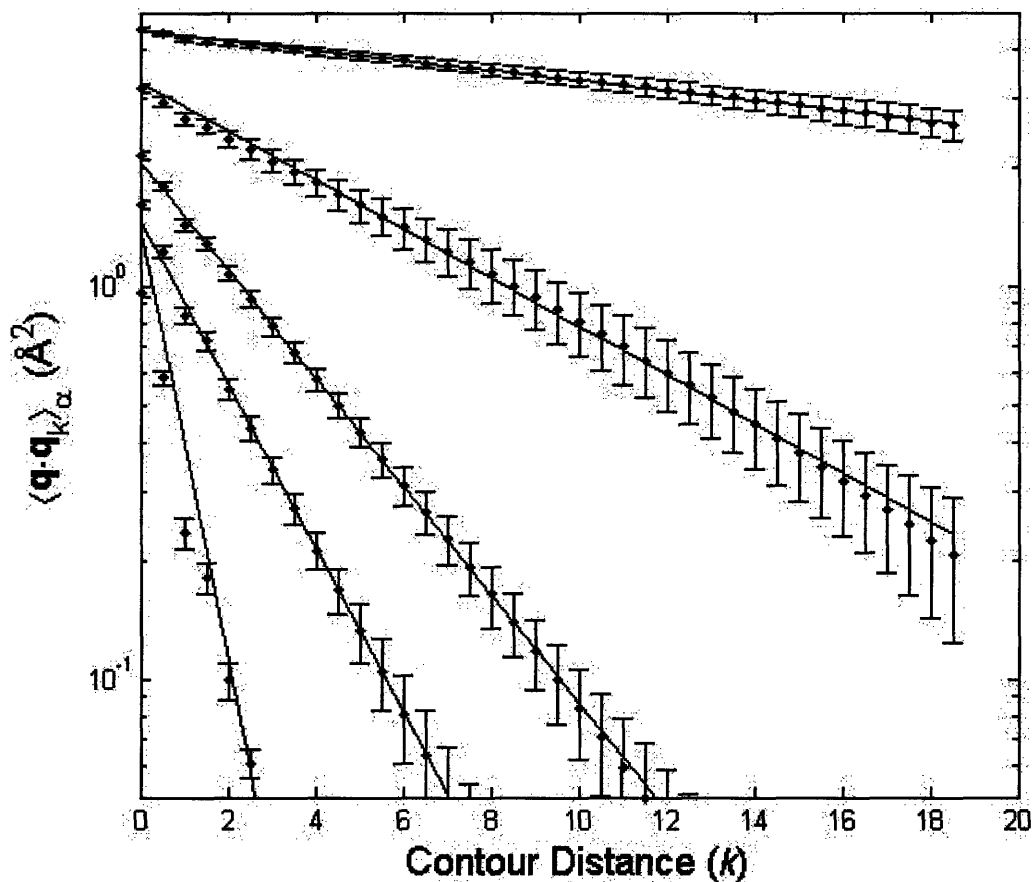
Figure 4.2. Semi-log plot of the connector vector **q** autocorrelation as a function of separation k along the chain contour. The points are the values of the components of the vectors obtained from simulation; error bars represent 95% confidence levels. The lines represent fits weighted to minimize the residual difference with the values at contour distance $k \geq k^*$. The data sets are, from top to bottom: μ=0.3, axial; μ=0.15, axial; μ=0; μ=0.15, transverse; μ=0.3, transverse for C_{78} system. Note: due to polydispersity arising from end-bridging and rebridging MC moves, the contour length for the shortest chains in the C_{78} simulations is 18.
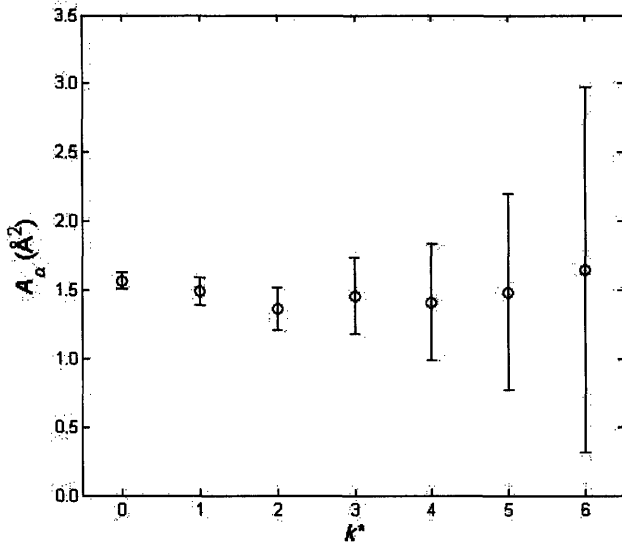
(a)
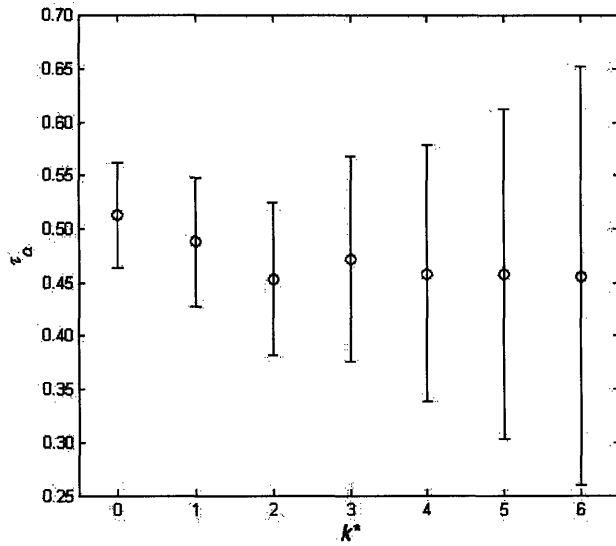
(b)

Figure 4.3. Estimates of the parameters (a) A_α and (b) τ_α as a function of k^* for the transverse component of the C_{78} system with μ=0.15. The rise in error of the parameters with increasing k^* results from increased noise in the simulation data at large k.
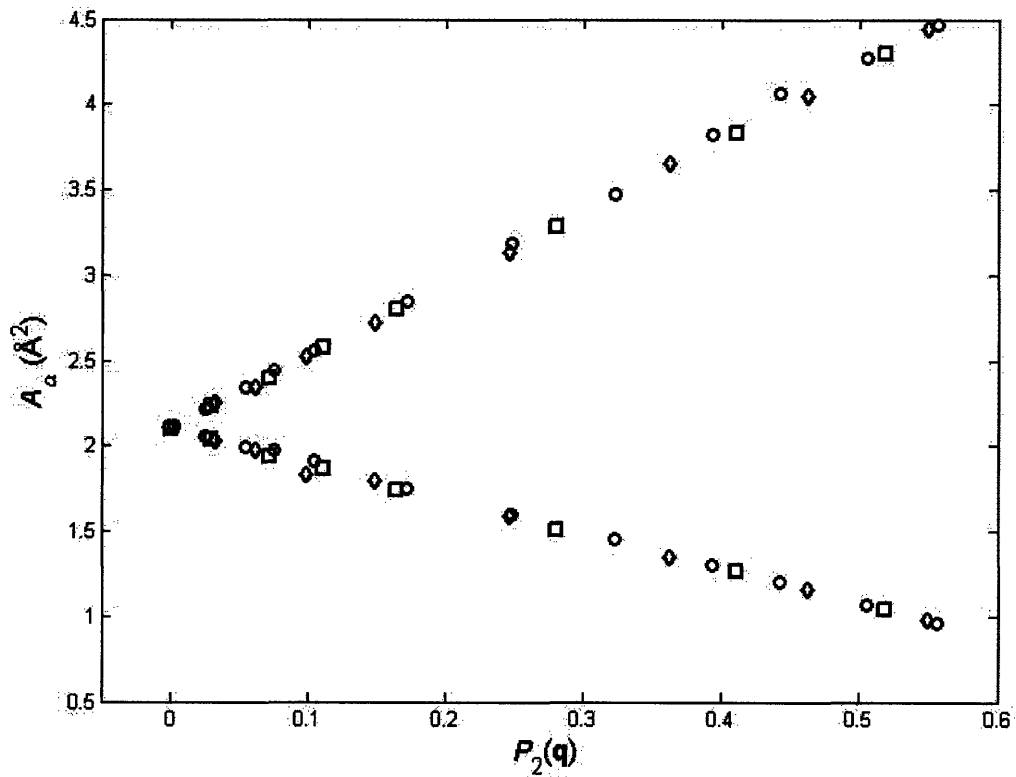
Figure 4.4. Intercept parameter A_α as a function of local orientation $<P_2(\mathbf{q})>$ for: C_{24} system (circles); C_{78} system (diamonds) and C_{156} system (squares). Upper curve is the axial component; lower curve is the transverse component.
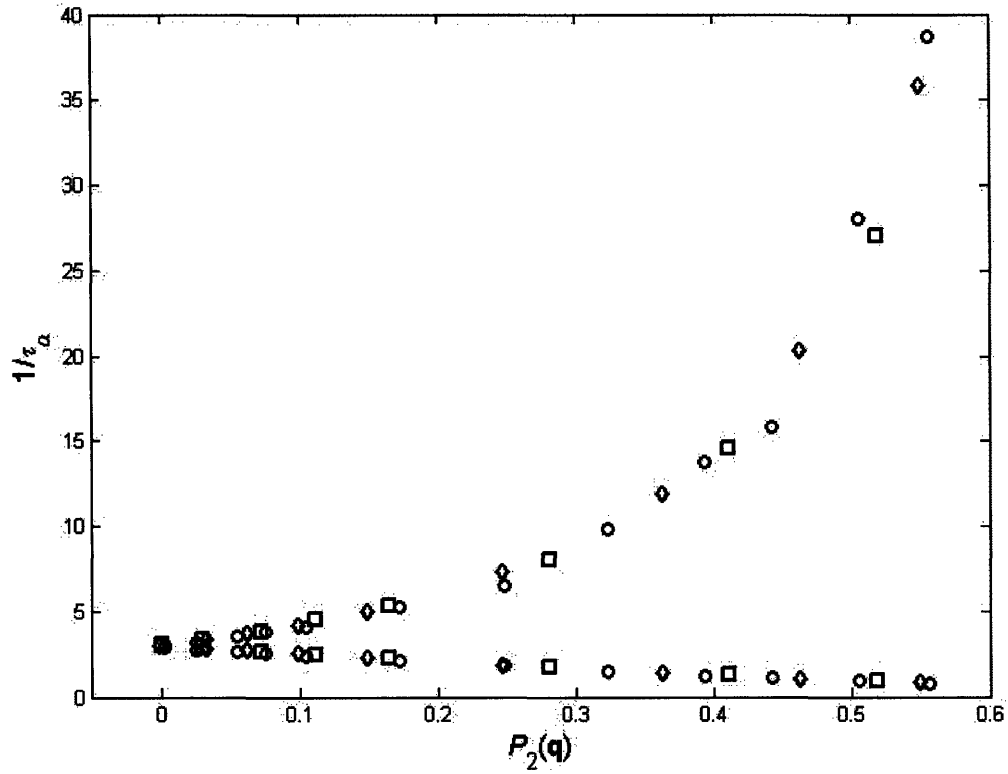
Figure 4.5. Characteristic length of correlation versus order parameter for the following simulations: C_{24} system (circles); C_{78} system (diamonds) and C_{156} system (squares). Upper curve is the axial component; lower curve is the transverse component.

4.3.2 Long Chain Limit.

Fig. 4.6 compares the principal components of $<\mathbf{QQ}>$ for a C_{156} system predicted by the three sets of PE simulations using the proposed method of persistence lengths, with those measured directly from the C_{156} simulation. There is no statistically significant difference between the predicted and directly measured values of $<\mathbf{QQ}>$. Figure 4.7 shows the evolution with $<P_2(\mathbf{q})>$ and N_j of the components of $<\mathbf{QQ}>$ computed using the method of persistence lengths. For a given value of $<P_2(\mathbf{q})>$, the components of $<\mathbf{QQ}>/N_j$ approach asymptotic values with increasing N_j; the asymptotic value for the axial component diverges, of course, as $<P_2(\mathbf{q})>$ approaches 1, corresponding to the fully extended chain. For values of $<P_2(\mathbf{q})>$ as high as 0.15, C_{100} provides an accurate value of the components of $<\mathbf{QQ}>/N_j$ for arbitrarily long chains; for values of $<P_2(\mathbf{q})>$ approaching 0.5, however, an order of magnitude increase in chain length is necessary to obtain the asymptotic value of the axial component of $<\mathbf{QQ}>/N_j$. The reason for this can be understood in terms of the previously explained transition from chain rotation to chain extension around $<P_2(\mathbf{q})>=0.15$. Fig. 4.8 shows how

$$\left\langle Q^2 \right\rangle = \left\langle Q^2_{axial} \right\rangle + 2\left\langle Q^2_{transverse} \right\rangle$$ varies with orientation. It remains relatively constant up to

$<P_2(\mathbf{q})>=0.15$, beyond which it increases dramatically, accompanied by changes in the torsion angle distribution and the internal energy of the molecule.

As discussed in the Introduction to this Chapter, these changes coincide with a breakdown in the ability of FENE-type models to provide accurate estimates of the stress at large deformations, due to the non-Gaussian nature of the resulting configurations. Since atomistic simulations can reproduce the stress-birefringence relation up to and beyond the linear region described by the stress-optical rule, as shown in the previous Chapter, it offers an implicit constitutive relation between stress and degree of flow-induced orientation for polymeric systems even at high deformation. In this respect, our method can serve as a component of "micro-macro" MD modeling approaches, which model the properties of macromolecular systems without the use of explicit constitutive equations. Examples of such approaches include the CONNFFESSIT method developed by Laso and Öttinger[14], as well as more recently developed methods like the Lagrangian
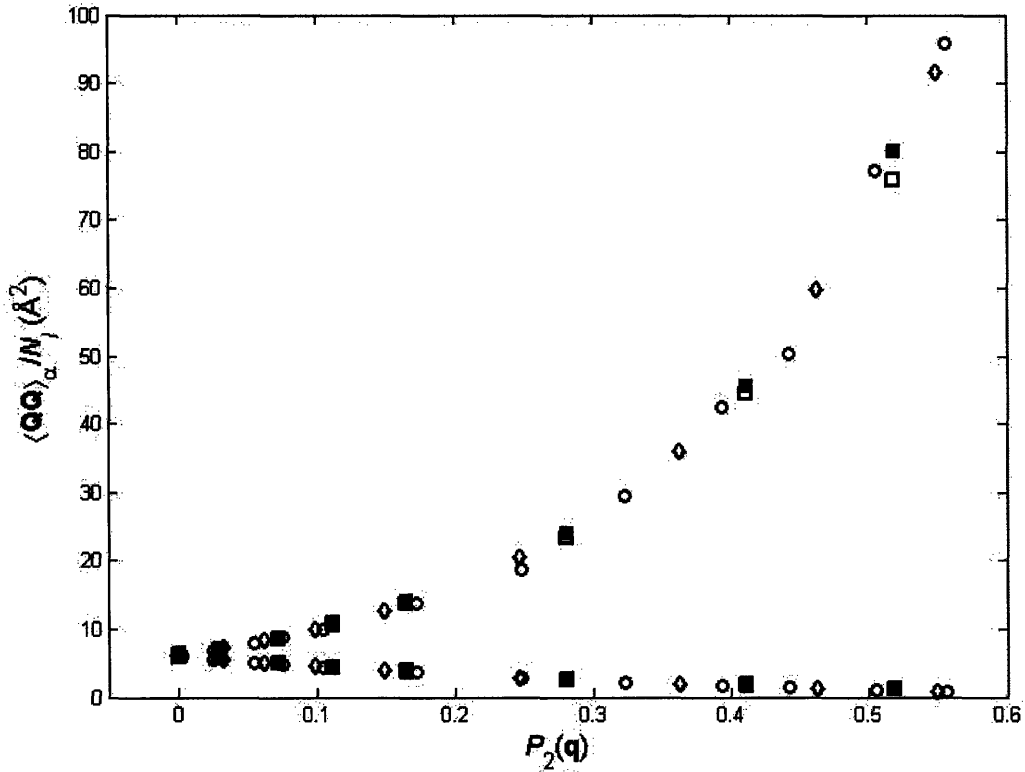
Figure 4.6. Principal components of <QQ> for C_{156} chains: Directly measured from simulation (filled squares); others calculated by the method of persistence lengths using parameters from the following simulations: C_{24} system (circles); C_{78} system (diamonds); and C_{156} system (squares). The upper curve is the axial component; the lower curve is the transverse component.
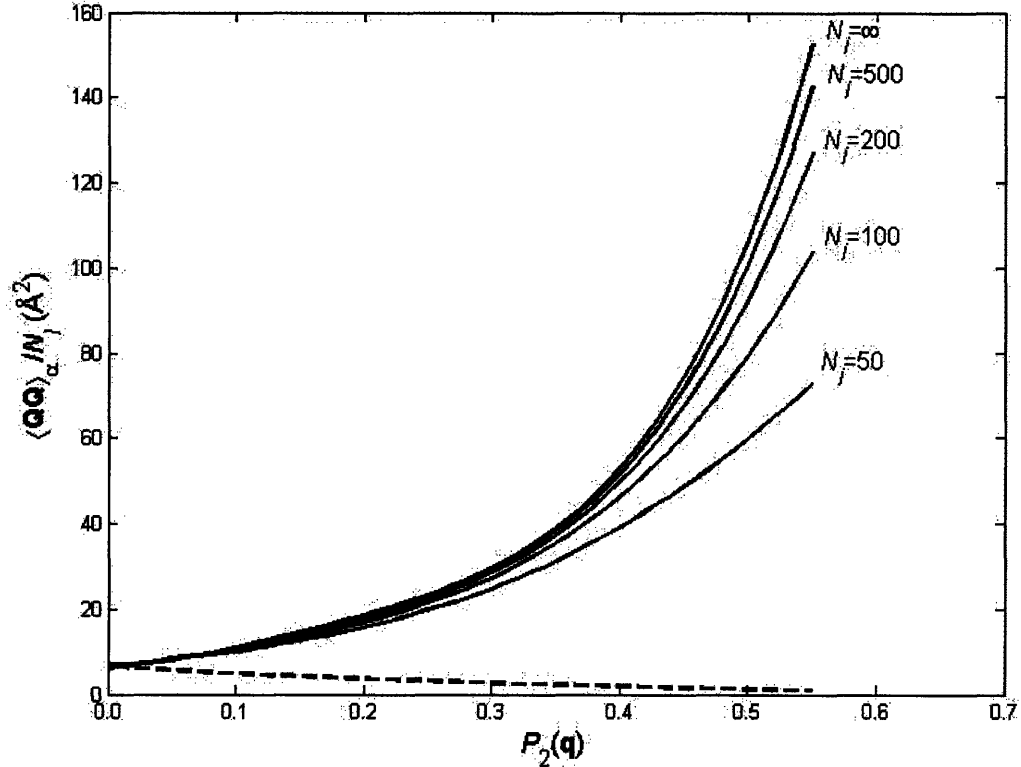
Figure 4.7. Principal components of <QQ> calculated using the persistence length method. The solid lines are the axial components; the dashed line represents the corresponding transverse components (not distinguishable at this scale for chains of different length). Lines are substituted for data particle method (LPM)[15], and Brownian configuration fields (BCF)[16]. However, as shown in figure 3.8, there is a molecular weight dependence of the stress-optical relationship at high deformation. Therefore, demonstration of convergence of the stress-optical relationship at high molecular weight and for high levels of stress would be necessary before such a constitutive relationship would really be useful.
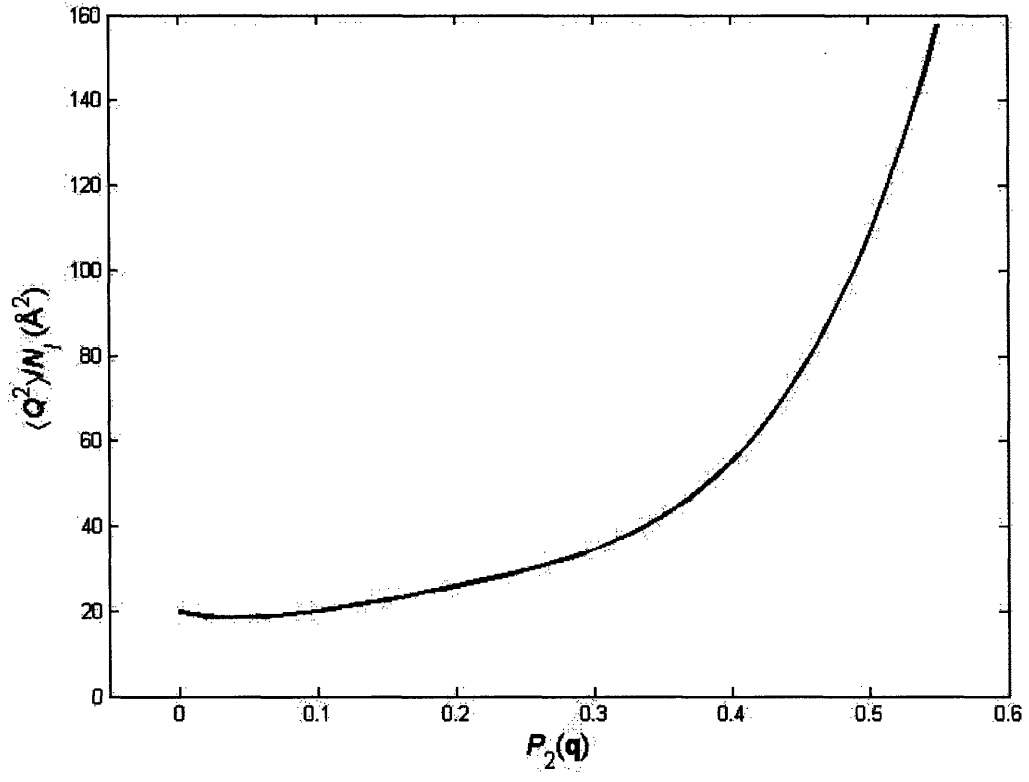
Figure 4.8. Mean-squared magnitude of end-to-end vector $<Q^2>$ vs. local orientation

4.3.3 Inverse Mapping.

The mapping procedure relating macromolecular configuration to oligomeric persistence lengths, demonstrated here for the uniaxial case, determines two molecular characteristics $\{<Q^2>_{axial}, <Q^2>_{transverse}\}$ given two others $\{<P_2(\mathbf{q})>, N_j\}$. In the long chain limit $<Q^2>_{axial}/N_j$ and $<Q^2>_{transverse}/N_j$ are asymptotically constant for a given $<P_2(\mathbf{q})>$, leaving only one independent quantity among $<P_2(\mathbf{q})>$ and $<Q^2>_{axial}/N_j$ in this limit. Thus, given values of the principal components of $<\mathbf{QQ}>$, one can infer the local orientation $<P_2(\mathbf{q})>$ from fig. 4.7. A simulation of oligomers of a chosen length and with the same level of local orientation can then be constructed using a value of μ interpolated from a plot of μ versus $<P_2(\mathbf{q})>$, such as the one previously generated for PE and shown in fig. 3.1; alternatively, in the absence of such a plot, μ can be found iteratively using procedures discussed elsewhere[10,17]. It is important to note that μ must be chosen according to the length of oligomers to be simulated. Nevertheless, a valuable feature of the persistence length methodology is that all of the information in fig. 4.7 can be obtained with a relatively modest amount of computing power. A handful of simulations of oligomers at the temperature of interest provide the necessary persistence vector information to link local and macromolecular conformations in oriented states. This in turn allows the connection between processing conditions defined at the continuum scale and simulations of structure-property relations arising from atomic scale interactions.

Implicit in all that has been presented above is the assumption that orientation is spatially and topologically homogeneous down to the atomic level. Lacking information to the contrary, we have minimized the free energy by inferring an orientation that is independent of both the spatial and chain contour coordinates. Nevertheless, there are examples where orientation is inhomogeneous; for example, upon cessation of shear[18], the relaxation of oriented polymer chains proceeds from the ends of the chain to the center, so there can be a period of time in which orientation is inhomogeneously distributed along the contour of the chains. Such cases can also be treated within the SGMC method when warranted, but require a more detailed analysis that is presented in Chapter 5.

4.4. Conclusion

We have demonstrated a general method for evaluating the average conformation tensor $<\mathbf{QQ}>$ for chains of arbitrary length in a state of orientation, based on a information obtained from simulations of oligomers constrained to a comparable state of local orientation. No significant difference is seen between the results obtained using systems whose minimum chain lengths vary from about 1.5 to ten times the intrinsic persistence length (i.e. in the absence of orientation). This method allows us to relate measurements of local orientation, such as birefringence, to macromolecular conformational properties using readily accessible oligomeric simulations. Conversely, it allows the determination of the appropriate local degree of orientation consistent with a rheological measurement of $<\mathbf{QQ}>$ for a high molecular weight polymer. This provides a means to cross length scales from the atomistic to the macromolecular for the purpose of describing systems with significant flow-induced orientation. This in turn allows the development of a unique non-equilibrium model that captures the chemical nature of the material and some aspect of the processing history. The method promises to be especially useful for modeling the deformation of chemically complex polymers, for which equilibration of chains larger than a few persistence lengths is problematic.

4.5. References

[1]   R. B. Bird, R. C. Armstrong, and O. Hassager, *"Dynamics of Polymeric Liquids, Vol. 2. Kinetic theory"*, 2nd ed., Wiley-Interscience, New York 1987.

[2]   A. N. Beris and B. J. Edwards, *"Thermodynamics of Flowing Systems"*, Oxford University Press, New York 1994.

[3]   M. Kröger, *Physics Reports* **2004**, *390*, 453.

[4]   I. Ghosh, G. H. McKinley, R. A. Brown, R. C. Armstrong, *J. Rheol.* **2001**, *45*, 721.

[5]   C. Baig, B. Jiang, B. J. Edwards, D. J. Keffer, H. D. Cochran, *J. Rheol.* **2006**, *50*, 625.

[6]   R. C. Picu, G. Loriot, J. H. Weiner, *J. Chem. Phys.* **1999**, *110*, 4678.

[7]   V. K. Kuppa, P.J. In 't Veld, G. C. Rutledge, *Macromolecules* **2007** (in press).

[8]   P. J. Flory, *J. Chem. Phys.* **1949**, *17*, 303.

[9]   M. Doi, *Introduction to Polymer Physics*, Oxford University Press, New York 1995, section 1.1.2.

[10]   G. C. Rutledge, *Phys. Rev. E* **2001**, *63*, 021111.

[11]   R. J. Chiang, *J. Phys. Chem.* **1966**, *70*, 2348.

[12]   W. Paul, D. Y. Yoon, G. D. Smith, *J. Chem. Phys.* **1995**, *103*, 1702.

[13]   P. J. in't Veld, M. Hutter, G. C. Rutledge., *Macromolecules* **2006**, *39*, 439.

[14]   M. Laso, H.C. Öttinger, *J. Non-Newtonian Fluid Mech.* **1993**, *47*, 1.

[15]   P. Halin, R. Lielens, R. Keunings, V. Legat, *J. Non-Newtonian Fluid Mech.* **1998**, *79*, 387.

[16]   M. A. Hulsen, A. P. G. van Heel, B. H. A. A. van den Brule, *J. Non-Newtonian Fluid Mech.* **1997**, *70*, 79.

[17]   M. Bathe, G. C. Rutledge, *J. Comput. Chem.* **2003**, *24*, 876.

[18]   M. Doi, *J. Polym. Sci: Polym. Phys.* **1983**, *21*, 667.

Chapter 5

Simulation of Mechanical Properties of Oriented Glassy Polystyrene

5.1. Introduction

A useful characteristic of polymeric materials is their processability into persistent, non-equilibrium structures that exhibit anisotropic mechanical and optical properties. For example, Hadley and coworkers showed that by subjecting polymer filaments to a draw ratio of approximately 6, one obtains an order-of-magnitude increase in the tensile modulus of low-density and high-density polyethylenes, polypropylene, and polyethylene terephthalate[1]. Other polymers follow the same trend, albeit with less dramatic increases in their tensile properties[1, 2].

In Chapters 3 and 4, I have studied polymer systems that are homogeneously oriented, both spatially and along the chain contour using the Semi-Grand Canonical Monte Carlo (SGMC) method. Using this approach, many aspects of dense polymer systems that are out of equilibrium can be inferred from simple structural measurements like birefringence. These include stress-optical relationships, average macromolecular conformations, and enthalpic and entropic contributions to the changes in free energy upon orientation. These homogeneously oriented simulations are appropriate for the local description of systems exhibiting macroscopic gradients in orientation, provided that the average orientation and stresses are effectively constant at the local (nanometer) scale. In such cases, the simulated homogeneous systems should be viewed as slices of the larger,

118

heterogeneous system. Such an approach can be readily used to investigate the spatial variation in, e.g., the orientation of injection-molded parts[3].

However, in many cases chain relaxation creates orientation differences at length scales on the order of, or smaller than, the simulation box size and cannot therefore be adequately described using a series of simulations with homogeneous orientation. One example of this inhomogeneity is the enhanced orientation of long chains *vis-à-vis* short chains during flow-induced crystallization of polyethylene[4], which is believed to be responsible for the "shish-kabob" morphology.

The simulations presented here explore another example of inhomogeneity - the variation of orientation along the contour of individual polymer chains. The current simulations are prompted by the results of a study of the effects of draw ratio and temperature on the development of orientation in atactic polystyrene (PS), and the resulting effects on the mechanical properties, by De Francesco and Duckett[5,6]. Based on the theories of contour-dependent relaxation of oriented polymer chains published by Doi[7], and by Milner, et al. [8], De Francesco and Duckett concluded that the variation in the mechanical properties could be explained by the inhomogeneity of the orientation along the chain contour, as illustrated in Fig 5.1 (similar to Fig 6 of ref. 5). The inhomogeneity arises from the fact that the chain relaxation propagates from the chain ends toward the center of the chain. Because the longest and shortest time scales of relaxation for polymer systems span many orders of magnitude, partial relaxation is a common feature of polymeric systems.

Although the study of systems out of equilibrium normally entails simulation of the real dynamics of the polymer, the longest time-scale of the polymer chain dynamics are not amenable to molecular dynamics (MD) simulation without substantial coarse-graining. While this coarse-graining may allow the exploration of polymer dynamics on the desired time scale, this comes with the loss of the unique chemical characteristics of the system, which are important for the accurate calculation of mechanical and rheological properties. In such cases, the use of a constrained Monte Carlo (MC) simulation offers an alternative approach to study a system far from equilibrium.

119

In the same way that we have used the SGMC method to provide a thermodynamically consistent ensemble to describe homogeneous states of orientation, we can also model systems that describe inhomogeneous states of orientation. This is achieved by applying an orientation potential selectively to a subset of segments within the chains, chosen according to criteria such as the length of chain in which such segments reside, or the contour distance of the segment from a chain end. This allows us to create simulations that can readily explore the evolution of microstructure and the dependence of properties like Young's modulus on such evolution. The resulting ensembles can also serve as a starting point for subsequent MD simulations of dynamic phenomena such as crystallization. Here, we focus on the dependence of mechanical properties of glassy polystyrene on process-induced orientation of either a homogeneous or inhomogeneous nature.

5.2 Theoretical Approach

5.2.1 Physics of Chain Relaxation

The Doi-Edwards theory[9] has been successful in explaining a number of observed dynamic phenomena of polymer chains. It is built upon a "tube" model that envisions an individual polymer chain as being constrained by entanglements with other chains to remain within a tube that follows the contour of the chain. The tube model establishes a number of characteristic times that explain various aspects of polymer dynamics. These include the entanglement time τ_e, the retraction time τ_r and the reptation time τ_d, where $\tau_e < \tau_r < \tau_d$. The entanglement time represents the characteristic time for equilibration of the density of polymer segments between entanglements; the retraction time characterizes the recoil after deformation of the tube contour to its original size, as well as fluctuation of the tube contour length at equilibrium; the reptation time characterizes the loss of memory of the original conformation of the tube.

120

Orientation of the polymer chains occurs when the Weissenberg number for reptation, the product of the strain rate and the reptation time $\gamma\tau_d$, is greater than unity, thus giving rise to deformation of tube. However, if the Weissenberg number for retraction, the product of the strain rate and the retraction time $\gamma\tau_r$, is less than unity, two dynamic processes contribute to the loss of deformation-induced orientation through partial relaxation of the tube: (1) the aforementioned retraction of the chain decreases its tube contour length and attenuates the orientation of the entire molecule; and (2) fluctuations of the contour length (or "breathing" modes) eliminate orientation preferentially at the chain ends by allowing the ends of the molecule to escape from the tube on a time scale short compared to the reptation time τ_d. The result is that even in the absence of reptation ($\gamma > 1/\tau_d$) there is a finite fraction of the chain that nevertheless escapes the tube and disorients on the shorter time scale of order τ_r. This effect was used by Doi to explain the value of 3.4 in the power law dependence of viscosity on molecular weight[7] and has also been used to correct other deviations of the Doi-Edwards (DE) model from experimental data[10]. The scaling of this effect goes as the inverse square root of the number of entanglement lengths; a prefactor of 1.3 was estimated by Doi using a variational calculation of the Rouse model and accounting for deformation of the tube under strain[11]. This prefactor is consistent with other studies as well[12, 13]. Thus, the fraction of the chain f that is has lost orientation on the sub-τ_d time scale is:

$$f = 1.3 \left(\frac{M_e}{M} \right)^{0.5} \tag{5.1}$$

where M_e and M are the entanglement molecular weight and chain molecular weight respectively.

The simplest way in which to model the partial loss of orientation at the molecular scale is to consider two populations of segments within each chain: the first population consists of the segments at each end of the polymer chain, which have fully relaxed on the time scale τ_r and are isotropically oriented; the second population consists of the central segments of each polymer chain, which relax on the time scale τ_d and are thus

oriented for much longer times. The average orientation of the system $<P_2>_{system}$ is the average of these two populations, where $f/2$ is the fraction of segments at each end of the chain that have fully relaxed:

$$\langle P_2 \rangle_{system} = f \langle P_2 \rangle_{population\,1} + (1-f)\langle P_2 \rangle_{population\,2} \qquad (5.2)$$

In order to simulate these partially relaxed chains, population 1 is allowed to sample local configurations independent of orientation and has an average orientation $<P_2>_{population\,1} \approx 0$; population 2 is constrained to provide the overall average orientation $<P_2>_{system}$ corresponding to the observed birefringence. Depending on the value of f, even a modest value of $<P_2>_{system}$ may indicate very high degrees of orientation for the inner segments of the chain. The orientation along the contour of the chain using this two-population model is shown schematically in figure 5.1.

While the addition of chain contour fluctuation represents an improvement in the ability of the DE model to explain the loss of orientation in polymer chains, this model of relaxation remains overly simplistic[14]. Nevertheless, the addition of a contour fluctuation to the DE tube model reproduces the observed phenomenon of a rapid loss of orientation of the chain ends followed by the slower loss of orientation throughout the remainder of the chain[10]. We proceed on the basis of well-separated relaxation times for which two distict conditions approximately describe the structure for $t<\tau_d$: the first is the case of the uniformly oriented chain ($f=0$); the second case is that of a chain relaxed to the extent described by eq. 5.1.

5.2.2 Application to Polystyrene

It has been demonstrated[5, 15] that the characterization of oriented samples of polystyrene by birefringence is insufficient to account for variations in the Young's modulus E_{33}. This has been explained by the fact that birefringence measures the average local orientation of the polymer chain, and is insensitive to any kind of inhomogeneity in
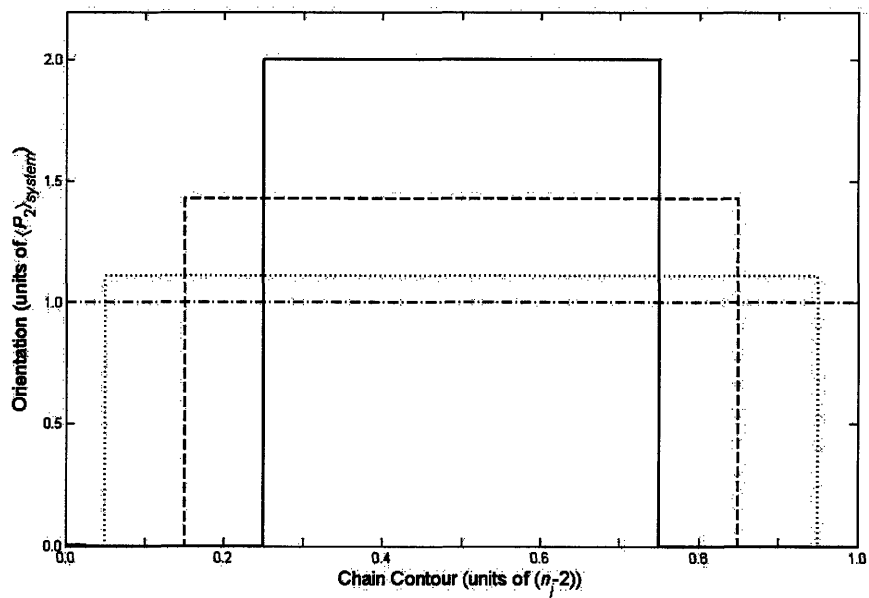
Figure 5.1. Schematic diagram showing f=0.0 (dot-dashed line), 0.1 (dotted line), 0.3 (dashed line), and 0.5 (solid line) for partial relaxation of the chain. While the curves represent different initial orientations, the overall average orientation $<P_2>_{system}$ is the same for all of the curves.

orientational order, such as that arising from the relaxation of chain ends. The experiments of De Francesco and Duckett[6] considered systems of MW=130 to 210 kg/mol and $T-T_g$ = 3 to 28 °C. The time constants for these systems covered a broad range: τ_e=0.05 to 425, τ_r= 9.0×10^0 to 1.0×10^5, and τ_d=3.0×10^2 to 9.0×10^6 seconds. For any given molecular weight and temperature, an order of magnitude or more separates these time constants; this separation is more pronounced for the higher MW systems since $\tau_e\sim MW^0$, $\tau_r\sim MW^2$, and $\tau_d \sim MW^3$. For a given molecular weight, the time constants all increase by a factor of about 15 as $T-T_g$ decreases from 28 to 18 °C. There is a more rapid increase as temperature nears T_g; the time constants increase by a factor of 10 over the smaller decrease of $T-T_g$ from 8 to 3 °C (see table 3 of reference 6). This illustrates the tremendous influence of temperature on the relaxation of polymers, especially for small values of $T-T_g$.

To study the partial chain relaxation hypothesis proposed, we model two pairs of drawn PS samples produced by De Francesco and Duckett having a birefringence $\Delta n \approx -$ $0.015^{[6]}$, or equivalently $<P_2>_{system} \approx 0.3$. This set comprises samples of molecular weights 130 and 180 kg/mol, each of which were deformed by drawing at a common initial strain rate of $1.2\times10^{-2}s^{-1}$. The strain ratios and temperatures were {3, 105°C} and {5.5, 110°C} for the 130 kg/mol sample and were {3, 105°C} and {4.5, 110°C} for the 180 kg/mol sample. The values of fractional relaxation that may be attributed to these samples correspond to 0 and 0.5 for the 130 kg/mol sample and 0 and 0.4 for the 180 kg/mol sample.

5.2.3 Molecular representation of PS

For a polymeric system comprised of N atoms or sites, distributed among N_{ch} chains, the Cartesian coordinate of the ith site of the jth chain can be written $\mathbf{r}_{i,j}$. Considering only the backbone of the chain, the intramolecular coordinates are equivalently represented in terms of connector vectors $\mathbf{q}_{i,j}^{(m)}$ of the n_j sites along the backbone in each chain, where the superscript m indicates the number of bonds spanned

by the connector. As in our previous work, we employ the use of a "local chain direction" $q_{ij}^{(2)}$ defined as follows:

$$q_{i,j}^{(2)} = r_{i+1,j} - r_{i-1,j}, \quad i = 2,3,\ldots,n_j - 1 \tag{5.3}$$

Additionally, for polystyrene we define a unit vector $q_{ij}^{(p)}$ normal to the plane of the phenyl ring of the side group. Both of these vectors are shown in figure 5.2.
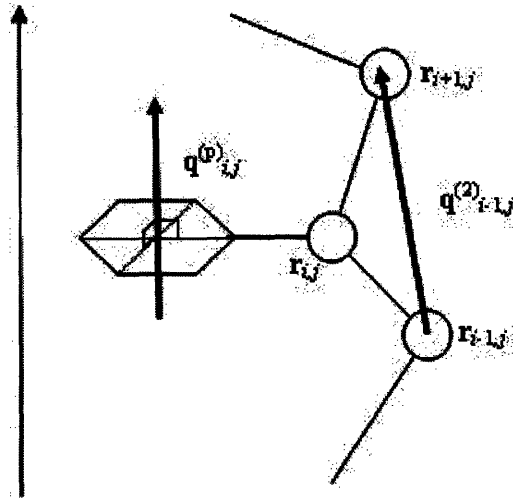
Figure 5.2. Vectors used to define the orientation of a polystyrene chain.

The description of the polystyrene (PS) chains in terms of $q_{ij}^{(2)}$ and $q_{ij}^{(p)}$ is motivated by the relationship between available experimental measurements and the physical organization of the molecules. Not only birefringence measurements, but also measurements of IR and Raman, produce results that depend on the orientation of these vectors through the value of the second Legendre polynomial $P_2^{(m)}$ of the direction vectors shown in fig. 5.2:

$$P_2^{(m)} = \frac{3(q_{ij,x}^{(m)})^2}{2(q_{ij}^{(m)})^2} - \frac{1}{2} \tag{5.4}$$

The birefringence Δn is defined as[16]:

125

$$\Delta n = \frac{2\pi}{9} \frac{N}{V} \frac{(n^2+2)^2}{n} (\alpha_{xx} - \frac{\alpha_{yy} + \alpha_{zz}}{2}) \langle P_2 \rangle = \Delta n_{max} \langle P_2 \rangle \qquad (5.5)$$

where n is the refractive index of the material, N/V is the number density of birefringent units, and $\{\alpha_{xx}, \alpha_{yy}, \alpha_{zz}\}$ are the diagonal components of the polarizability tensor of the birefringent unit in the frame of reference of the sample orientation. In general, the orientation of the phenyl rings are expected to mirror that of the chain backbone, since $\mathbf{q}^{(2)}$ and $\mathbf{q}^{(p)}$ are parallel in the energetically favored conformation of the styrene unit. However, libration of the phenyl rings leads to a reduction in orientational order for the rings relative to the chain backbone, so the overall birefringence must be written as the sum of the contributions of the phenyl ring and the backbone. For polystyrene, the individual birefringences Δn_{max} were calculated according to eq. 5.5 using the polarizability tensors of Abe, et al.[17] for the phenyl ring (α_{xx}=-2.981, α_{yy}=0.383, α_{zz}=2.598) and the backbone (α_{xx}=1.741, α_{yy}=-0.953, α_{zz}=-0.788) and by using a refractive index for PS of n=1.59[18]. This leads to the relationship between Δn and the orientational order parameters for the chain backbone $<P_2^{(2)}>$ and phenyl ring $<P_2^{(p)}>$:

$$\Delta n = \frac{N}{V} \left[23.5 \langle P_2^{(2)} \rangle - 40.2 \langle P_2^{(p)} \rangle \right] \qquad (5.6)$$

where N/V is the number density of monomer units in Å^{-3}.

5.3 Simulation Procedure

The force field used in these simulations is based on the united-atom model proposed by Mondello et al.[19] They showed that this united-atom force field successfully reproduced two independent sets of X-ray data for PS within experimental error. In the united-atom force field, each carbon and associated hydrogens of the PS molecule are lumped together into a single site and labeled as indicated in fig 5.3. In order to adapt the Mondello force field to our existing code, the bond lengths along the backbone of the polymer were modeled as harmonic springs rather than as rigid bonds. The force constant was chosen to be consistent with the General Amber Force Field of

Wang, et al.[20], and did not introduce any measurable changes in the average bond lengths and angles. The force field is as follows:

$$U = \sum_{\substack{backbone \\ bonds}} \frac{1}{2}k_b\left(b_i - b_0\right)^2 + \sum_{\substack{backbone \\ angles}} \frac{k_\theta}{2\sin^2\theta}\left(\cos\theta_i - \cos\theta_0\right)^2 + \sum_{\substack{backbone \\ torsions}} \frac{1}{2}k_\phi\left[1 - \cos 3\phi_i\right]$$

$$+ \sum_{rings}\left\{\sum_{i=1,3} k_{\xi,i}\left(\xi_i - \xi_{0,i}\right)^2 + k_{oop}\varphi_i^2 + k_\chi(\chi_i - \chi_0)^2 + k_\tau \cos^2\left(\tau_i - \tau_0\right)\right\} \qquad (5.7)$$

$$+ \sum_{sites\ i,j} 4\varepsilon\left[\left(\frac{\sigma}{r_{ij}}\right)^{12} - \left(\frac{\sigma}{r_{ij}}\right)^6\right]$$

In the equation above, the first term is the harmonic bond stretching potential, applied to the backbone bonds, where b_0= 0.153 nm and k_b =3761 kJ/mol/nm^2. The C–C bonds in the phenyl ring were fixed at 0.140 nm and the C2–C3 bond connecting the phenyl ring to the chain backbone was fixed at 0.151 nm. The second term is the harmonic bond angle bending potential, applied only to the C–C–C angles in the chain backbone. For the angle C1'-C2-C1, θ_0=1.91 rad and k_θ=502.1kJ/mol; for the angle C2'-C1-C2, θ_0=1.91 rad and k_θ=527.2 kJ/mol. The C–C–C angles in the phenyl ring were fixed at 2.095 rad. The third term is the backbone torsion potential, which accounts for all intramolecular interactions between atoms separated by three bonds; ϕ_i is defined to be zero in the *trans* state and k_ϕ=5.86 kJ/mol. The fourth through seventh terms are specific to the phenyl rings. The fourth term arises due to bending of the phenyl ring relative to the chain backbone and has three contributions per ring: $\xi_{0,i}$=1.91rad and $k_{\xi,i}$=502.1kJ/mol for bond angle C1-C2-C3; $\xi_{0,i}$=2.095 rad and $k_{\xi,i}$=585.8kJ/mol/rad^2 for bond angles C2-C3-C7 and C2-C3-C8. The fifth term is the out-of-plane bending energy, where φ_i is the angle defined by C2–C3–C6 and k_{oop}=334.7 kJ/mol/rad^2. The sixth term is the improper torsion, which serves to maintain the chirality of the molecule. χ_i is the angle between the normal to the plane defined by C1'-C2-C1 and the bond C2-C3. Depending on the chirality of the C2 site, the equilibrium angle χ_0 will be either 0.6116 rad or 2.530 rad. The force constant is k_χ=209.2 kJ/mol/rad^2. The seventh term is the ring torsion, where τ_i is defined by projection onto the plane normal to C2–C3 of the angle between the normal to the ring, and the vector connecting sites C1 and C1', and k_τ=8.37 kJ/rad^2/mol with τ_0=1.571

rad. The last term is the Lennard-Jones (LJ) potential, which is used to compute the nonbonded interactions between all united atom pairs that are on different chains or that are separated by four or more bonds on the same chain. The nonbonded potential parameters are: C1, $\sigma=0.385$ nm and $\varepsilon=0.5021$ kJ/mol; C2, $\sigma=0.370$ nm and $\varepsilon=0.3766$ kJ/mol; CX, X $\neq$1,2, $\sigma=0.370$ nm and $\varepsilon=0.5021$ kJ/mol. Lorentz-Berthlot mixing rules were used for interactions between all unlike sites. The cut-off distance for all nonbonded interactions was 0.770 nm, or twice the largest value of σ. A corresponding long-range correction based on g(r)=1, where g(r) is the radial distribution function between any pair of atom types, was applied to the simulation.

The polymer chains are 30 mers long, regio-regular head-to-tail, atactic with a meso dyad fraction of 0.5±0.03, and terminated with a CH_3 group at each end. Thus, each molecule has 61 backbone sites and 30 phenyl rings, for a total of 241 sites/molecule. Each individual system consists of four such chains. All results were averaged over six independent simulations. The root mean squared values of the radius of gyration $<r_g^2>^{1/2}$ for samples of 40-mer and 80-mer polystyrenes were also simulated, to confirm agreement in conformational properties between our simulations and those of Lyulin and Michels[21], who also used a version of the Mondello force field, modified to relax the rigidity of the phenyl ring angles.
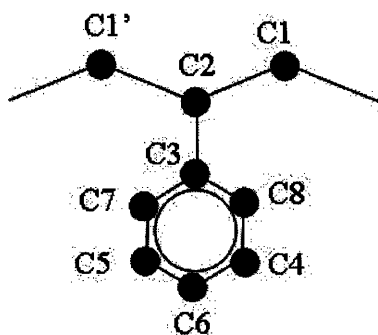
Figure 5.3. Diagram of nomenclature for a styrene monomer

The acceptance criterion for the SGMC simulation of uniaxially oriented molecules employed in this work differs from the corresponding isotropic *NPT* simulations by the addition to the Hamiltonian of the measure of chain backbone anisotropy, $P_2^{(2)}$, and its thermodynamic conjugate, the scalar physical potential μ. The relative probability of a configuration is related to the thermodynamic variables as follows:

$$\ln(p) \propto -\beta \left[U(r^N) + PV - \mu \sum_{i,j} P_2^{(2)} \right] + N \ln V \qquad (5.8)$$

The value of $P_2^{(p)}$ was not constrained since the time scale of ring libration (i.e. the β relaxation) is much faster than that of the chain backbone. Addition of a term containing $P_2^{(p)}$ to eq. 5.8 was found to bias the orientation of the rings relative to the chain backbone, thus producing improbable conformations.

For the purposes of mechanical property determination, the [NσTμ] ensemble was used, with the following Hamiltonian:

$$\ln(p) \propto -\beta \left[U(r^N) + \sum \sigma_{z'} A_{x'y'} (\ell_{z'} - \ell_{z',0}) - \mu \sum_{i,j} P_2^{(2)} \right] + N \ln V \qquad (5.9)$$

where [x',y',z'] is cycled over [x,y,z], [y,z,x], and [z,x,y]; the axes of the simulation box were kept orthogonal. The change in the normal stress difference attributable to the applied physical potential (μ) was determined according to the eq. 3.41. Because the strains were small, $<P_2^{(2)}>$ did not change significantly, and the contribution of this term to the stress was unimportant.

Simulations of homogeneously oriented systems (using eq. 5.8) were run for $<P_2^{(2)}>_{system}$=0.0, 0.1, 0.2, 0.3, 0.4 and 0.5. Simulations of inhomogeneously oriented systems that account for the partial loss of orientation at the chain ends were run for $<P_2^{(2)}>_{system}$=0.3 and f= 0.0, 0.4 and 0.5. All simulations were run in four stages: (1) generation of independent configurations that match the target $<P_2^{(2)}>_{system}$ through the application of an appropriate value of μ for PS "ghost" chains (i.e. with LJ potentials turned off), called "amorphization"; (2) application of the LJ potentials to equilibrate the PS melt at the target $<P_2^{(2)}>_{system}$ at T=550K in the [NPTμ] ensemble, called "melt

equilibration"; (3) generation of glassy samples using a series of [NPTμ] simulations by reducing temperature from 550K to 300K while the value of the physical potential μ was continuously updated to maintain $<P_2^{(2)}>_{system}$, called "quench"; and (4) evaluation of the elastic modulus using the relationship between stress and strain obtained from simulations with five applied stresses σ_x, ranging from -30MPa to 30MPa in the [NσTμ] ensemble, called "glass deformation".

In each of stages (1) to (3), the physical potentials (μ) were iterated using a procedure reported by Bathe and Rutledge[22], based on the method developed by Lyubartsev and Laaksonen[23]; for inhomogeneously oriented systems ($f{\neq}0$) the potential μ was applied only to population 2, the central fraction (1-f) of the chain. Stage 1 was run for 20,000 MC cycles; stage 2 was run for 175,000 to 250,000 cycles; the temperature was reduced in stage 3 from 550K to 300K over 750 steps of 200 cycles each; elastic properties were evaluated in stage 4 over 450,000 cycles. Because the systems rapidly loses orientation in the absence of the applied physical potential, the value of μ obtained from the cooling stage was applied and held constant during the application of stress in stage 4. The equilibration was judged on the basis of a stable value of orientation without drift in the value of μ for stages 1 and 2; in subsequent stages, convergence of volume and energy was used as an indicator of equilibration. Table 1 summarizes the simulation protocol described above.

During any given simulation, the following Monte Carlo moves were employed: (1) site translation; (2) reptation; (3) re-bridging; (4) end rotation; (5) pendant move; and (6) volume change. Other than the pendant move, all of these moves were performed as described in Chapter 3. The added pendant move attempts at random to perturb one of the following: a ring torsion, an out-of-plane bending angle, an improper torsion, or a ring bending angle. The maximum sizes of these perturbations were continuously updated to maintain 50% acceptance. The attempt frequency and typical fraction of accepted moves (for the isotropic melt) were, respectively: site translation, 0.44 and 0.50; reptation, 0.11and <0.001; re-bridging, 0.11and 0.01; end rotation, 0.11 and 0.50; pendant move, 0.22 and 0.50.

The decorrelation times of the end-to-end vectors for polystyrene are extremely long compared to our earlier polyethylene simulations, due in large part to the absence of variable connectivity moves, which were found to be ineffective for PS due to the presence of the large phenyl side group. A similar problem was previously encountered with variable connectivity moves for polypropylene, and resolved through the use of an expanded ensemble in Hamiltonian space[24]; this was not attempted here. The longest relaxation time, and consequently the time for orientation to react to the application of a given μ (i.e., for orientation to propagate throughout the polymer chain), scales as the square of the chain length, n_j^2. Thus, a trade-off was necessary between the length of chain that could be equilibrated in an oriented state practically, and the length of chain required to obtain quantitative estimates of mechanical properties (as evident below). The current simulations of 30-mer PS were each run in parallel over the course of several weeks on 1.6MHz Pentium processors; these 30-mers were sufficient to reproduce realistic densities and orientation in the glassy state.

As an aside, the original Mondello force field was developed using simulations in the NVT ensemble and was not confirmed to yield the correct pressure. In applying this force field to studies of 80-mers of polystyrene in the NPT ensemble, Lyulin and coworkers found it necessary to introduce a pressure correction in order to match the melt phase density. Even so, the density of the polymer glass so obtained underestimates the experimental density by about 2% (see figure 3 of ref. 21); as reported below, our simulation densities range from about 3% above to 2% below the same set of experimental values. Since we obtain comparable agreement with the experimental density data in the glassy state for these 30-mers, we used the force field without this pressure correction.

Table 5.1. Simulation Protocol

Stage	Simulation Parameters
1: Amorphization	$T = 550K$ $\mu \Rightarrow iterated$
2: Melt Equilibration $[NPTN_{ch}\mu]$	$P = 0.1MPa$ $T = 550K$ $\mu \Rightarrow iterated$
3: Quench $[NPTN_{ch}\mu]$	$P = 0.1MPa$ $300K < T < 550K$ $\mu \Rightarrow iterated$
4: Glass Deformation $[N\sigma TN_{ch}\mu]$	$\sigma_y = \sigma_z = 0.1MPa$ $\sigma_x - \sigma_y (MPa) = -30, -15, 0, 15, 30$ $T(K) = 300K$ $\mu \Rightarrow value\ from\ previous\ step$

5.4 Results and Discussion

5.4.1 Melt Configurations

The ensemble average chain orientations are shown in figure 5.4 as a function of the applied potential for the melt equilibration stage. The absolute values of μ obtained at the end of the cooling stage did not differ significantly from those of the melt stage; however, due to lack of ergodic sampling at the lower temperatures of the glassy state, these μ values should be viewed only as "locally relevant" to a particular region of phase space at low temperature. Since μ was iterated to maintain a specific orientation for each sample, there are a distribution of values corresponding to each value of <P2>. For the PS melt, figure 5.4 is analogous to figure 3.1. In that case, the sampling of polyethylene was much more robust and did not suffer from equilibration problems.

132
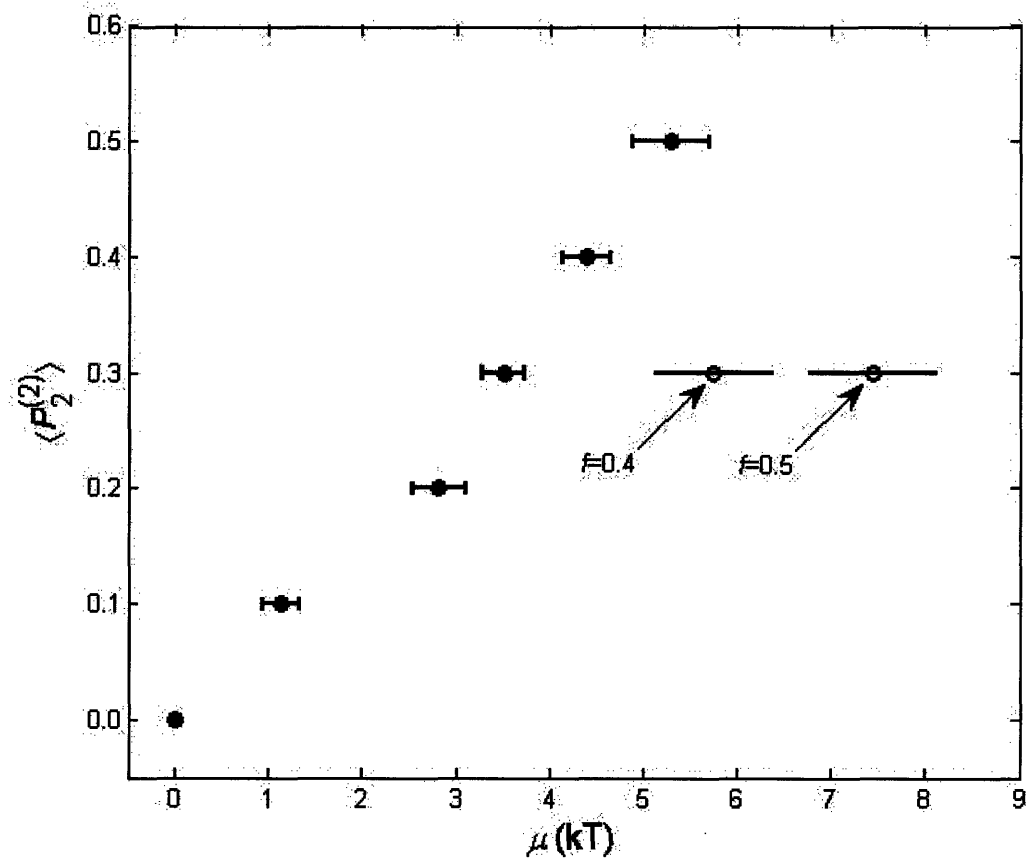
Figure 5.4. Ensemble orientation of chain orientation $<P_2^{(2)}>$ as a function of orientation potential μ obtained during melt equilibration. Filled circles represent the f=0.0 systems; the open circles represent the $f \neq 0.0$ systems as labeled. Bars represent the range of values for μ that produced the specified values of $<P_2>$.

Fig 5.5 shows the distribution of orientation as a function of position along the chain, for the cases of a homogeneously oriented system ($f=0$) and an inhomogeneously oriented system ($f=0.5$), generated during the melt equilibration stage. The most important aspect of fig. 5.5 is that the average distributions indicative of effective sampling of the possible conformations at each level of orientation and at each position along the chain. As can be seen, the application of the physical potential is very effective in creating the desired orientation distribution; the resulting plots may be compared with the hypothesized samples shown in Fig 5.1. However, the use of a single orientation potential μ through the chain does create some artifacts in the contour orientation. This is most apparent for the orientation at the chain ends and for the abrupt transition between the oriented and isotropic portions for the case of $f=0.5$. The value of μ may, in general, depend on the proximity of the segment to the chain ends or to the change in potential. Due to the connectivity of the chains, these effects are distributed over several segments and account for the curvature in the orientation distributions. These effects could be corrected using a chain position-dependent μ, but this was not done here since the effects are relatively minor and sampling for a position-dependent would be extremely difficult.

5.4.2 Glass Transition

Figure 5.6 shows a cooling curve for the isotropic polystyrene melt obtained from the quench stage. From this, we estimate a T_g of 415 ± 30 K for this model of polystyrene using data between 300 K and 500 K. This is somewhat higher than the value of 380 K obtained by Lyulin et al[25]. This difference is most likely due to the addition of the pressure correction term and the lower density obtained by Lyulin and Michaels[21], as discussed above. Although our results indicate a high value for the glass transition, the T_g is sensitive to the range of data used for the determination of the melt phase coefficient of thermal expansion, because of the large volume change and the rapid quench rate; excluding values above 480 K provides a glass transition temperature of about 390 K, which is very close to the expected value of 380 K.

134

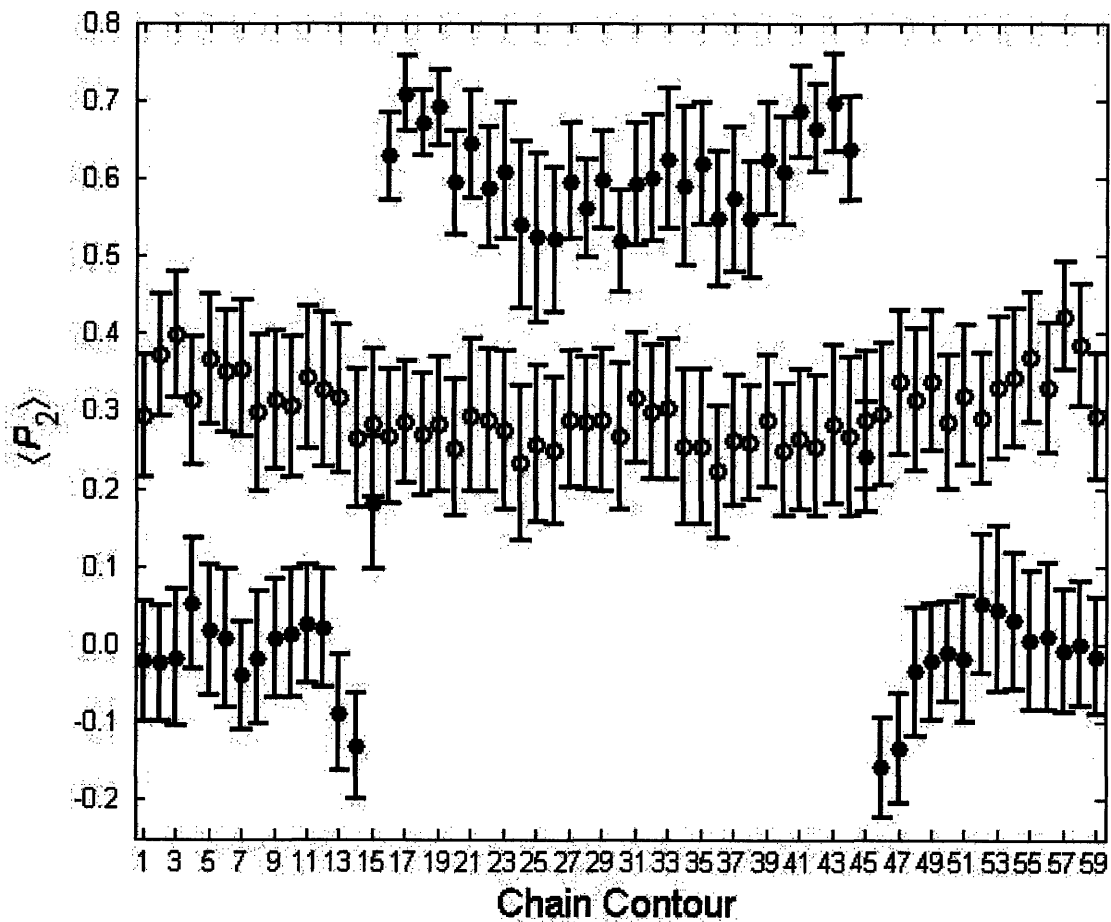Figure 5.5. Ensemble average orientation over the chain contour for $<P_2>_{system}$=0.3: f=0.0 (open circles) and f=0.5 (filled circles) during the melt equilibration stage. The chain contour represents the 59 $q^{(2)}$ vectors along the chain.
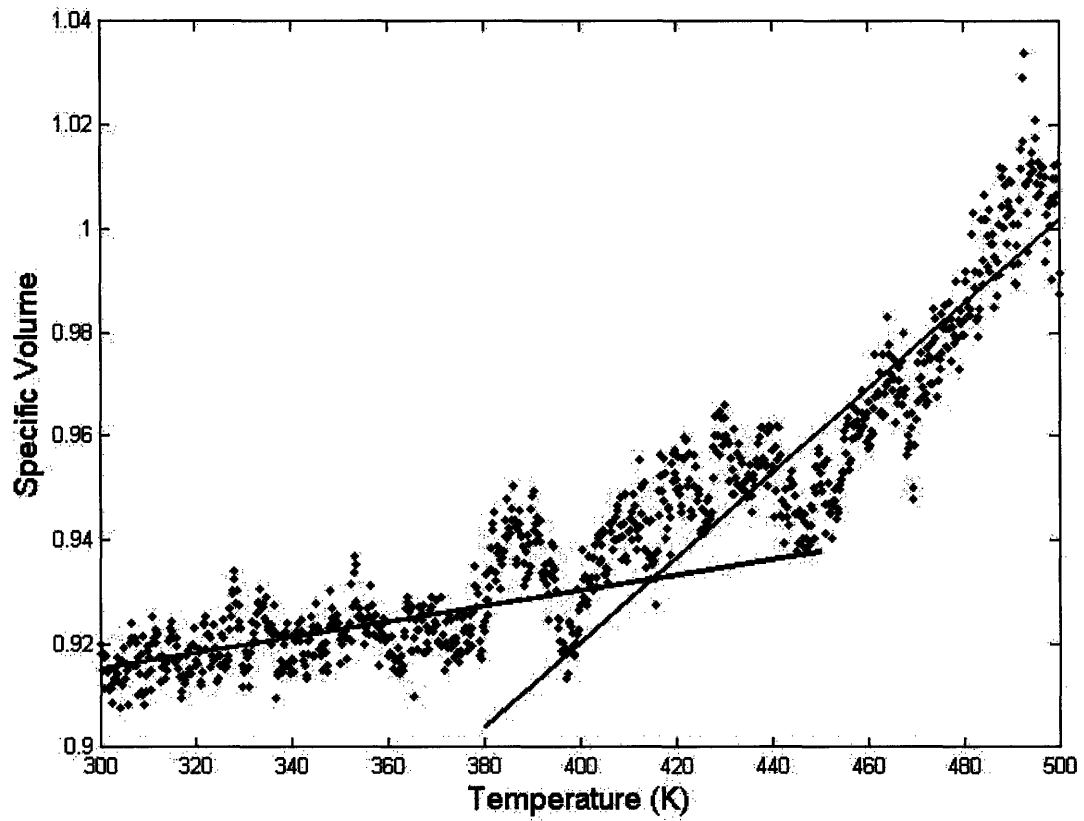
Figure 5.6. Cooling curve for atactic PS, MW=3135 (30-mer). The resulting Tg is approximately 415±30 K. Lines were fitted using data between 300K and 500K.

The density obtained for glassy polystyrene chains of 30-mers and 80-mers at 300K was about 1.08 g/cm^3, comparable to the literature value of 1.05 g/cm^3 for PS[26]; simulations of polystyrene chains of 20 mers gave a density of 0.95g/cc, which was deemed to be too low to be representative of polystyrene. The densities obtained through our simulations ranged from 1.08 g/cc to 1.03 g/cc, with the oriented systems generally having lower density compared to the isotropic system.

5.4.3 Birefringence

Figure 5.7 shows the variation of birefringence with orientation. The overall birefringence was obtained using eq. 5.5 with the coefficients obtained from Abe[17] and the orientation averages independently obtained from the simulations. By extrapolation to <P$_2$>=1.0, we obtain a value of Δn_{max} (the value of birefringence at full orientation) equal to –0.0489. This is in excellent agreement with the value of –0.048 obtained by Vancso, et al. using WAXS and birefringence[27] from a similar study of the relationship between birefringence and average chain orientation over this same range.

5.4.4 Elasticity of Homogeneously Oriented Polystyrene

The determination of the modulus E_{33} was made from the results of the [NσTμ] simulations through fitting to the relationship:

$$\sigma_3 = E_{33}\varepsilon_3 \qquad\qquad (5.10)$$

where $\varepsilon_3 = \delta L_x/L_{x0}$ and atmospheric pressure was maintained in the lateral directions, y and z. Voigt notation is used for Young's modulus. The strains obtained from the simulations spanned the range +/-1.0% for the most oriented PS systems, and +/-2.0% for the isotropic systems, well within the range of elastic behavior for PS[28].
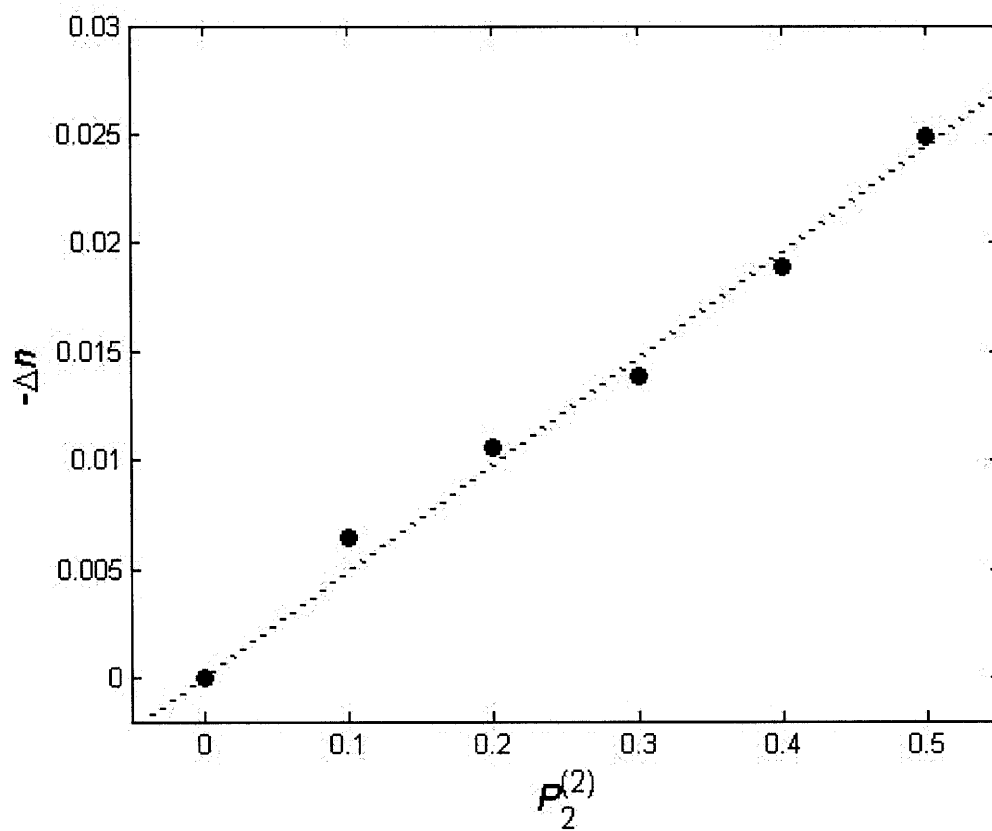
Figure 5.7. Birefringence as a function of the chain orientation. Dashed line represents a linear least squares regression of the birefringences obtained for each value of chain orientation.

Figure 5.8 shows the increase of the Young's modulus E_{33} with increasing birefringence, or equivalently $<P_2>$, for simulations with homogeneously distributed orientation, $f=0$. Looking first at the results for simulations without any orientational bias, i.e. $-\Delta n=0$, the simulated value is $E_{33}=1.7$ GPa. This falls significantly below experimental values of the isotropic Young's modulus, which are typically in the range of 2.3-3.3GPa[26]. However, additional simulations of 80-mer PS predict a modulus of 2.3GPa for the isotropic case, which agrees significantly better with the experimental values and with the value of 2.9GPa obtained by MD simulations of 160-mer chains at the same temperature by Lyulin, et al[29]. From this, we conclude that the downward shift of 0.65 GPa for the simulation results using 30-mer PS are due to the low molecular weight, relative to the experimental systems.

Secondly, Figure 5.8 shows the variation of the simulated modulus with increasing birefringence. Despite the downward shift relative to the experimental data attributed to molecular weight mismatch, the trend in modulus with increasing birefringence agrees well with the experimental data of De Francesco and Duckett[5]. The relevant experimental values for this comparison are the lowest values of modulus, which exhibit the least amount of contour inhomogeneity. The simulated values of the modulus increase by 1.2 GPa between $-\Delta n=0$ and 0.025, compared to approximately 1.6 GPa for the experimental data over the same range. In each case, there is an approximate doubling of the Young's modulus for systems with a birefringence $\Delta n=-0.025$ relative to the isotropic systems. As mentioned earlier, the decision to simulate 30-mers was made as the result of a trade-off between practical considerations required for accurate equilibration of orientation and quantitative accuracy of properties such as density for the isotropic system. The downward shift in mechanical properties appears to be systematic and entirely due to molecular weight. Nevertheless, we believe these results are promising with regard to the ability of the SGMC method to reproduce the relationship between two macroscopically observable quantities, birefringence and tensile Young's modulus. The variation of modulus in fig. 5.8 is discussed below.

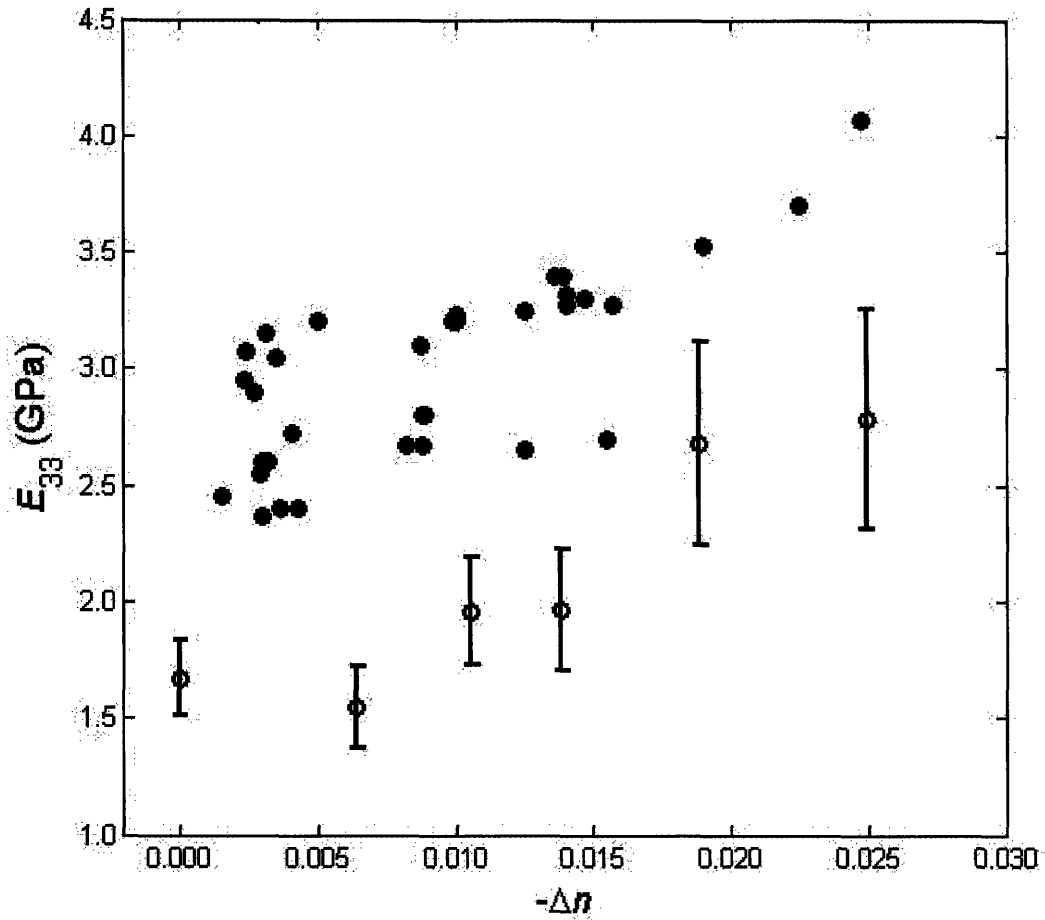Figure 5.8. Increase of tensile modulus with the birefringence from simulations and experiments. Simulations assuming homogeneously oriented (f=0) 30-mer PS (open circles); experimentally observed measures of tensile modulus versus birefringence (filled circles) for samples of PS reproduced from figs. 3 and 4 of ref 5. Variation in the moduli can be attributed to the processing conditions, as explained in the text.

5.4.4 Elasticity of Inhomogeneously Oriented Polystyrene

In order to explain the range of modulus values they observed for samples with similar birefringence, De Francesco and Duckett[5] hypothesized the presence of inhomogeneities in the distribution of the backbone orientation of the chain, as originally proposed by Doi[7]. The tensile moduli obtained by De Francesco and Duckett[5] are shown in Figure 5.8. At any given birefringence, samples that were more highly drawn at a higher temperature exhibited a higher modulus. De Francesco and Duckett[5] concluded that the existence of inhomogeneity in the chain is responsible for increase the mechanical properties, i.e., that the increase in modulus due to a more highly oriented center of the chain more than offsets the decrease due to less highly oriented chain ends.   Fig 5.9 shows the increase in modulus with the increase of the fraction of chain with relaxed orientation for the cases selected in the Theoretical Approach – Application to Polystyrene. For purposes of comparison, the simulation results are shifted by 0.65 GPa to compensate for the average downward shift of the 30-mer moduli. The increase of the modulus due to inhomogeneous orientation predicted by the simulations is consistent with the increase in the modulus observed experimentally for samples drawn at high temperature[5].

For comparison, we provide an analysis of the relationship between the distribution of orientation and mechanical properties using the Aggregate Model of Ward[30]. This model describes a polymer system as an aggregate of identical, non-interacting mechanical units. Parameterization proceeds by equating the mechanical properties of an individual unit to that of the fully oriented material. The mechanical properties of the aggregate can thus be expressed as a function of the orientation distribution of the individual mechanical units. The Aggregate Model predicts that the change in the modulus with increasing f at a fixed birefringence is proportional to the quantity $(2s_{13} + s_{44} - s_{11} - s_{33})$, where the s_{ij} are compliance constants in Voigt notation. Experimental estimates of this quantity for PS indicate that it is negative[2, 31, 32]. This means that the Aggregate Model predicts a decrease of E_{33} with increasing $<P_2^{(2)}>_{population2}$ at constant $<P_2^{(2)}>_{system}$, in contradiction to the experimental results and

141
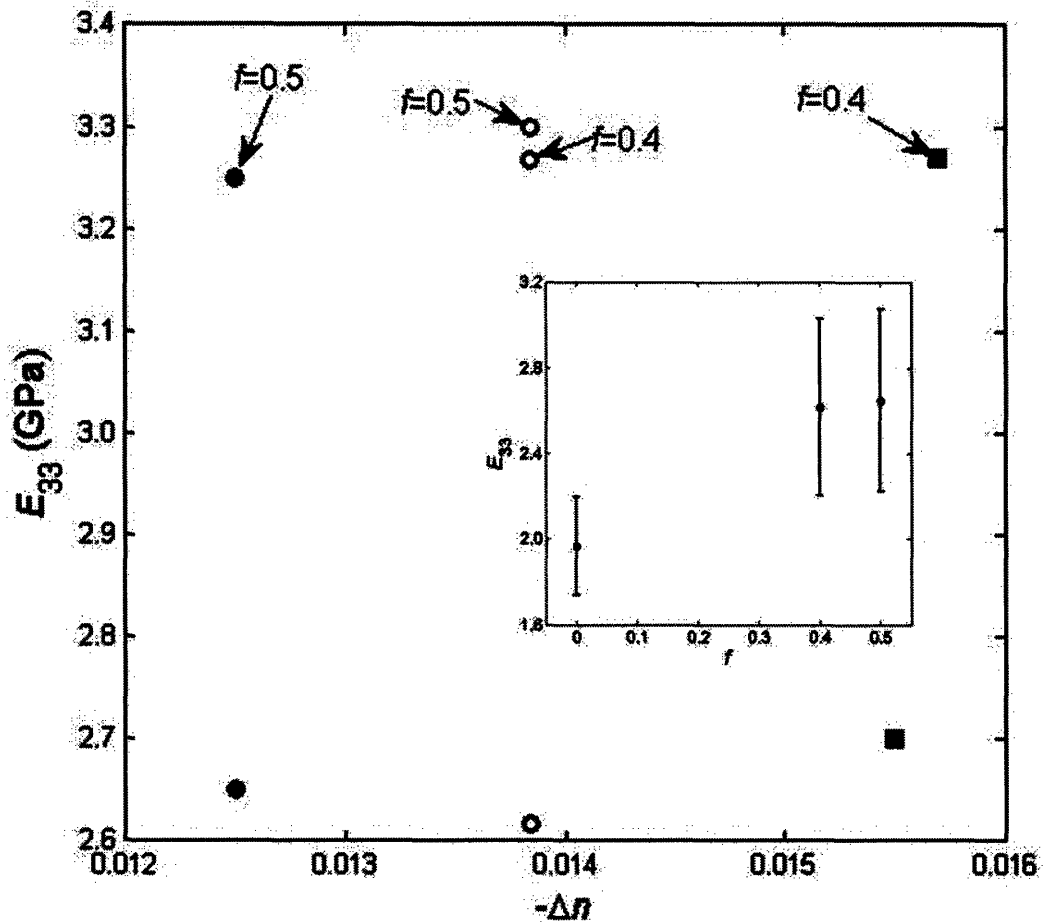
Fig 9. Modulus as a fraction of chain inhomogeneity for simulations $<P_2>_{system}=0.3$ ($\Delta n=-0.0139$). The choice of experimental data points, and the determination of values of f are described in the Theoretical Approach – Application to Polystyrene. Plot shows shifted data for simulations (open circles), and experimental data for MW=130kg/mol, $f=0$, 0.5 (filled circles) and for MW=180kg/mol, $f=0$, 0.4 (filled squares). All lower values of moduli correspond to $f=0$; other values are labeled. Inset shows the uncorrected values of modulus for the simulations as a function of f including error.

the simulations reported here. This qualitative difference underscores the value of atomistic simulations to understand phenomena such as the effect of the distribution of orientation on the mechanical properties of polymers.

5.5 Conclusion

There are two novel aspects to the methodology presented here to analyze the connection between the structural and mechanical properties of PS. First, there is the use of an atomistic-level Monte Carlo method to probe the properties of glassy PS. Second, there is the ability to constrain the orientation of the polymer chains to mimic desired states of anisotropy. Both of these aspects are necessary to provide conformations tailored to exhibit features of homogeneously oriented ($f=0$) and partially relaxed ($f>0$) PS chains. This method is unique in that it allows us to access systems characterized by partially relaxed orientation, which is not typically accessible using MD. This provides the opportunity for a more complete understanding of the effects of microstructure on the mechanical properties.

The simulation results obtained for oriented PS support the explanation of De Francesco and Duckett[5] for the variation of modulus with processing conditions due to partial relaxation in the more highly-drawn, high temperature systems. Our results show quantitative agreement with the experimentally observed increase of tensile modulus with overall orientation as measured by birefringence. Significantly, the simulations also reproduce the experimentally observed increase of the tensile modulus with inhomogeneity by evaluating different conditions of partial relaxation of the PS chains.

Atomistic simulations are shown to be particularly useful in the case of PS, because they provide qualitatively different results from the behavior predicted by the Aggregate Model. We believe this difference is indicative of the importance of the distribution of orientation along the chain and the nature of interactions between different parts of the chain. The importance of the atomic-level interactions is not unique to PS, and we expect that the additional information provided through atomistic simulation will

similarly provide insight to the structural problems of other polymers. Because of its flexibility, the SGMC methodology can be tailored to produce spatial, or other, heterogeneities, thereby providing the tools to investigate a wide variety of polymer structural problems at the atomic level. This ability to mimic conditions inaccessible by direct MD simulation provides not only the means to evaluate their structural thermodynamic properties, but also a starting point for MD simulations to probe their dynamic properties.

5.6. Appendix – Orientation of Polystyrene using Second and Fourth Legendre Coefficients

The original strategy for simulating the results of De Francesco and Duckett[5, 6] was to homogeneously constrain the orientation of PS molecules using an expanded basis expansion suggested by equation 3.17. Using the second and fourth Legendre coefficients provides the ability to describe a more complex set of orientation distributions. Moreover, since the birefringence depends only on the second Legendre coefficient, the fourth Legendre coefficient could be increased or decreased to mimic the possible spectrum of microstructures that correspond to a given birefringence value. The strategy for the simulations differed from those described in this chapter in that the eqn 5.8 was modified to include an additional term:

$$\ln(p) \propto -\beta \left[U(r^N) + PV - \mu_2 \sum_{i,j} P_2^{(2)} - \mu_4 \sum_{i,j} P_4^{(2)} \right] + N \ln V \qquad (5.11)$$

where the μ's are subscripted to designate which Legendre coefficient is being constrained and $P_4^{(2)}$ is the Fourth Legendre coefficient of the chain direction vector, defined analogously to $P_4^{(2)}$ in eq. 5.4:

$$P_4^{(m)} = \frac{35(q_{ij,x}^{(m)})^4}{8(q_{ij}^{(m)})^4} - \frac{15(q_{ij,x}^{(m)})^2}{4(q_{ij}^{(m)})^2} + \frac{3}{8} \qquad (5.12)$$

144

For simplicity, the Fourth Legendre coefficient will be denoted P_4. The inhomogeneous systems described earlier in this chapter correspond to systems with higher values of P_4 than for the homogeneous cases.

Simulations were run using the protocol described in Table 5.1 to produce systems with values of P_4 chosen to be significantly higher, and lower, than the value of the unconstrained value for $P_2=0.2$. Systems with unconstrained P_4 correspond to the homogeneously oriented simulations performed above; the unconstrained value of P_4 in this case was 0.07. For the constrained simulations, values of $P_4=0.2$ and $P_4=-0.05$ were chosen.

Figure 5.10 shows the change in modulus that accompanied the changes in the value of P4. The modulus of the high- P_4 system did not show a significant difference from that of the unconstrained P_4 system. The low- P_4 system showed a noticeable decrease in the modulus with respect to the other systems. Although this result follows the trend observed by De Francesco and Duckett that lower values of P_4 correspond to a decreased modulus, it must be recognized that none of the systems in that study correspond structurally to this case.

One could ask whether the degree of change in the structure was significant enough to expect the changes in modulus observed above in the case of inhomogeneous orientation. In fact, the value of P_4 for the $P_2=0.3$ system studied above in going from $f=0$ to $f=0.5$ only increases from 0.11 to 0.18. Therefore, in terms of the value of P_4 the differences were much more significant here than for the introduction of inhomogeneity detailed in this chapter. This serves to further highlight the importance of structural inhomogeneity, such as that introduced through polymer dynamics, to the properties of polymer systems.
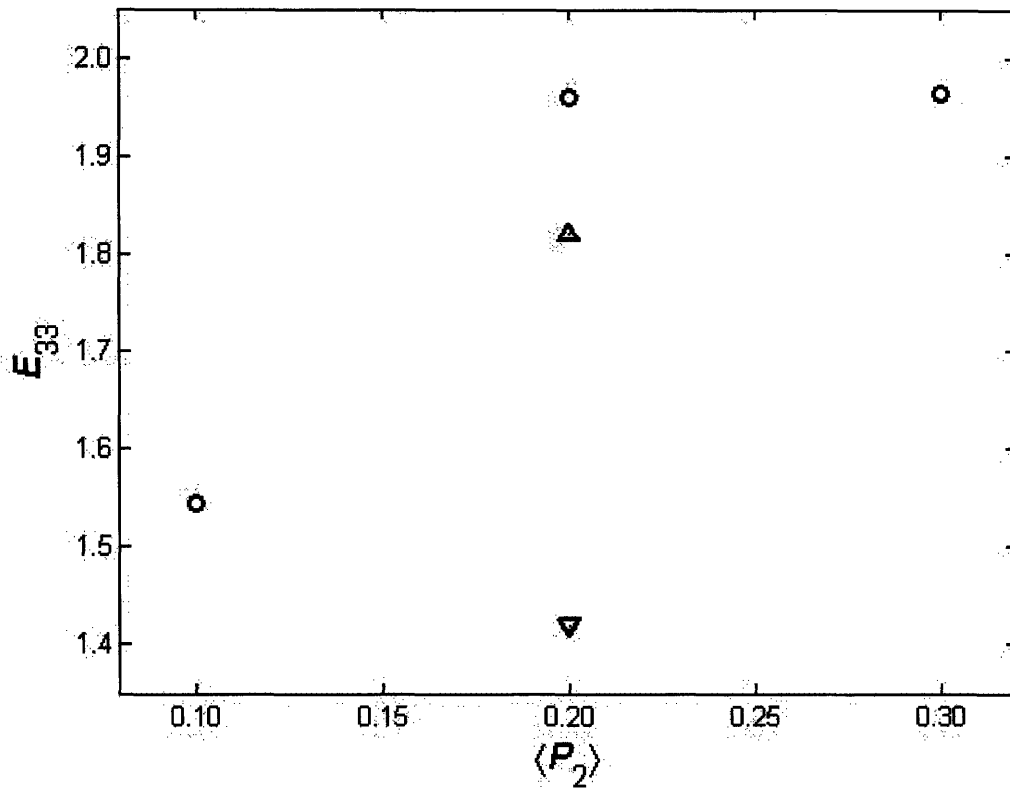
Figure 5.10. Variation of modulus obtained by constraining the values of P_4. Unconstrained values are shown for $<P_2>=0.1$, 0.2, and 0.3 to provide context for the shift in moduli; constrained values of $<P_4>=0.2$ (triangle) and $<P_4>=-0.05$ (upside-down triangle) are shown for $<P_2>=0.2$.

5.7. References

[1]   D.W. Hadley, P.R. Pinnock, I.M. Ward, *J Mater Sci* **1969**, *4*, 152.

[2]   H. Wright, C.S.N. Faraday, E.F.T. White, L.R.G. Treloar, *J. Phys. D:Appl. Phys.*, **1971**, *4*, 2002.

[3]   S. Dreher, S. Seifert, H.G. Zachmann, N. Moszner, P. Mercoli, G. Zanghellini, *J Appl Polym Sci* **1998**, *67*, 531.

[4]   R.H. Somani, L. Yang, B.S. Hsiao, *Polymer* **2006**, *47*, 5657.

[5]   A. DeFrancesco, R.A. Duckett, *Polymer* **2004**, *45*, 8005.

[6]   A. DeFrancesco, R.A. Duckett, *Polymer* **2004**, *45*, 4297.

[7]   M. Doi, *J Polym Sci Polym Phys Ed* **1983**, *21*, 667.

[8]   S.T. Milner, T.C.B. McLeish, A.E. Likhtman, *J Rheol* **2001**, *45*, 2.

[9]   M. Doi, *J. Chem. Soc. Faraday Trans. II* **1979**, *75*, 32.

[10]   J.F. Tassin, L. Monnerie, L.J. Fetters, Macromolecules **1988**, *21*, 2404.

[11]   *Theory of Polymer Dynamics*, M. Doi and S.F. Edwards, Oxford Univ., New York 1986; section 7.4.2.

[12]   J. des Cloizeaux, *J. Physique Lett* **1984**, *45*, 17.

[13]   Needs, R.J., *Macromolecules* **1984**, *17*, 437.

[14]   H. Watanabe, Prog. Polym. Sci. **1999**, *24*, 1253.

[15]   D.A. Carey, C.J. Wust, D.C. Bogue, *J. Appl. Poly. Sci.* **1980**, *25*, 575.

[16]   E. Riande and E. Saiz, *Dipole Moments and Birefringence of Polymers*, Prentice-Hall, Englewood Cliffs, NJ, 1992.

[17]   Y. Abe, Y., A.E. Tonelli, P.J. Flory, *Macromolecules* **1970**, *3*, 294.

[18]   *Prediction of Polymer Properties*, J. Bicerano, Marcel Dekker, New York, 2002.

[19]   M. Mondello, H.-J. Yang, H. Furuya, R.-J. Roe, *Macromolecules*, **1994**, *27*, 3566.

[20]   J. Wang, R. Wolf, J. Caldwell, P. Kollman, D. Case, *J. Comp. Chem.* **2004**, *25*, 1157.

[21]   A.V. Lyulin, M.A.J. Michels, *Macromolecules* **2002**, *35*, 1463.

[22]   M. Bathe, G.C. Rutledge, *J. Comput. Chem.* **2003**, *24*, 876.

[23]   A.P. Lyubartsev, A. Laaksonen, *Phys. Rev. E* **1995**, *52*, 3730.

[24]   V.K. Kuppa, P.J. in 't Veld, G.C. Rutledge, *Macromolecules* **2007**, *40*, 5187.

[25]   A.V. Lyulin, B. Vorselaars, M.A. Mazo, N.K. Balabaev, M.A.J. Michels, *Europhys. Lett.* **2005**, *71*, 618.

[26]   Modern Plastics Encyclopedia '99, *Modern Plastics* **1998**, *75(12)*, B207

[27]   G. Vancso, D. Snétivy, I. Tomka, *J. Appl. Polym. Sci* **1991**, *42*, 1351.

[28]   T.S. Chow, *Polymer* **1993**, *34*, 541.

[29]   A.V. Lyulin, J. Li, T. Mulder, B. Vorselaars, M.A.J. Michels, Macromol. Symp. **2006**, *237*, 108.

[30]   I.M. Ward, *Proc. Phys. Soc.* **80**, *1176*, 1962.

[31]   D.S. Hughes, J.L. Kelly, *Phys. Rev.* **1953**, *92*, 1145.

[32]   J.K. Kruger, C. Grammes, K. Stockem, R. Zietz, M. Dattenmaier, *Coll. Polym. Sci.* **1991**, *269*, 764.

Chapter 6

Conclusion and Future Work

6.1 Summary

The modeling and conceptual understanding of non-equilibrium systems present enormous challenges. One reason is that non-equilibrium conditions are characterized by what they are not, i.e. equilibrium, and not by virtue of the specific characteristics which are not at equilibrium; each non-equilibrium condition is unique. Although the constantly increasing computational power is an important component of the ability to use methods such as Monte Carlo simulations for these, it is just as important to devise efficient and creative methods to apply this power; brute force calculation is only useful in the simplest of cases. This failure of brute force methods is a common feature of highly interacting systems, for which it is possible to sample only with difficulty a sufficient portion of phase space, and thus obtain the answers to outstanding problems. This is especially true for polymer systems, because of the huge number of degrees of freedom and the highly interactive nature of polymer systems, i.e. their connectivity. This thesis has proposed a number of interconnected methods and tools to investigate non-equilibrium systems, with an emphasis on the application to oriented polymer systems. Below, I summarize the most important contributions to the achievement of the goals outlined in the first chapter of this thesis. These goals are:

1. Representation of experimental non-equilibrium information.
2. Bridging atomic-molecular length scales.

3. Representation of inhomogeneous non-equilibrium systems.

4. Demonstration of ability to reproduce macroscopic observations

6.1.1 SGMC representation of experimental non-equilibrium information.

The first, and most fundamental of these goals is the question of how to interpret experimental data. While the tools developed here are general to atomic level measurements of structure, I have focused on the specific problem of interpreting atomic level measurements of polymer orientation provided by birefringence measurements. The measurement of birefringence provides an average measurement of the average second moment of the orientation of specific units of the polymer. In the case of PE, this orientation is approximated as that of the chain itself; for polymers with side-groups, the relationship is more complex. By incorporating this information in a consistent manner, without a priori assumptions about the meaning of the data, we can allow the measurements guide us to an interpretation of the underlying structural relationships. The SGMC method is one such method which allows the incorporation of data in a way that ensures the uniqueness of the interpretation by specifying that the minimum-energy solution that is consistent with the experimental measurement and the known information about the system be chosen.

The SGMC method is shown in Chapter 3 to provide the 'best' interpretation of non-equilibrium experimental information. In this case the 'best' interpretation is the one that is most likely given only what we know about the system. In the specific cases of oriented polyethylene, I infer the microstructure from a single measure of anisotropy obtainable from the birefringence measurements, and from a reliable force field that describes the intrinsic properties of PE. The SGMC method is shown to be the appropriate framework for the interpretation of measurements of the non-equilibrium system by providing an ensemble of configurations that is the lowest free energy state that is consistent with all of the information we know about the system. Because of the thermodynamic consistency of the method, we can use the ensemble of configurations to

150

understand aspects of the system that are not, or cannot, be measured. Such attributes are density, molecular shape and size, torsion distribution, orientation at arbitrary length scales, free energy, and normal stress. This final attribute can be used in conjunction with the birefringence to obtain the stress-optical coefficient C. The veracity of our other structural inferences is supported by the fact that the value of C obtained in this study matched its experimental value.

Another aspect that is apparent from my results is the delineation of two modes of orientation available to a polymer chain. This is the orientation of the chain as a whole, followed by the distortion of the chain to obtain further orientation. The application of the SGMC method shows that the transition to distortion of the molecules occurs at an orientation of $P_2 \approx 0.15$. This point is the transition of a number of interrelated phenomena, which include the rapid increase in the energy of orientation, the increase in the radius of gyration, and the increase of the fraction of trans torsions. Again, the SGMC method allows a quantitative assessment of the onset of the transition between these different orientations as well as a quantitative estimate of the degree to which torsions, molecular dimensions, and free energy increase upon the onset of distortion. While the verification of these structural changes is not yet possible, the degree to which these results agree with future structural analyses will test the usefulness of a single measurement of birefringence for the characterization of microstructure.

6.1.2 Bridging Atomistic-Molecular Length Scales.

In Chapter 4, I have addressed the present impossibility of using atomistic simulations to directly obtain macromolecular characteristics for polymers of industrial interest. This stems from the fact that of carrying out an atomistic simulation of a chain hundreds of thousands of repeat units in length is orders of magnitude beyond current computational capabilities. I provide a solution to the challenge of bridging these scales by considering the intrinsic behavior of a portion of a polymer chain. This information is used to calculate a coarse grain descriptor that preserves the important characteristics of

the system while averaging out unnecessary atomic-level details. The selected characteristics common to both oligomers and macromolecules is the orientation and persistence in each principal direction α, represented respectively by the parameters A_α and τ_α. These parameters provide the means for calculating the size and shape of an arbitrary molecular system at the simulated oligomer conditions.

A correction was also introduced for the possible short-range deviation from the exponential decay of orientation assumed by the method. It was therefore recognized that there may be k^* terms that require correction due to bonded interactions. These parameters were found to be consistent for oligomers of polyethylene covering an order of magnitude from C_{12} to C_{234}, and gave results that matched the measured simulation results of the highest molecular weight system.

The proposed method allows the determination of the coarse grain descriptor of polymer molecules, the configuration tensor <QQ>, for very long chains that are beyond the scope of atomistic simulations alone, which is used in equations of state to determine the stress on the systems. This method extends the SGMC method elaborated in Chapter 3 since it relies on the information obtained from an SGMC simulation of oligomers in order to determine the macromolecular properties of the system. Therefore, it preserves the determination of properties based on the addition of no extra information; the application of the method relies on a similar lack of structure that is not a part of the experimental measurement. Similar to the results of the previous section, the degree to which these results agree with future structural analyses, i.e. simultaneous SANS measurements, will test the usefulness of a single measurement of birefringence for the characterization of the conformation at the macromolecular scale.

6.1.3 Representation of inhomogeneous non-equilibrium systems.

In Chapter 5, I make a concrete application of the SGMC method to experimental data by exploring the hypothesis that the relaxation processes in polymer systems lead to measurable differences in the mechanical properties of the system. Specifically, the

152

experimental data document an increase in the Young's modulus that accompanies the increasing inhomogeneity of the orientation. The ability to impose the characteristic inhomogeneous orientation of this system in a MC simulation highlights the flexibility of the SGMC method to apply the relevant constraints to a system. Due to the nature of the SGMC method, these constraints can cover any arbitrary distribution of average orientation; the modeling of inhomogeneities of orientation along the chain contour is only one possible application.

The increasing modulus with degree of orientation as measured by birefringence, although consistently lower than the experimental modulus, reproduced the trend quantitatively. More importantly, the increase of the Young's modulus with increasing inhomogeneity was also reproduced quantitatively. This latter result is important because the results of inhomogeneity depend on the specific chemical nature of the polymer; inhomogeneity could very well decrease the modulus in some cases. In fact, for polystyrene, the Aggregate Model predicts that inhomogeneity should *decrease* the modulus, in contrast to the experimental and simulation results. Therefore, the atomistic simulations presented here are necessary to elucidate the properties due to the chemical specificity of the system, and to understand the development of mechanical and optical properties. In this case, the simulations using the SGMC method provide a consistent link between the measurements of orientation and of mechanical properties. This provides supporting evidence for the ability of this method to be extrapolated to provide properties for other cases in which direct measurement is not feasible.

6.1.4 Demonstration of ability to reproduce macroscopic observations

Whenever possible we make comparisons between the computational models and the experimental systems. The most important reproductions of data were mentioned above as part of the previous goals. However, since our ultimate goal is to apply simulations to systems that cannot be measured, it is important to understand the limits of our ability to reproduce experimentally observable characteristics. The most concrete

examples of this are the measurement of the stress-optical coefficient of polyethylene, and the Young's modulus of oriented PS.

In Chapter 3, the stress-optical coefficient C was determined from the application of an orientation potential to the system. Neither the birefringence nor the stress is a simple function of the orientation potential; both quantities were evaluated for a given orientation potential. We found that although the low MW systems underestimated the stress-optical coefficient, its value asymptotically approaches the literature value for the higher MW systems; a MW of 100 repeat units appeared sufficient to reproduce this value. This sets a lower limit for simulations that can properly reproduce the stress-optical relationship.

In chapter 5, I focused on the ability to reproduce aspects of the mechanical properties of polystyrene for a number of structural conditions. The underestimate of the Young's modulus can be attributed in part to the fact that the simulations used 30-mer oligomers, which lie below the point at which the mechanical properties in the glassy phase become independent of the molecular weight. While this was recognized as a potential problem, higher MW simulations were not run because of the expense of PS simulations described earlier. Nonetheless, the simulations showed quantitative trends that matched those of the experimental systems. Just as with the stress-optical coefficient above, useful estimates of the large MW polymer can be obtained even at these oligomeric sizes, although care must be taken in the application of specific numeric values.

Nevertheless, the success of these simulations to quantitatively reproduce experimentally verifiable properties in the first case, and trends in the second case, argue strongly for the usefulness of computational simulations to understand orientation phenomena that are unobservable in the laboratory, using the SGMC methodology elaborated here.

6.2 Future Work

In many respects the topics of this thesis represent forays into completely unexplored territory. As is typical in such cases, the number of new questions raised by this research is as great as the number of answers it provides, leaving open many possible avenues for future work. The future work encompasses areas that were left unresolved because of constraints on time, computational resources, or conceptual development. Below, I outline what I feel are the most important unanswered or undeveloped questions brought up over the course of this research.

6.2.1 Expansion of Variable-Connectivity Moves

Variable connectivity moves, such as end-bridging provide the means for investigating relatively high molecular weight polyethylene. However its application to polymers with side groups is severely limited because of the steric hindrances. Such problems were the fundamental cause of the inability to simulate higher molecular weight PS in Chapter 5. The ability to extend the variable connectivity moves, through a more complex reformulation of the attempted moves, would greatly enhance the study of linear polymers with side groups. Even minimal acceptances ($\sim$0.01%) would provide a tremendous increase in the ability to investigate more complex polymer systems such as PS. The use of expanded ensembles has recently been applied to polypropylene to provide efficient sampling for a nonlinear polymer molecule[1].

6.2.2 Expansion of the use of moments

The descriptions provided in this thesis were based primarily on the second legendre coefficient of the orientation; the application of higher Legendre coefficients in a homogeneous system, as could be measured by IR or Raman, has not been explored.

Such effects would be most important in cases where the higher moments give indications of bimodal distributions of orientation. Another possible avenue in which a bimodal distribution occurs is the suggested exploration of orientational inhomogeneity based on the identity of the chain, i.e. long vs. short. The investigation of the behavior of chains whose inhomogeneity is based on molecular weight would give insight into the formation of the "shish" morphology. The methodology of this investigation would follow that of Chapter 5, except that the populations contributing to the overall orientation would be determined according to chain identity in place of contour position.

6.2.3 Application of results to MD simulations

Part of the motivation of using MC simulations to describe the polymer system is the relative efficiency with which they can reach a desired state point. Therefore, if one is interested in the dynamic properties of oriented systems, the methods detailed here can provide a starting point for a MD simulation that would be otherwise inaccessible. Such studies could probe the necessary orientation to provide crystallization. The ability of providing inhomogeneous systems allows hypothesized formation of the shish-kebab polymer morphology to be explored in conjunction with the bimodal orientations mentioned above. As explained by Tóth and Baranyai[2], the thermodynamic consistency of methods such as SGMC allows the potentials to be directly applied to subsequent MD simulations in order to investigate the dynamic behavior of these constrained systems.

6.2.4 Use of simultaneous measurements

One aspect of the SGMC method that is promising for the determination of structure is its ability to incorporate measurements of orientation at different length scales. Different couplings of techniques to provide this information were provided in the Chapter 2. Although such measurements exist, there are complications that precluded

this direction of inquiry here. The most important is that the measures for PE would have to also account for the added complication of crystallinity. For this reason the development of variable-connectivity techniques applicable to non-crystallizable polymers (i.e., those with non regular side groups) would be especially beneficial.

6.3 References

[1]   V.K. Kuppa, P.J. in 't Veld, G.C. Rutledge, *Macromolecules* **2007**, *40*, 5187.

[2]   G. Tóth, A. Baranyai, *J Phys. - Condens. Mat* **2005**, *17*, S159.